3/9/88

FERMILAB PROPOSAL P-789

STUDY OF NON-CHARM DI-HADRON DECAY OF NEUTRAL B MESONS AND Λ_b

Spokesmen: D. M. Kaplan and J. C. Peng

Participants: D. M. Alde, H. W. Baer, T. A. Carey, J. S. Kapustinsky, A. Klein, M. J. Leitch, J. W. Lillberg, P. L. McGaughey, C. S. Mishra, J. M. Moss, J. C. Peng,
Los Alamos National Laboratory

C. N. Brown, W. E. Cooper, Y. B. Hsiung,
Fermilab

D. M. Kaplan, R. S. Preston,
Northern Illinois University

M. L. Barlett,
University of Texas

ABSTRACT

We propose using an upgraded version of the E605/E772 spectrometer to measure a large sample ($\sim 10^3$ events) of two-body, two-prong decays of neutral b-quark hadrons. An integrated luminosity of 1.1×10^{41} cm^{-2} combined with $\sim 2\%$ acceptance at the B mass gives an effective luminosity of 2×10^{39} cm^{-2}. The excellent mass resolution (~3 MeV at m = 5.3 GeV) and high-rate capabilities of this spectrometer are uniquely suited to this objective. Masses and lifetimes of the B_d^0, B_s^0, and Λ_b^0 will be determined, as well as branching ratios for two-body non-charm decay into π, K, and protons. Major upgrades to the spectrometer are: a) addition of a vertex array employing silicon strip detectors, b) refurbishing of the E605 ring-imaging Cherenkov detector, and c) construction of a new station of high-precision, high-rate drift chambers (6 planes).

I. PHYSICS MOTIVATIONS

This proposal is motivated by two important recent discoveries in b-quark physics. The first is the observation[1,2] of unexpectedly large mixing in the neutral meson system, B^0 and $\bar{B}^0$. This result suggests the possibility that CP-violation could be observed in a high-statistics study of B^0 meson decays. The second discovery[3] is that the amplitude for b $\rightarrow$ u conversion is surprisingly large. The absence of non-charm decay of B mesons led to the determination $0 < |V_{ub}| \leq 0.008$ by the Particle Data Group[4] in 1986. This situation was changed by the recent discovery by the ARGUS[3] group of the decays $B^+ \rightarrow \bar{p}p\pi^+$ and $B^0 \rightarrow \bar{p}p\pi^+\pi^-$. Combined with previous data, the reported branching ratio of $(3.7 \pm 1.3 \pm 1.4) \times 10^{-4}$ for $B^+ \rightarrow \bar{p}p\pi^+$ and $(6.0 \pm 2.0 \pm 2.2) \times 10^{-4}$ for $B^0 \rightarrow \bar{p}p\pi^+\pi^-$ implies[5] $0.07 < |V_{ub}|/|V_{cb}| < 0.19$. The large magnitude of V_{ub} suggests that the branching ratios for $B^0_{d,s} \rightarrow h^+h^-$ non-charm decays could be of order 10^{-4} to 10^{-5}. Such di-hadron decays have not yet been observed experimentally. It is clear that the observation of non-charm h^+h^- decays will have important impact on the determination of V_{ub}.

Even though the existing data on B meson production and decay originate almost exclusively from e^+e^- collider experiments, the luminosity at existing colliders severely limits the production rate. An alternative[6] is the detection of b decays in fixed-target experiments at FNAL, where the production rate of b-quark hadrons is orders of magnitude greater than that at current e^+e^- colliders. The crucial questions to be answered of course are: (a) How many b's can be produced? and (b) To what extent can non-b-physics events be rejected from the data set. We propose that the existing E605/E772 spectrometer, characterized by its superb mass resolution and high-rate capability, is uniquely suitable for detecting the hadron pairs $(\pi^+\pi^-, K^+K^-, p\bar{p}, \pi^\pm K^\mp, p\pi^-, \bar{p}\pi^+, pK^-, \bar{p}K^+)$ emitted in the decays of neutral B mesons (B_d, B_s) and b-baryons $(\Lambda_b, \bar{\Lambda}_b)$. Based on the total number of b decays estimated for a single fixed-target running period — of order one thousand — we will be able to measure the masses of the B^0_s and Λ^0_b for the first time and accurately determine their lifetimes.

Beyond these goals it is interesting to note that measurements of the time dependence of $\Gamma(B \rightarrow h^+h^-)$ could lead to the observation of $B^0 - \bar{B}^0$ mixing and CP-violation provided

that a large production asymmetry exists between B^0 and $\bar{B}^0$. It is straightforward to derive[7]

$$\Gamma(B^{neutral}_{d,s} \to K^-\pi^+) \quad \propto \quad e^{-\Gamma_{d,s}t}\left(\frac{1}{2}(1+e^{-\Delta\Gamma_{d,s}t}) - \frac{\bar{N}-N}{\bar{N}+N}cos\Delta m_{d,s}t\right) \qquad (1)$$

where $N, \bar{N}$ are the numbers of B^0, $\bar{B}^0$ produced.

Equation (1) shows that even without flavor tagging of the B mesons, it is possible to observe an oscillatory component in the time evolution of $B^0 \to K^\mp\pi^\pm$ decay. Such an observation could lead to the determination of Δm and $(\bar{N}-N)/(\bar{N}+N)$. Unfortunately, it is difficult to predict the best kinematic region for a large production asymmetry.

The asymmetry in $B^0 \to K^\mp\pi^\pm$ decays is also sensitive to CP-violation. Bigi and Stech[7] obtain the following relation

$$\frac{Yield(K^-\pi^+)_B}{Yield(K^+\pi^-)_B} = \frac{1+Af(t)}{1-Af(t)}\frac{|Ampl(\bar{B}\to K^-\pi^+)|^2}{|Ampl(B\to K^+\pi^-)|^2} \qquad (2)$$

where $A = (\bar{N}-N)/(\bar{N}+N)$, and $f(t) = 2e^{-1/2\Delta\Gamma t}/(1+e^{-\Delta\Gamma t})cos\Delta mt$. CP-violation is established if the second factor in Eq. (2) is different from unity. For $B^0_d \to K^\mp\pi^\pm$ decays, CP asymmetry as large as 10% could occur.[7]

II. PROPOSED MEASUREMENTS

The goals of this experiment are the following:

(1) To determine the values (or upper limits) of the branching ratios of the following decays:

(a) $B_d \to \pi^+\pi^-$

(b) $B_d \to K^+K^-$

(c) $B_d \to p\bar{p}$

(d) $B_d \to \pi^\pm K^\mp$

(e) $B_s \to \pi^+\pi^-$

(f) $B_s \to K^+K^-$

(g) $B_s \to p\bar{p}$

(h) $B_s \to \pi^\pm K^\mp$

(i) $\Lambda_b \to p\pi^-$

(j) $\Lambda_b \to pK^-$

(k) $\bar{\Lambda}_b \to \bar{p}\pi^+$

(l) $\bar{\Lambda}_b \to \bar{p}K^+$

None of these decays has been observed.

(2) To search for B_s and Λ_b.

Neither the B_s nor the Λ_b has been seen. This experiment could lead to the first observation of these particles.

(3) To measure the mass and lifetime of B_d, B_s and Λ_b.

The Si strip vertex detectors, necessary for rejecting the backgrounds originating from the target, will determine the time evolution of various decays. We also expect excellent mass resolution ($\sigma \simeq 3$ MeV at mass $\cong 5$ GeV) with the E605/E772 spectrometer.

(4) To study the dynamics of b-quark production in hadron-hadron collisions.

We expect to measure the cross section and the x_F and p_t distributions of B_d production in p+W collisions at 800 GeV.

Strictly speaking, our proposed measurements are only sensitive to the product of the production cross sections times the branching ratio for a specific decay channel, $\sigma \cdot$BR. However, it is quite likely that we could determine σ and BR separately. For example, some of the decays we propose to detect could also be observed in future experiments at e^+e^- colliders. Furthermore, we expect to have some acceptance for the decay channel $B^\pm \to J/\psi K^\pm \to \mu^+\mu^- K^\pm$. The branching ratio for this decay is already known from e^+e^- experiments.

The proposed experiment would also provide useful information on several other decays:

(5) Search for B $\to \mu^\pm e^\mp$ decay.
No data exist on the upper limit of the branching ratio of this rare decay. We expect to have a sensitivity of order $10^{-5} - 10^{-6}$.

(6) Search for B $\to \mu^+\mu^-$ and B $\to e^+e^-$ decays.
The Drell-Yan continuum originating from the target will be greatly suppressed by the vertex detectors, allowing very sensitive measurements of the branching ratios of these decays (or upper limits).

(7) Search for $\eta_b \to p\bar{p}$ decay.
The η_b $b\bar{b}$ quarkonium state has not yet been discovered. The production cross section for η_b is predicted to be even greater than for Υ states. $\eta_b \to p\bar{p}$ could be an interesting channel to search for η_b. The branching ratio for $\eta_c \to p\bar{p}$ was measured[4] to be $(1.2 \pm 0.6) \times 10^{-3}$. Even though the branching ratio for $\eta_b \to p\bar{p}$ is expected to be lower, the excellent mass resolution ($\sigma \sim 8$ MeV for mass ~ 10 GeV) would lead to a sensitive search for η_b through the $\eta_b \to p\bar{p}$ decay.

Measurements 5), 6), and 7) are by-products of the proposed experiment and do not require additional beam time.

III. EXPERIMENTAL DETAILS

A schematic diagram of the E605/E772 spectrometer is shown in Figure 1. The large magnets SM12 (p_t kick $\sim 4.5GeV$) and SM3 (p_t kick $\sim 1.0GeV$) provide excellent momentum resolution. Figure 2 shows[8] the well-separated peaks of the Υ states in the dimuon mass spectrum obtained in E605. This spectrometer has been used in the 1987-1988 fixed-target run for experiment 772. Several modifications are required by this proposal:

1) Aperture

For P789 the spectrometer will be used in the open aperture configuration, with the aperture reduced in size to optimize acceptance for 5.3-GeV mass while minimizing singles rates. Results of a February 1988 test run under the approximate conditions of P789 are described in Section VI.

2) Cherenkov Detector

A ring-imaging-Cherenkov detector (RICH), operational for the 1983 and 1984 E605 runs, was not used in E772. The present proposal obviously requires the RICH detector for particle identification. An important task for P789 is to make the RICH detector operational again.

3) Silicon Strip Detectors

A crucial component of the P789 detector system is the silicon strip detectors which are required for reconstructing the decay vertices of B $\rightarrow h^+h^-$. We propose to have a total of 8 planes of Si strip detectors, placed 63 and 126 cm downstream of a thin target (3 mm long W), and covering the range 18 mr $\leq |\theta_y| \leq$ 65 mr and -26 mr $\leq \theta_x \leq$26 mr. The proposed locations and specifications of these Si strip detectors are given in Table I and Figure 3. A question which comes immediately to mind is whether these detectors can tolerate the expected high rate environment. In particular, will the detectors suffer significant radiation damage, and what will their average hit multiplicities be? We addressed these questions in the February 1988 test, the results of which are discussed in Section VI.

4) Drift Chambers

The sensitivity of the proposed experiment depends critically on the mass resolution one can achieve. Impressive mass resolution (δ(mass)$\simeq$ 30 MeV at mass $\simeq$ 9.5 GeV) was already obtained in the E605 experiment[8] with closed aperture and an extended target. The use of the Si detectors together with an open-aperture configuration will lead to excellent vertex determination and also improve the mass resolution. In addition, we propose replacing the existing station 1 MWPCs with high-rate drift chambers to obtain better position resolution at station 1. This will improve not only the mass resolution but also the ability to associate downstream tracks with tracks in the silicon vertex spectrometer. The proposed dimensions of these new drift chambers are listed in Table II. Monte-carlo simulation of the expected mass resolution (Section IV) yields $\sigma \sim 3$ MeV at m = 5.3 GeV.

5) Hodoscope Scintillators

For the proposed spectrometer setting, the profile of accepted 5.3-GeV-mass events at station 1 is about half the vertical size of the existing station 1 hodoscopes. We propose to rebuild the station 1 hodoscopes with the same number of scintillators but half the current vertical size. This will improve the trigger matrix definition at the lowest trigger level.

6) Target

We will employ a tungsten target with the dimension 3 mm$\times$ 0.5 mm $\times$ 10 mm (length $\times$ height $\times$ width). The short length of the target will facilitate the separation between primary and decay vertices. The small height of the target will help to reject those background tracks whose 3-momenta point back to the target and to provide a further cut on the 3-momenta of the dihadron which will be required to point to the target.

IV. MONTE-CARLO SIMULATIONS OF SPECTROMETER PERFORMANCE

1) Acceptance

The dynamics of b-quark production in hadron interactions was recently investigated by E. Berger.[9] His model is capable of reproducing the existing data from UA1[10] and π+nucleus[11] experiments. Figure 4 shows the x_F and p_t distributions predicted by Berger for b-quark production in p+p collisions. We assume similar distributions for B meson production in our monte-carlo simulation (x_F distribution $\propto e^{-x_F^2/2\sigma^2}$, $\sigma = 0.17$; p_t distribution $\propto e^{-(p_t^2/7GeV^2)}$). Figures 5(a) and 5(b) show the acceptance of the spectrometer as a function of SM12 current and target location, respectively. The choice SM12 = 2000 amps and Z = -80 inches is used throughout this proposal. Data taken during the February 1988 test on singles rates in the spectrometer vs. target location and magnet excitation will be used to optimize further the tradeoff among acceptance, resolution, and singles rates.

Figures 6(a) and 6(b) show the spectrometer acceptance as a function of the x_F and p_t of the B meson. The acceptance as a function of dihadron mass is shown in Figure 6(c). Note that the acceptance for mass $\sim$ 9.5 GeV is quite large. Therefore the search for $\eta_b \rightarrow p\bar{p}$ decay does not require different spectrometer settings. Figures 7(a) and 7(b) show the acceptance folded with Berger's production model for x_F and p_t; the p_z distribution is shown in Figure 8(a). At 800 GeV, the accepted B mesons have rather large momentum ($< P_z > \simeq 165GeV$). This implies that the average distance between the primary production vertex and secondary decay vertex is $\sim$ 1.0 cm, as shown in Figure 8(b).

To determine the dimensions of the Si strip detectors, we show in Figure 9 the distribution vs. θ_x and θ_y in the upper hemisphere for events accepted by the downstream spectrometer. The symmetry of the spectrometer implies nearly identical acceptance for the lower hemisphere.

2) Mass Resolution

To simulate the mass resolution of the spectrometer, multiple-scattering in the various materials and the finite position resolutions of the chambers are taken into account. Figure 10 shows the result of the monte-carlo simulation of mass resolution at the B meson mass. The large p_t kick of the SM12 magnet and the vertex determination by the Si vertex detectors are responsible for the excellent mass resolution of $\delta M/M \simeq 0.6 \times 10^{-3}$.

3) Vertex Reconstruction

Figure 11(a) shows the Z-vertex resolution for accepted B meson events, and Figure 11(b) shows the corresponding distribution in proper lifetime. Figure 11(c) shows the distribution of the reconstructed impact parameter of the $h^+ - h^-$ events.

V. SIGNALS AND BACKGROUNDS

1) Expected Yields of $B, \Lambda_b \to h^+h^-$

The expected number of events is calculated as

$$N_{det} = N_{beam} \times N_{targ} \times \sigma \times \epsilon \times BR \times Acc \times Eff \tag{8}$$

Assuming 10^5 spills for a fixed-target run with 3×10^{10} protons/spill, the total number of beam particles (N_{beam}) is 3×10^{16}. A 3mm-long W target (3% interaction length) gives $N_{targ} = 3.5 \times 10^{24}$ nucleon/cm^2. The production cross section $\sigma(pp \to b\bar{b}X)$ is estimated by Berger[9] to be $9nb > \sigma > 2nb$. ϵ is the probability that the produced $b, \bar{b}$ quarks will hadronize into a particular B meson or b-baryon. Bjorken has estimated[6] that $\epsilon(b \to B_d) \simeq 30\%$, $\epsilon(b \to B_s) \simeq 15\%$ and $\epsilon(b \to \Lambda_b) \simeq 15\%$. BR is the expected branching ratio for a specific $B, \Lambda_b \to h^+h^-$ decay. As discussed earlier, the spectrometer acceptance Acc is calculated to be $\sim 2\%$ at 5.3-GeV mass. Eff represents the efficiency of the B events to survive the various background-rejection cuts (mainly mass and Z-vertex cuts). We estimate Eff to be ~35%. Table III lists the number of surviving events (N_{det}) after all cuts for various decay channels. In Table III we assume $\sigma(pp \to b\bar{b}X)$ to be 4.5 nb and BR $= 5 \times 10^{-5}$ for all decay modes. With the assumed branching ratios, the total number of reconstructed $B, \Lambda_b \to h^+h^-$ events is expected to be of order one thousand.

2) Backgrounds

There are two major types of background. The first arises from production of a pair of relatively long-lived particles which decay downstream of the target. The second is due to direct hadron pairs produced in the target. The nature of these backgrounds and the estimated efficiency to reject them are discussed below.

(a) Background from decays of pairs of long-lived particles

First we consider the production of D-meson pairs $D\bar{D}$ followed by $D \to K\pi$, $D \to K\pi\pi$, $D \to K\pi\pi\pi$ decays. The lifetimes of D mesons are comparable to those of B mesons but with production cross sections three orders of magnitude larger. The probability for a

pion pair produced in the D-pair decays to fake a $B \rightarrow \pi\pi$ event has been simulated and the results are summarized in Appendix A. Cuts in invariant mass, Z-vertex, and track distance of closest approach, combined with the spectrometer acceptance, efficiently reject these backgrounds. Indeed, Appendix A shows that this background contributes less than 1/1000 of the $B \rightarrow \pi\pi$ signals.

Another background is the production of $K^0\bar{K}^0$ pairs followed by $K_S \rightarrow \pi^+\pi^-$ decays. This background has been simulated and the results are given in Appendix B. The spectrometer acceptance for this background is much larger than that for D-pair decays, and the background is estimated to be about 4% of the $B \rightarrow \pi^+\pi^-$ signal. We conclude that the backgrounds from decays of pairs of long-lived particles do not pose a significant problem.

(b) Backgrounds from direct hadron-pair production

It is well known that hard parton-parton scattering at high energies can lead to the production of pairs of high-p_t hadrons. This background affects the proposed experiment in two ways. First, it sets a lower limit to the trigger rate. Second, it determines the ultimate sensitivity in the off-line analysis. The cross sections for hadron-pair production have been measured both in a fixed-target experiment by the CFS group[12,13] and in the CCOR experiment at the ISR.[14] Figure 12 shows the CFS data[12] and the CCOR data.[14] Also indicated on Figure 12 is the CFS cross section extrapolated to ISR energy using the CFS scaling fit.[13] It is seen that the two experiments disagree by an order of magnitude. This is not surprising considering the extremely small ($< 10^{-3}$), and hence model-dependent, acceptance of the CFS spectrometer and the large extrapolation factor involved.

To resolve the question of what cross section to use in estimating the hadron-pair background, we turn to the results of the February 1988 test run. Figure 13 shows the observed yield of hadron pairs originating in the target vs. mass. The CCOR data extrapolated to our mass and beam energy are a factor of two higher than these test run yields. Preliminary results from E605 extrapolated to the 5 GeV mass region are also a factor of two higher than the test run results. To be conservative, we therefore use the test run results normalized upwards by a factor of two in estimating the hadron-pair back-

ground. Normalizing to the proposed P789 beam intensity, we observe a total of 2×10^3 hadron-pair events originating in the target per spill. This is a trigger rate which our data acquisition system is capable of handling. More details on trigger rates are presented in Section VI.

In principle, the direct QCD dihadron backgrounds originate from the target and can be rejected in the off-line analysis using vertex information from the Si strip detectors. In practice, the Z-vertex resolution, the multiple-scattering in the Si detectors, and the ambiguities in the track reconstruction will determine the rejection efficiency. A detailed monte-carlo simulation is underway to study this issue and the results will be presented at the April 1988 PAC meeting. To evaluate the level of rejection required in this experiment, we show in Table IV the estimated number of events for the $B \rightarrow h^+h^-$ signals and for the backgrounds. We have used the CFS identified-hadron-pair fractions to convert our February test results to yields for particular particle-species combinations. We assume that a 5 MeV cut in invariant mass and a decay-time $> 0.7\tau$ cut in Z-vertex will give a background rejection factor of 10^4. Table IV shows that the statistical significances of all proposed measurements are very high. It is worth noting that even if a rejection factor of only $\sim 10^3$ is obtained or if the QCD dihadron background is ten times larger than we have assumed, good statistical significance is still obtained.

VI. RESULTS FROM TEST RUN

In January and February 1988, after the completion of experiment 772, we performed several tests to evaluate the spectrometer configuration of P789. The major goals of these tests were:

a) To check the singles rates in various detectors in the proposed open-aperture configuration.

b) To measure the rate of charged-particle production from the interaction of an 800 GeV proton beam with a 3mm tungsten target. The neutron flux was also measured. These measurements are crucial for evaluating the radiation damage of and count rates in the Si strip detectors.

c) To measure the trigger rate.

For the tests, we removed from E772 the SM0 magnet and the hadron absorber wall. The SM12 current was set at 2000 amps and the SM3 current at -4250 amps. The exit of SM12 was collimated to 20" high × 28" wide. 1mm and 3mm W targets and beam intensities varying between a few × 10^{10} and a few × 10^{11}/spill were used. We present results normalized to the proposed beam intensity of 3 × 10^{11}/spill.

1) Singles rates on hodoscopes and chambers

Table V lists the singles rates at the various hodoscope stations. The maximum rate is ~6 MHz, well within the rate capability of these counters. The currents drawn by the wire chambers at stations 1, 2 and 3 were 50, 100 and 300 μamps, respectively. The hit multiplicities on the stations for reconstructed dihadron events were 12, 10, and 15. These chamber currents and multiplicities are similar to or less than those observed during E605 data taking.

2) Rates on the Si strip detectors

We installed a Si strip detector (5 cm × 5 cm, 50 μm pitch) 60 inches downstream

of the target. In addition, a finger scintillator (3" × 1/8" × 1/8") was mounted on a motor-driven frame 49 inches downstream of the target. The minimum ionization band was clearly visible on the photo-tube output of the scintillator. The vertical position of the finger scintillator was varied between 6mr $\leq |\theta_y| \leq$ 90 mr. Figure 14 shows the scintillator count rates as a function of the vertical position of the counter. Also shown are target-out rates. The beam axis can be well determined from Figure 14. The preamp output of the Si detector also showed a clear minimum ionization band. Three adjacent strips of the Si detector were read out. The Si detector was placed at two different heights corresponding to θ_y = 50 mr and θ_y = 96.5 mr. The rates measured by the finger scintillator are in agreement with the rate measured by the Si detector within a factor of two.

From the count rates measured by the finger scintillator (Figure 14), we can now make a realistic prediction of the rates on the Si strip detectors to be used in P789. We consider a Si detector located 63 cm downstream of the target covering -26 $\leq \theta_x \leq$ 26 mr, 18 mr $\leq \theta_y \leq$ 65 mr. This detector has 512 horizontal strips of 70 μm pitch with a total area of 2" × 1.4". In Table VI we list the predicted count rate/strip on various strips as a function of θ_y, as well as the flux per cm^2 integrated over one running period. (The integrated fluxes for a plane located 126cm downstream of the target are given for comparison.) The results in Table VI are also plotted in Figure 15. Table VI implies that the average count rate/strip is 1.4 MHz and the average number of hits per RF bucket on the Si detector is ~14. Assuming the radiation damage limit for Si detectors is 10^{14} minimum-ionizing particles/cm^2, we conclude that the upstream Si detector should last for a few months of beam time. We anticipate that the upstream planes can be replaced part-way through the run, should this prove necessary, at a cost of $7K per silicon wafer.

The neutron flux was measured in the target cave behind a few inches of concrete shielding. This was done in order to estimate the possible radiation damage to the silicon detector and its preamplifiers. The neutron rates were considerably lower than the direct charged particle rates from the target. With a modest amount of shielding, the neutron rates 1/2m east and west of the beam axis (where the preamplifiers will be located) can be reduced to less than 50 krads for 10^5 pulses. We have been assured by D. Christian that this level should prove not to be a problem for the new generation of preamplifiers.

The neutron rates on axis will cause less damage to the silicon wafers than the charged particle rates.

3) Trigger Rate

As indicated in a previous section, it is expected that 2×10^3 target di-hadrons per spill will be accepted by the spectrometer. Unless a highly efficient trigger can be devised which selects only such events, the resulting volume of data would most likely exceed the maximum storage of our data buffering system (4096 events or 4 megabytes per pulse). While we intend to increase this storage limit at least fourfold, it is essential that a clean di-hadron trigger be constructed. Past experience suggests that our existing low-level hadron-pair trigger, which is based upon hodoscope roads in combination with calorimeter energy deposition, could be the starting point for this trigger. The rejection power of the trigger processor, calculating the mass of the apparent hadron pair, should then bring the data rate within the capacity of the buffer.

Several tapes of di-hadron test data were recorded using a variety of hodoscope and calorimeter based triggers under various beam and target conditions. These serve to measure the relevant trigger rates and to check the di-hadron production cross sections. The results of these studies are shown in Table VII. The various trigger conditions applied are defined as follows: The 3/4 L·R hodoscope coincidence requires 3 out of 4 hodoscope planes on the both the left and right side of the apparatus to record hits. E_{tot} requires a total energy deposition threshold in the calorimeter of at least 70 GeV. h^+h^- is a 6-fold matrix hodoscope hit pattern consistent with two oppositely charged particles originating from the target.

By using all three of these trigger conditions in coincidence a raw trigger rate of 1.2×10^4 per spill was observed at 1.4×10^{11} protons per spill incident on a 3mm W target. This is expected to scale up to about 4×10^4 at 3×10^{11} incident protons per spill. Table VII indicates that about half of the event rate is due to particles coming from the beam dump. These beam dump triggers will be more efficiently rejected by the trigger matrix when the new, finer-grained Y1 hodoscope is employed. Furthermore, a requirement on the presence of two energy clusters in the calorimeter can be applied to remove the background of high

energy single hadrons. Nevertheless, this trigger rate is already well within the bandwith of our trigger processor, which requires only 10 to 20 μsec per event. In past running the trigger processor has provided a trigger rate reduction of 5 to 10 times by requiring a pair of opposite-sign tracks originating near the target. This would place the number of events per spill safely inside the anticipated capacity of the upgraded data buffer. If necessary, the processor is capable of making a tight mass cut on these target-track pairs to reduce the data rate still further. While we are planning on adding a silicon vertex track processor to our triggering system, it is not anticipated that this information will be needed in the trigger, but will merely serve to reduce the amount of tapewriting and hence also the off-line computing load.

VII. COST ESTIMATES

A number of changes to the E605/772 spectrometer are required for P789. These include the installation of a silicon vertex detector and a new station 1 drift chamber, construction of a partially-open aperture wall in the SM12 magnet, rehabilitation of the RICH detector, upgrades to the data acquisition system including a vertex processor, and rebuilding of two hodoscope planes. The total estimated cost is $590K. This is based primarily on the P789 impact statement written by D. Christian dated November 29, 1987 and assuming that the existing 6000 channels of MWPC electronics will be used for the silicon vertex detector readout. The breakdown of the costs is as follows:

1) Silicon Detectors

Silicon (8 planes + spares)	$150K	
Mounts	35K	
Preamps (6K channels)	55K	
A/C & RF shielding	30K	
Re-shielding target cave	30K	
Total		$300K

2) New Station 1 Drift Chamber

Mechanical	$40K	
Readout electronics	10K	
Total		$50K

3) Partially Open Magnet Aperture

Machining and rigging	$50K	
Total		$50K

4) RICH Detector

Readout electronics (2000 chan.)	$120K	
Misc. rehabilitation	20K	
Total		$140K

5) DAQ Upgrade

Megamemory replacement	$30K	
Si vertex processor	10K	
Total		$40K

6) Hodoscope rebuild

Rebuild 2 planes - mechanical	$10K	
Total		$10K

Total Estimated Cost $590K

VIII. SUMMARY

We propose to reconfigure the E605/772 spectrometer to study the two-body, two-prong decay modes of neutral B mesons and baryons. The superb mass resolution and high-rate capability of this instrument are uniquely suited to this objective. Based upon plausible assumptions for cross sections and branching ratios, a sample of order 10^3 b-decays can be obtained. These data will provide important first measurements of the masses, lifetimes and branching ratios for a variety of non-charm decays into π, K, and protons. While some upgrades to the spectrometer are required, the anticipated cost ($590K) and level of effort involved are reasonable in light of the potential physics insight that can be obtained.

References

1. H. Albrecht *et al.*, *Phys. Lett.* **192B** (1987) 245.

2. C. Albajar *et al.*, *Phys. Lett.* **186B** (1987) 247.

3. W. Schmidt-Parzefall, Invited talk at the 1987 International Symposium on Lepton and Photon Interactions at High Energies, Hamburg, W. Germany, July 27–31, 1987.

4. Particle Data Group, *Phys. Lett.* **170B** (1986) 74.

5. F. J. Gilman, Invited talk at the Workshop on High Sensitivity Beauty Physics at Fermilab, Batavia, Illinois, Nov. 11–14, 1987.

6. J. D. Bjorken, Invited talk at the International Symposium for the Fourth Family of Quarks and Leptons, UCLA, Los Angeles, California, February 26–28, 1987.

7. I. I. Bigi and B. Stech, Contribution to the Workshop on High Sensitivity Beauty Physics at Fermilab, Batavia, Illinois, Nov. 11–14, 1987. SLAC-PUB-4495.

8. E605 Collaboration, to be published.

9. E. L. Berger, Invited paper at the XXII Rencontre de Moriond, Les Arcs, France, March 15–21, 1987.

10. C. Albajar *et al. Phys. Lett.* **186B** (1987) 237.

11. M. G. Catanesi *et al. Phys. Lett.* **187B** (1987) 431.

12. R. D. Kephart *et al. Phys. Lett.* **39** (1977) 1440.

13. H. Jöstlein *et al.*, *Phys. Rev.* **D20** (1979) 53.

14. A. L. S. Angelis *et al*, *Nucl. Phys.* **B209** (1982) 284.

Table I. Si strip detector configuration.

Plane	Z (cm)	Size (X cm × Y cm) (H × V)	No. of strips	Spacing (μm)
Y1	60	4.0 × 3.4	512	66
U1	60	4.0 × 3.4	244	200
Y1′	68	4.0 × 3.4	512	66
V1	68	4.0 × 3.4	244	200
Y2	124	7.0 × 6.8	512	132
U2	124	7.0 × 6.8	244	400
Y2′	132	7.0 × 6.8	512	132
V2	132	7.0 × 6.8	244	400

Total number of strips = 3024 × 2 = 6048.

The U,V strips are on the reverse side of the Y silicon wafers.

Table II. New station 1 drift chambers.

Chamber	Size (cm × cm) (H × V)	No. of channels	Cell size (cm)
Y1	110 × 72	72	1
Y1′	110 × 72	72	1
U1	110 × 72	96	1
U1′	110 × 72	96	1
V1	110 × 72	96	1
V1′	110 × 72	96	1

Table III. Estimated number of events (per 10^{15} interactions).

Decay Mode	ε	BR	No. of events
$B_d, \bar{B}_d \to \pi^+\pi^-$	0.6	5×10^{-5}	100
$B_d, \bar{B}_d \to K^\pm\pi^\mp$	0.6	5×10^{-5}	100
$B_d, \bar{B}_d \to K^+K^-$	0.6	5×10^{-5}	100
$B_d, \bar{B}_d \to p\bar{p}$	0.6	5×10^{-5}	100
$B_s, \bar{B}_s \to \pi^+\pi^-$	0.3	5×10^{-5}	50
$B_s, \bar{B}_s \to K^\pm\pi^\mp$	0.3	5×10^{-5}	50
$B_s, \bar{B}_s \to K^+K^-$	0.3	5×10^{-5}	50
$B_s, \bar{B}_s \to p\bar{p}$	0.3	5×10^{-5}	50
$\Lambda_b, \bar{\Lambda}_b \to p^\pm\pi^\mp$	0.3	5×10^{-5}	50
$\Lambda_b, \bar{\Lambda}_b \to p^\pm K^\mp$	0.3	5×10^{-5}	50

Table IV. Number of signal and background events.

Decay Mode	No. of Events	Background	Significance
$B_d, \bar{B}_d \to \pi^+\pi^-$	100	40	8σ
$B_d, \bar{B}_d \to K^+K^-$	100	4	10σ
$B_d, \bar{B}_d \to p\bar{p}$	100	4	10σ
$B_d \to K^+\pi^-$	50	20	6σ
$\bar{B}_d \to K^-\pi^+$	50	10	6σ
$B_s, \bar{B}_s \to \pi^+\pi^-$	50	40	5σ
$B_s, \bar{B}_s \to K^+K^-$	50	4	7σ
$B_s, \bar{B}_s \to p\bar{p}$	50	4	7σ
$\Lambda_b \to p\pi^-$	25	30	3σ
$\Lambda_b \to pK^-$	25	5	5σ
$\bar{\Lambda}_b \to \bar{p}\pi^+$	25	5	5σ
$\bar{\Lambda}_b \to \bar{p}K^+$	25	2	5σ

Table V. Maximum count rates in hodoscopes (3×10^{11} protons on 3mm W).

Plane	Rate (MHz)
X1R	3.0
Y1R	2.4
Y2R	1.6
X3R	4.4
Y3R	6.5
X4R	0.25
Y4R	0.10

The X1R,Y1R rates are shown for the reduced size planes.

Table VI. Si detector count rate/strip (3×10^{11} proton/spill on 3mm W).

θ_y(mr)	Rate (MHz) per strip	Hits/RF bucket	Integrated flux/cm^2 Z = 63cm	(per 10^{15} interactions) 126cm
18.1	2.99	0.059	2.5×10^{14}	0.62×10^{14}
21.2	2.49	0.050	2.1×10^{14}	0.52×10^{14}
26.2	1.92	0.038	1.6×10^{14}	0.40×10^{14}
31.2	1.74	0.035	1.4×10^{14}	0.36×10^{14}
36.2	1.38	0.028	1.1×10^{14}	0.28×10^{14}
46.4	0.95	0.019	0.78×10^{14}	0.20×10^{14}
56.4	0.68	0.014	0.55×10^{14}	0.14×10^{14}

Table VII. Results of Trigger Rate Study with 3mm W Target.

Trigger	Target	Protons/spill	Triggers/spill
$(3/4L{\cdot}R){\cdot}E_{tot}$	In	$3.4{\times}10^{10}$	$1.9\ {\times}10^{4}$
$(3/4L{\cdot}R){\cdot}E_{tot}$	Out	$3.6{\times}10^{10}$	$1.2\ {\times}10^{4}$
$(3/4L{\cdot}R){\cdot}E_{tot}$	In	$9.8{\times}10^{10}$	$7.5\ {\times}10^{4}$
$(3/4L{\cdot}R){\cdot}E_{tot}$	Out	$1.4{\times}10^{11}$	$7.0\ {\times}10^{4}$
$(3/4L{\cdot}R){\cdot}E_{tot}{\cdot}(h^{+}h^{-})$	In	$2.6{\times}10^{10}$	$1.2\ {\times}10^{3}$
$(3/4L{\cdot}R){\cdot}E_{tot}{\cdot}(h^{+}h^{-})$	Out	$2.1{\times}10^{10}$	$5.2\ {\times}10^{2}$
$(3/4L{\cdot}R){\cdot}E_{tot}{\cdot}(h^{+}h^{-})$	In	$1.4{\times}10^{11}$	$1.2\ {\times}10^{4}$
$(3/4L{\cdot}R){\cdot}E_{tot}{\cdot}(h^{+}h^{-})$	Out	$1.3{\times}10^{11}$	$6.7\ {\times}10^{3}$

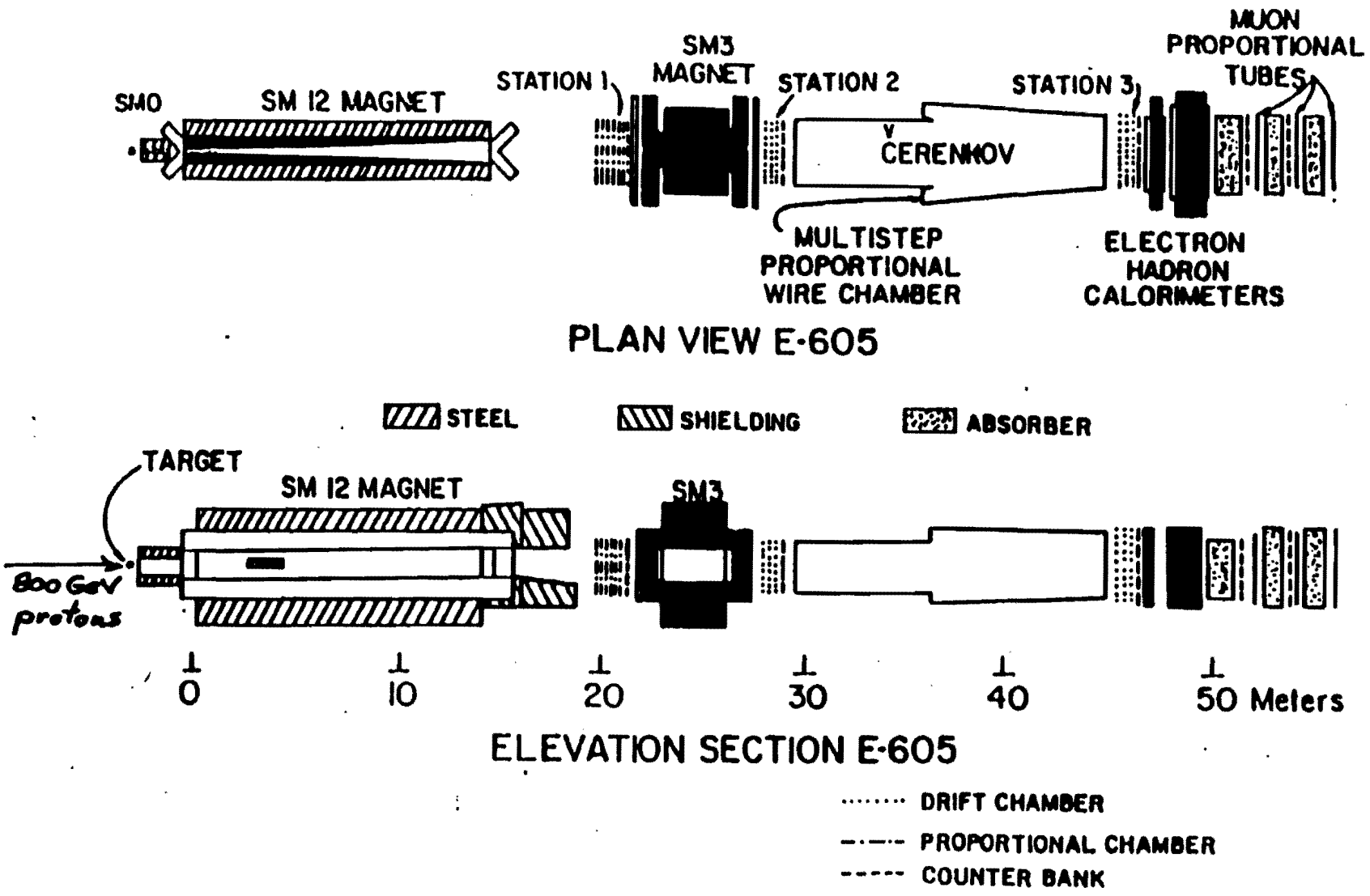
SM0
SM 12 MAGNET
STATION 1
SM3
MAGNET
STATION 2
STATION 3
MUON
PROPORTIONAL
TUBES
CERENKOV
MULTISTEP
PROPORTIONAL
WIRE CHAMBER
ELECTRON
HADRON
CALORIMETERS
PLAN VIEW E-605
STEEL
SHIELDING
ABSORBER
TARGET
SM 12 MAGNET
SM3
800 GeV
protons
0
10
20
30
40
50 Meters
ELEVATION SECTION E-605
DRIFT CHAMBER
PROPORTIONAL CHAMBER
COUNTER BANK

Figure 1.

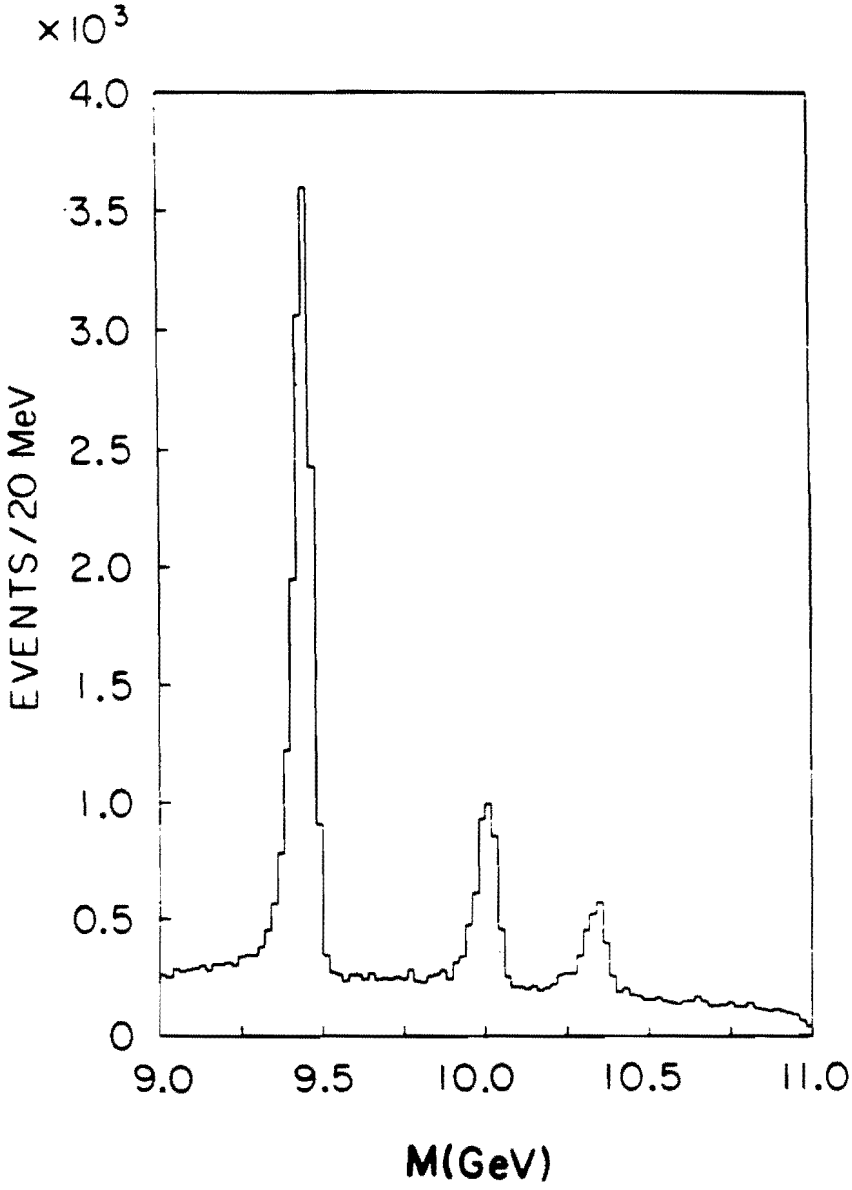

Figure 2.

Figure 3.

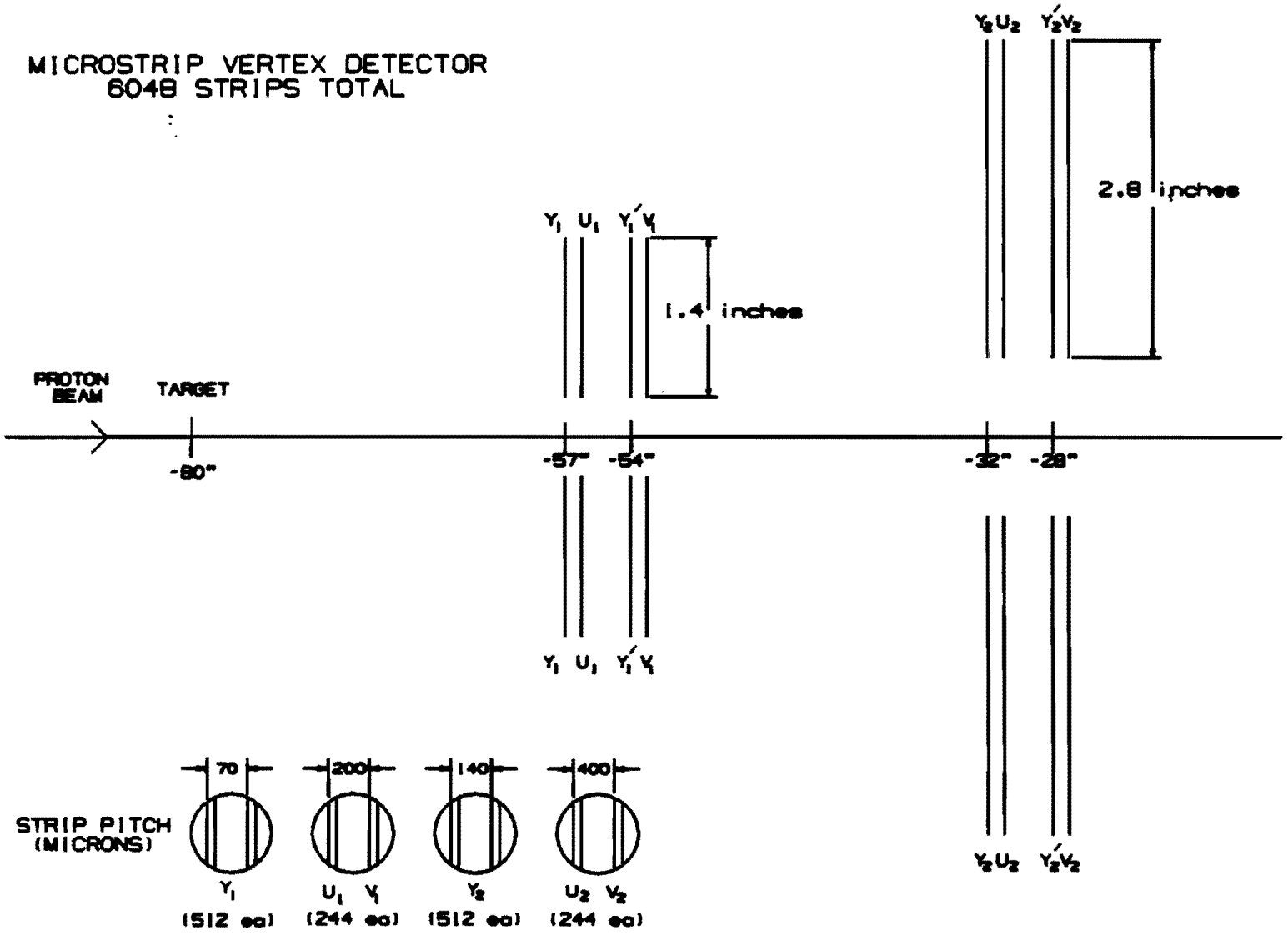

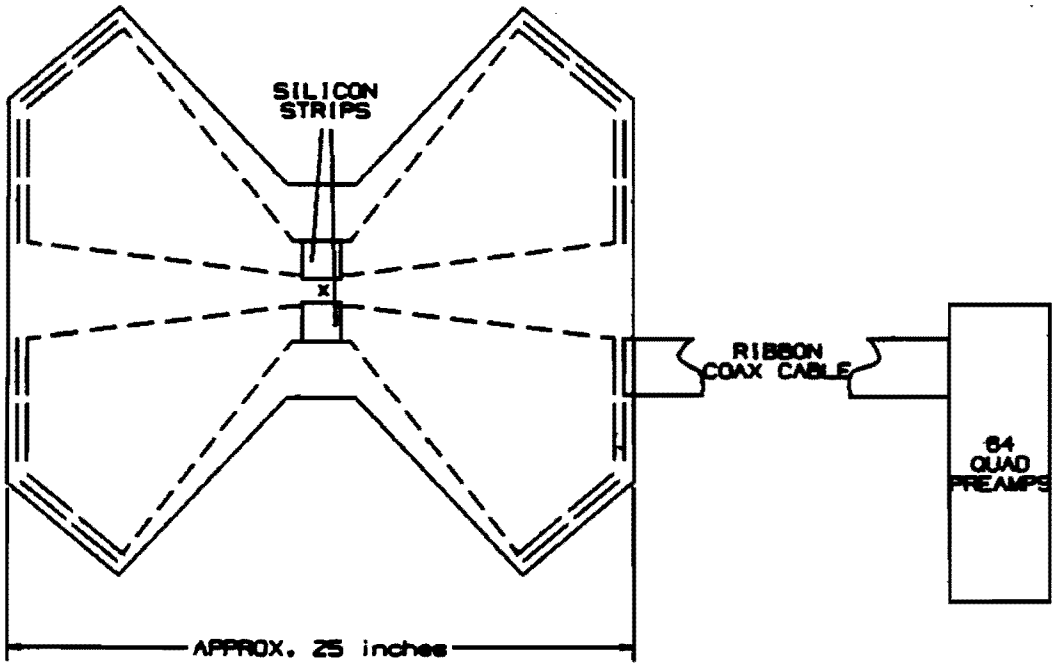

Y_1 U_1

UPSTREAM FACE

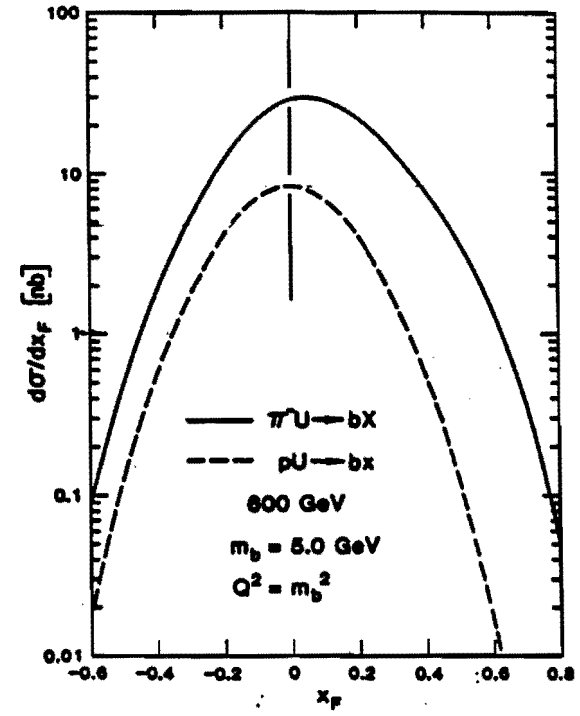
100
10
1
0.1
0.01
$d\sigma/dx_F$ [nb]
$\pi^-U \rightarrow bX$
$pU \rightarrow bx$
800 GeV
m_b = 5.0 GeV
$Q^2 = m_b^2$
-0.6
-0.4
-0.2
0
0.2
0.4
0.6
0.8
x_F

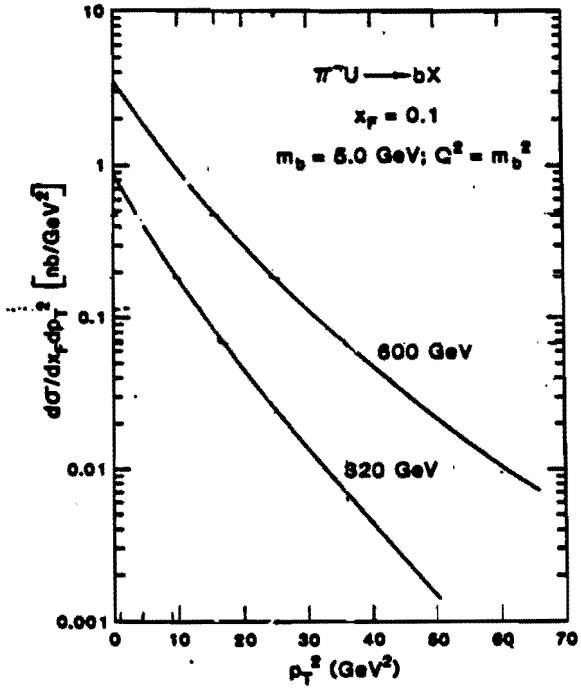
10
1
0.1
0.01
0.001
$d\sigma/dx_F dp_T^2$ [nb/GeV^2]
$\pi^-U \rightarrow bX$
x_F = 0.1
m_b = 5.0 GeV; $Q^2 = m_b^2$
800 GeV
820 GeV
0
10
20
30
40
50
60
70
p_T^2 (GeV^2)

Figure 4.

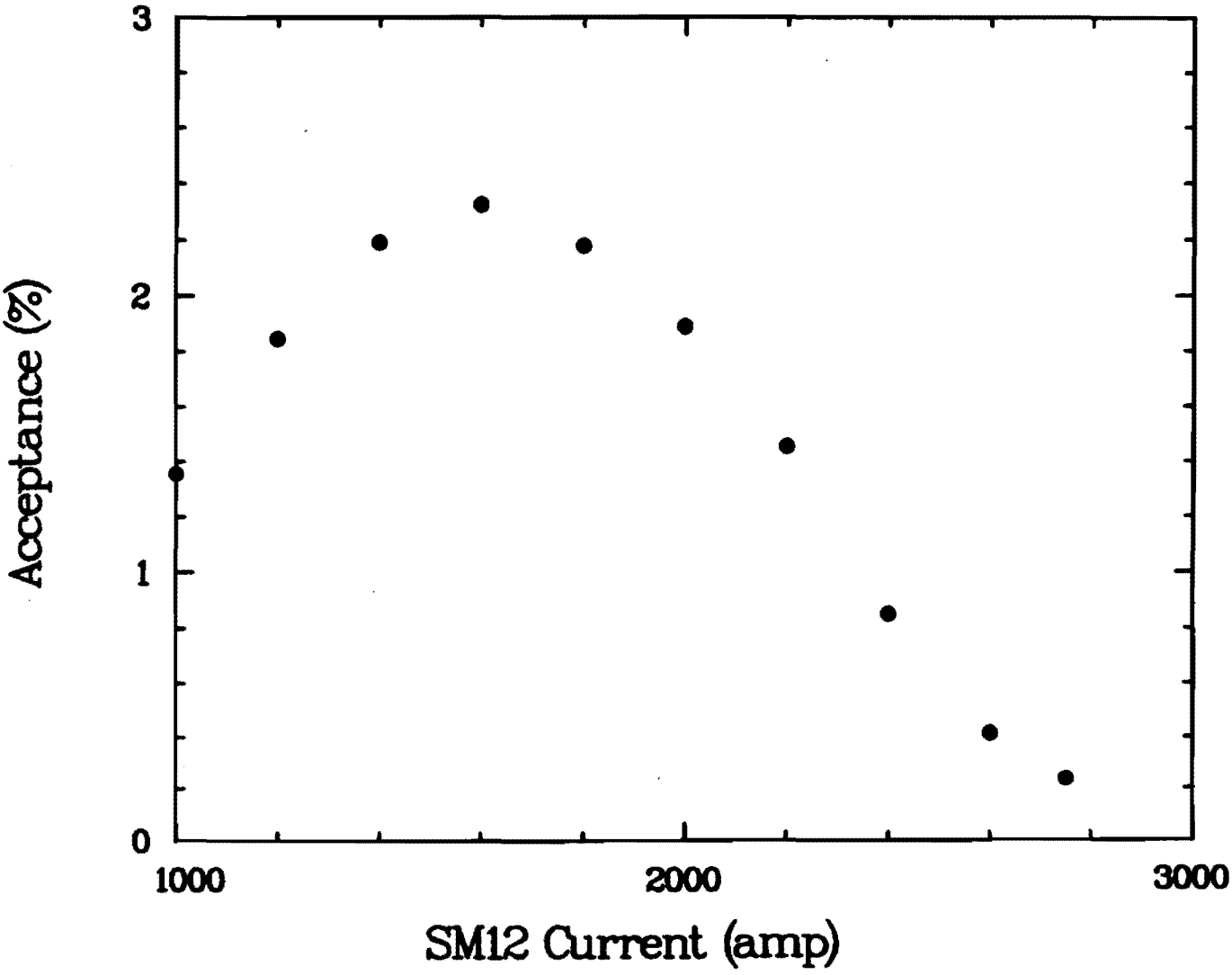

Figure 5(a).

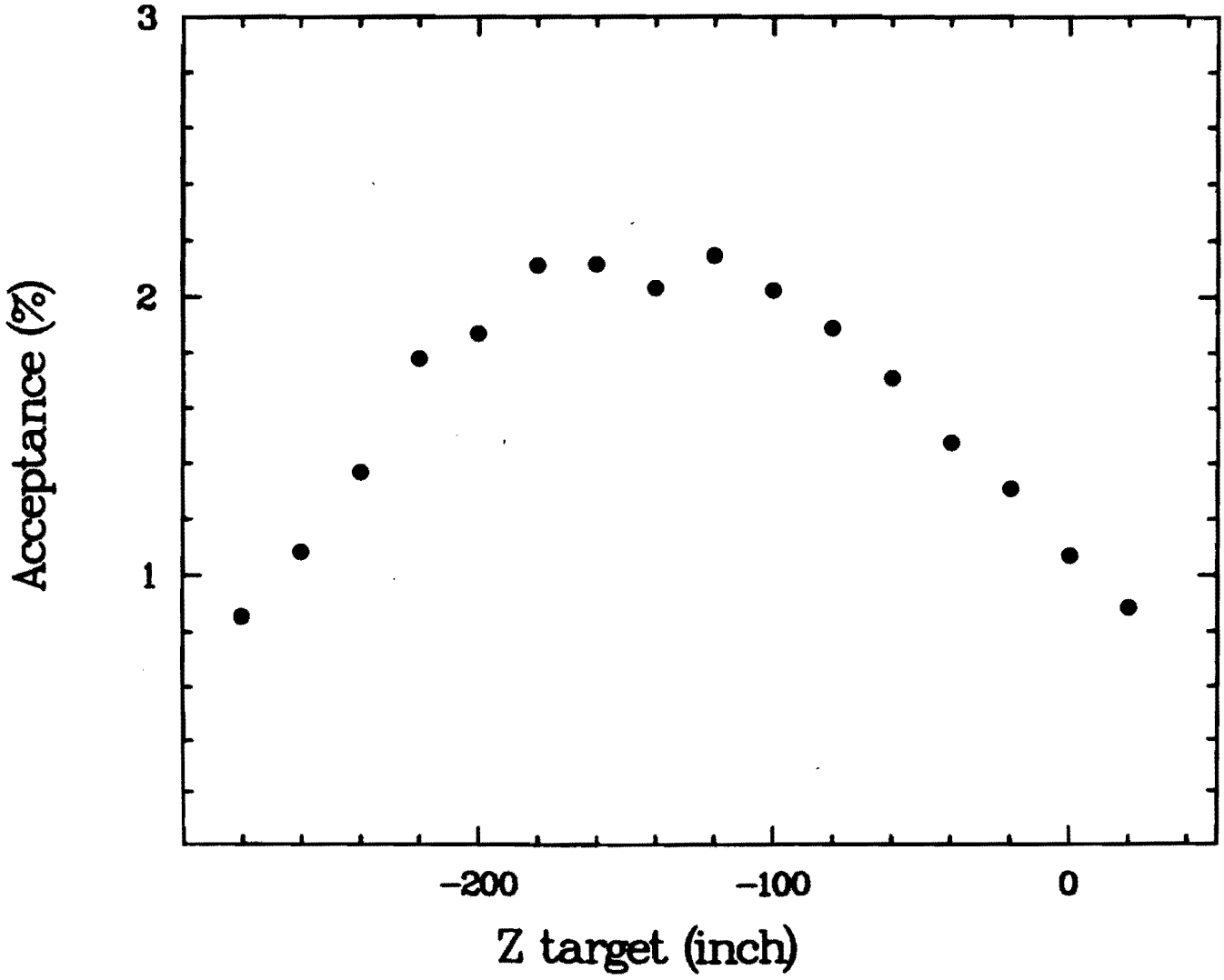

Figure 5(b).

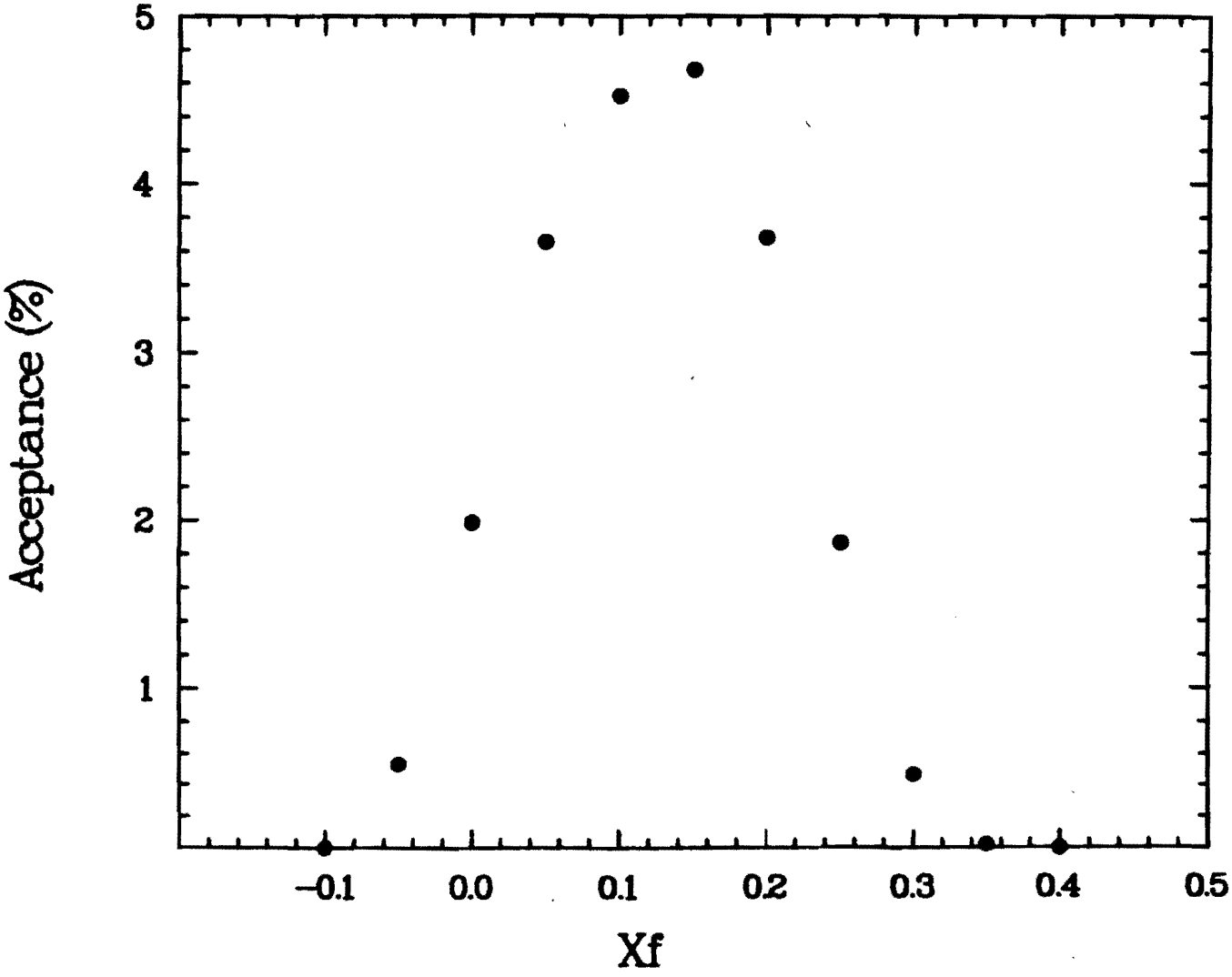

Figure 6(a).

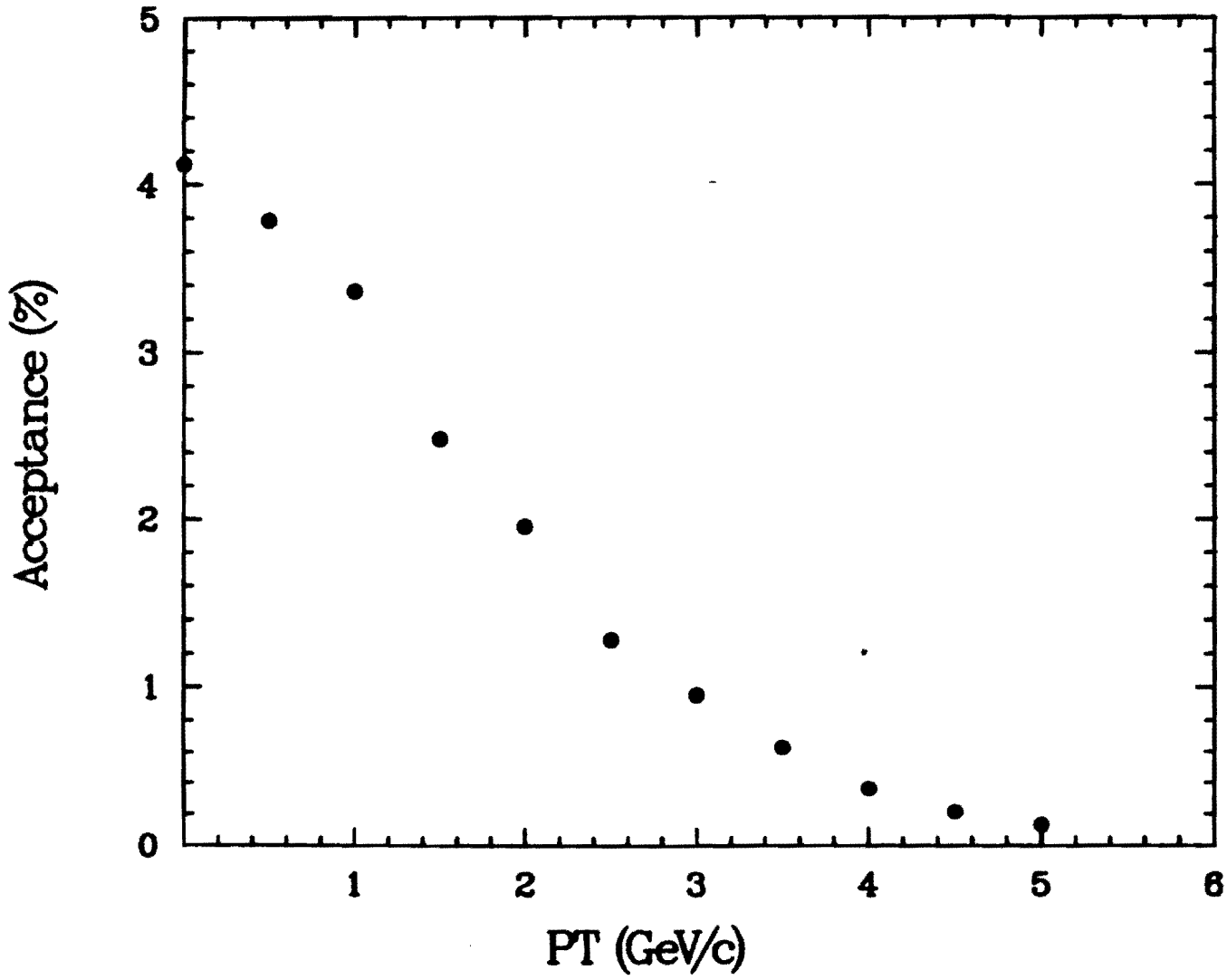

Figure 6(b).

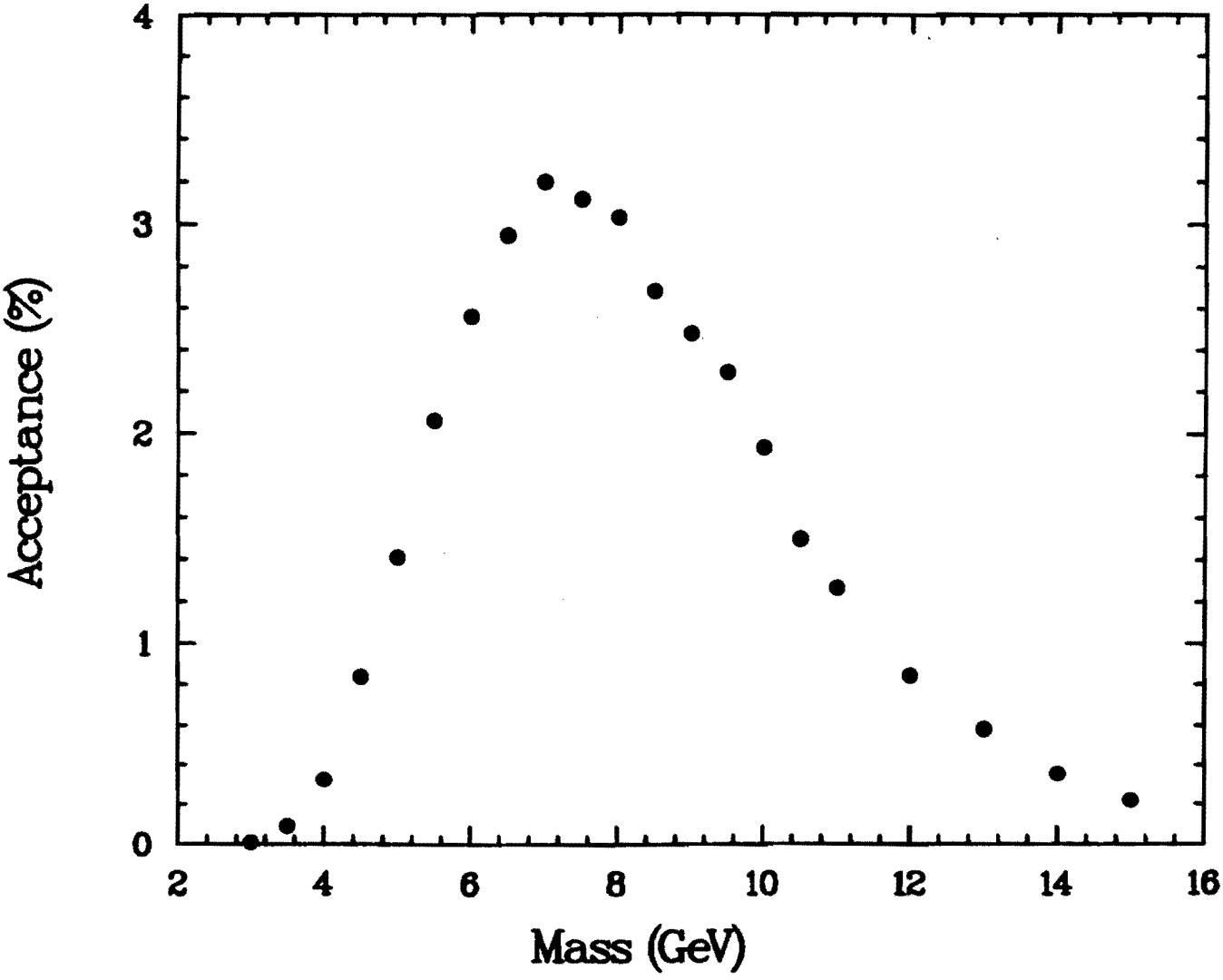

Figure 6(c).

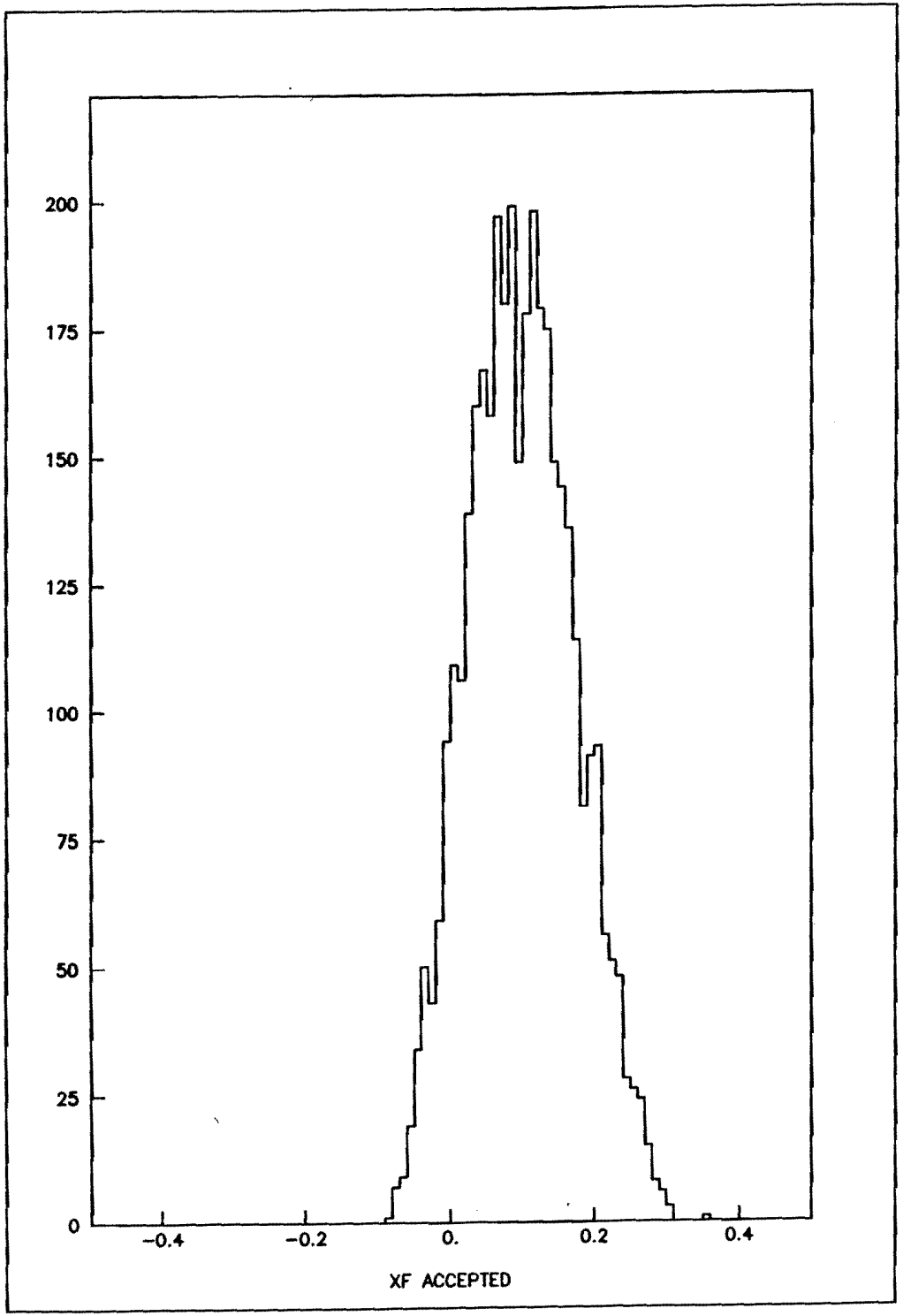

Figure 7(a).

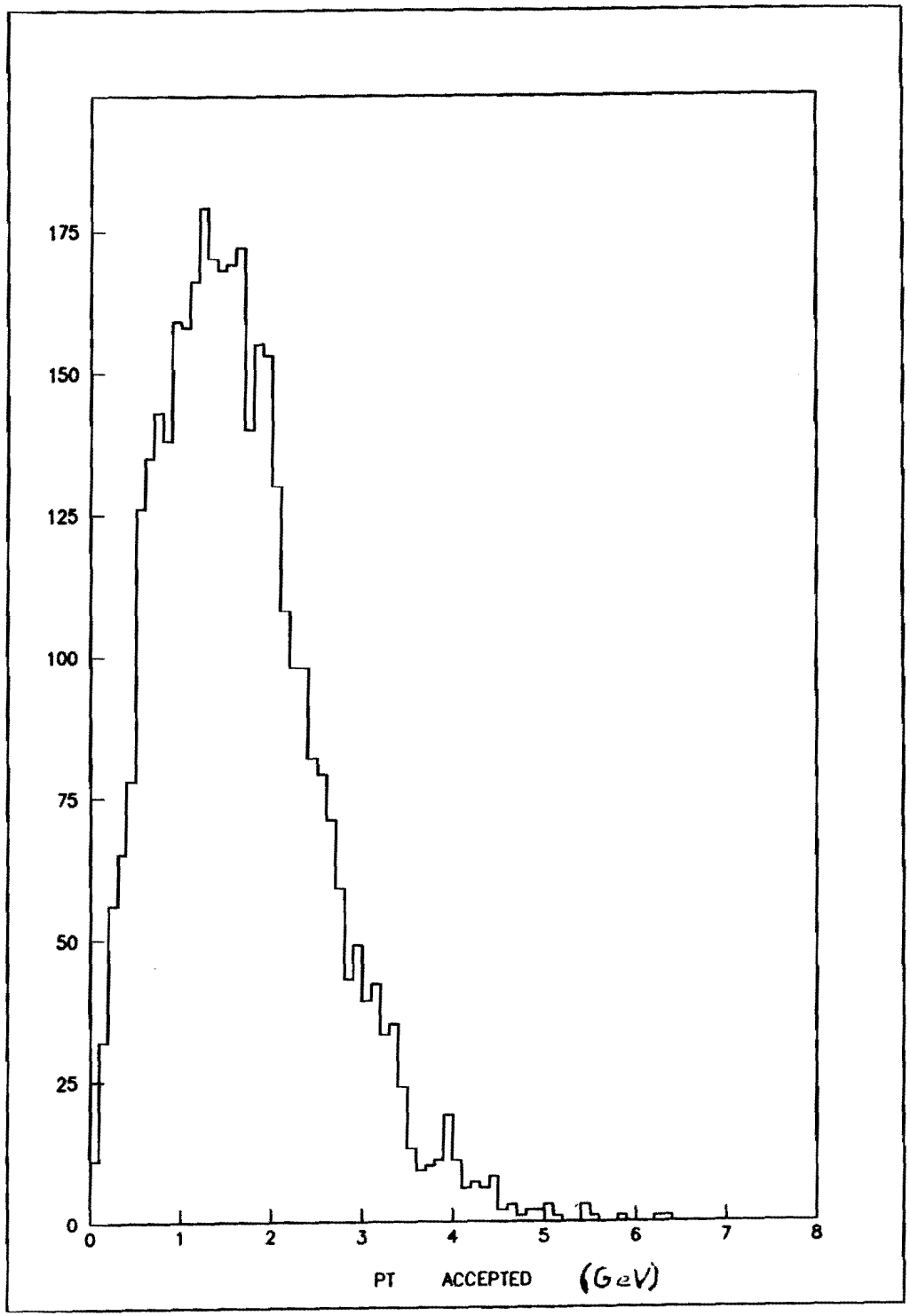

Figure 7(b).

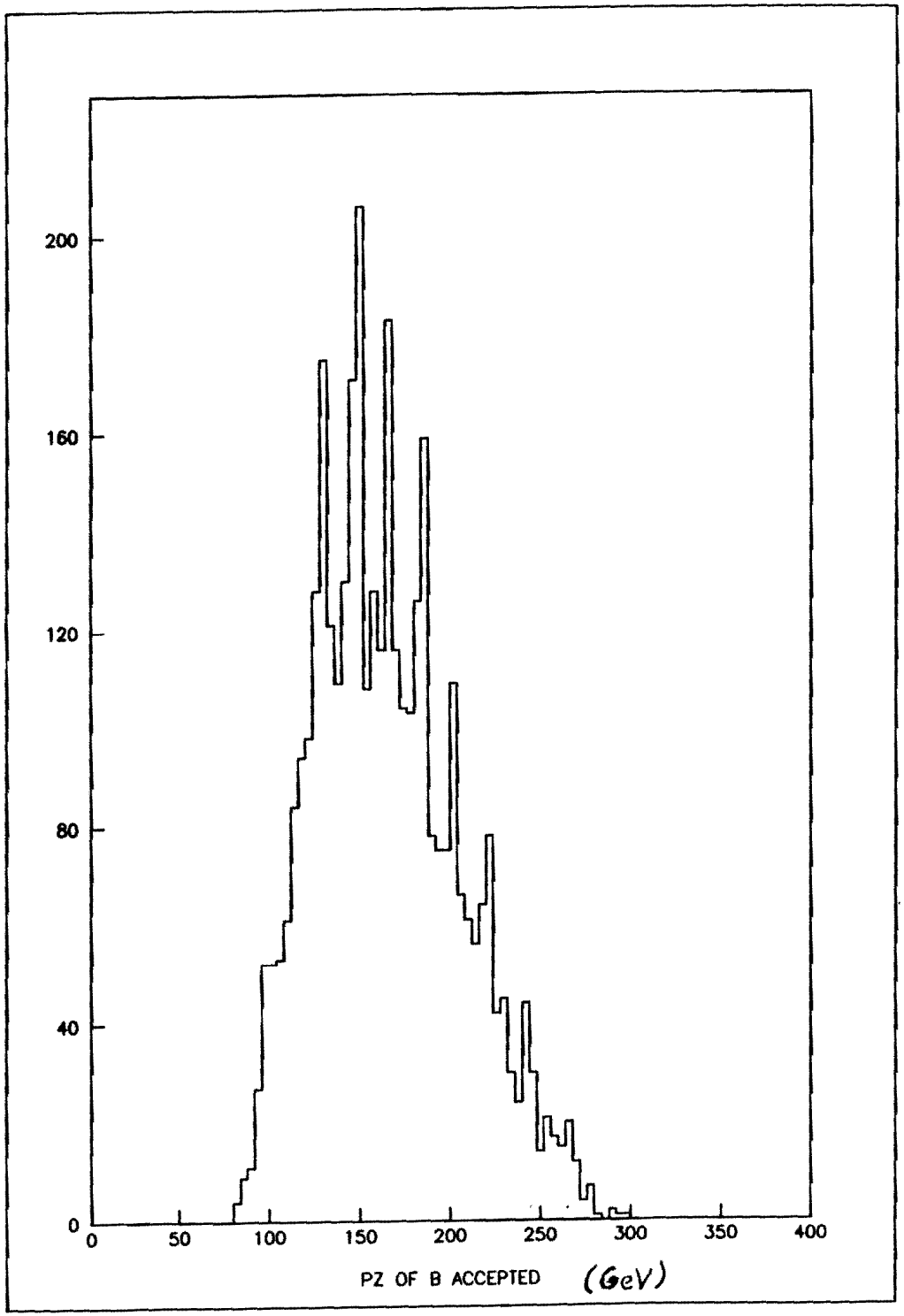
200
160
120
80
40
0
0
50
100
150
200
250
300
350
400
PZ OF B ACCEPTED (GeV)

Figure 8(a).

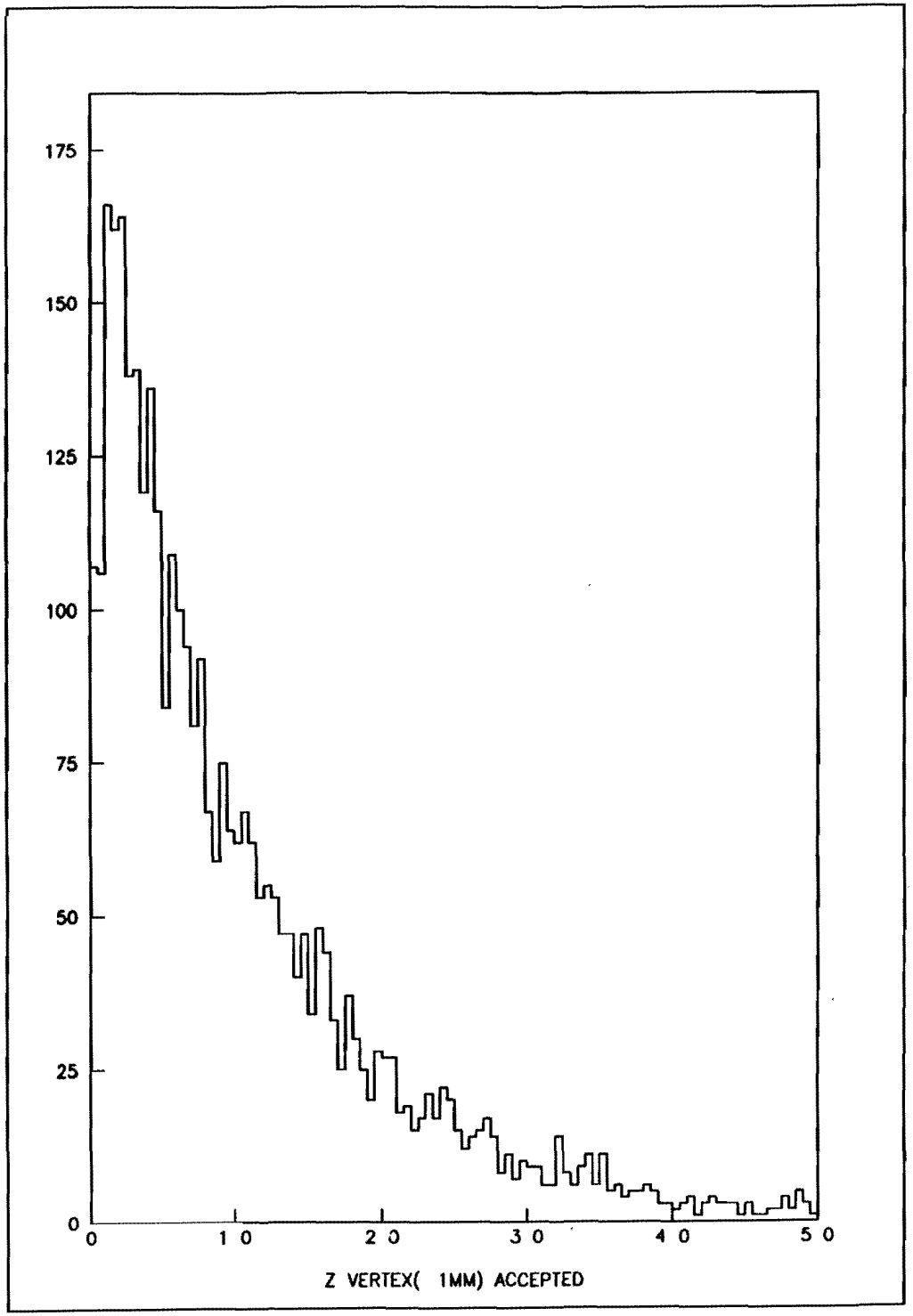

Figure 8(b).

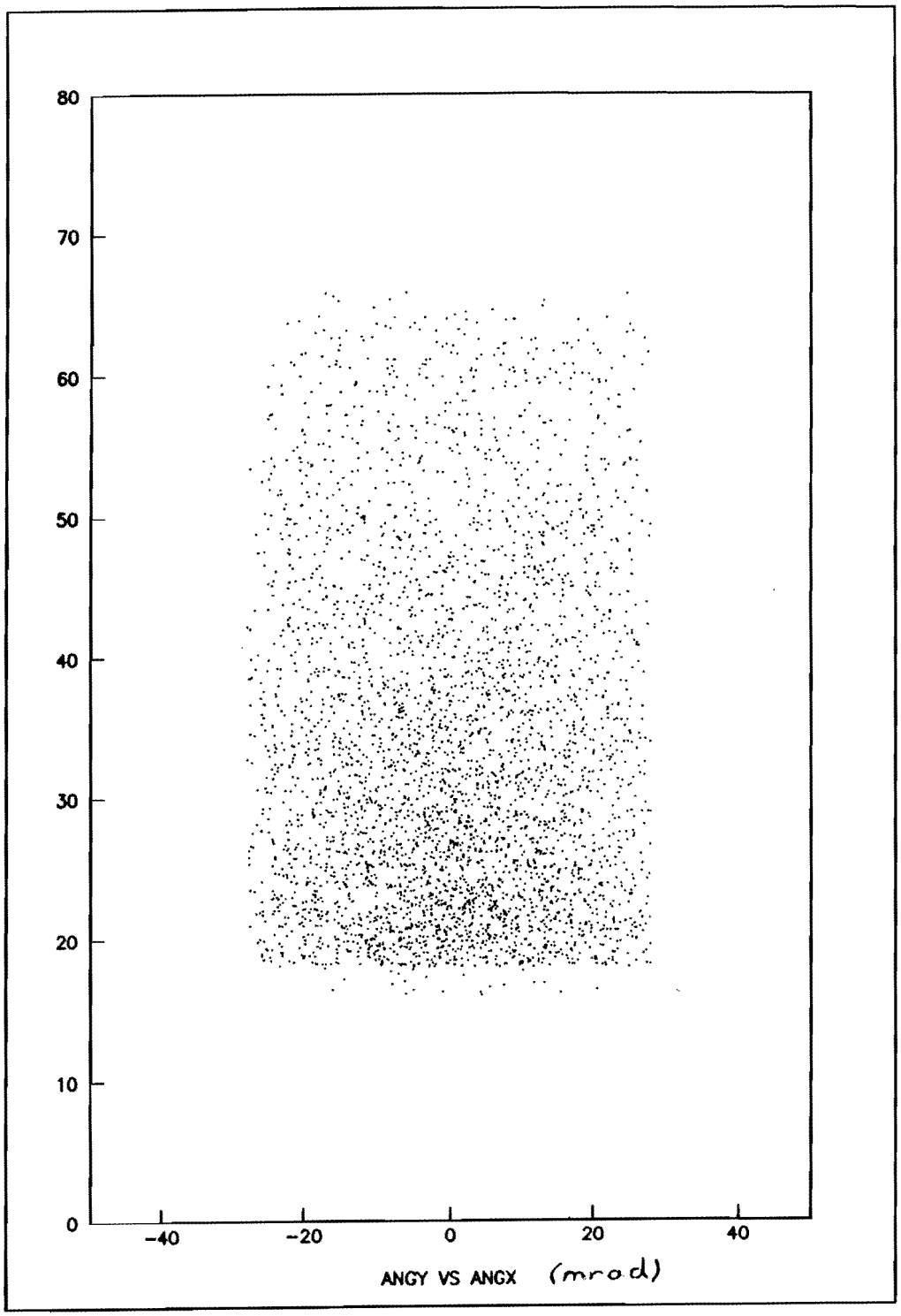

Figure 9.

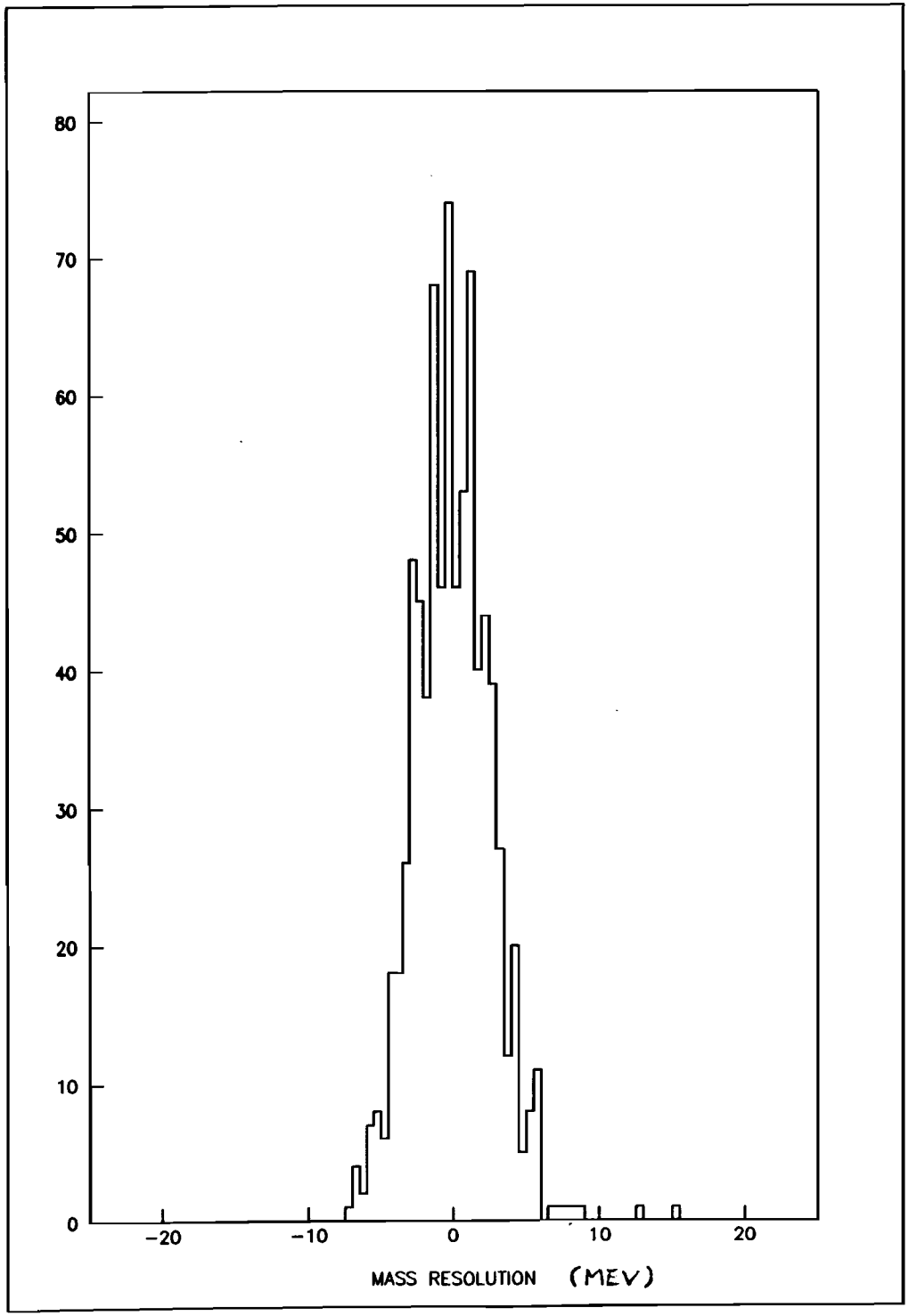

Figure 10.

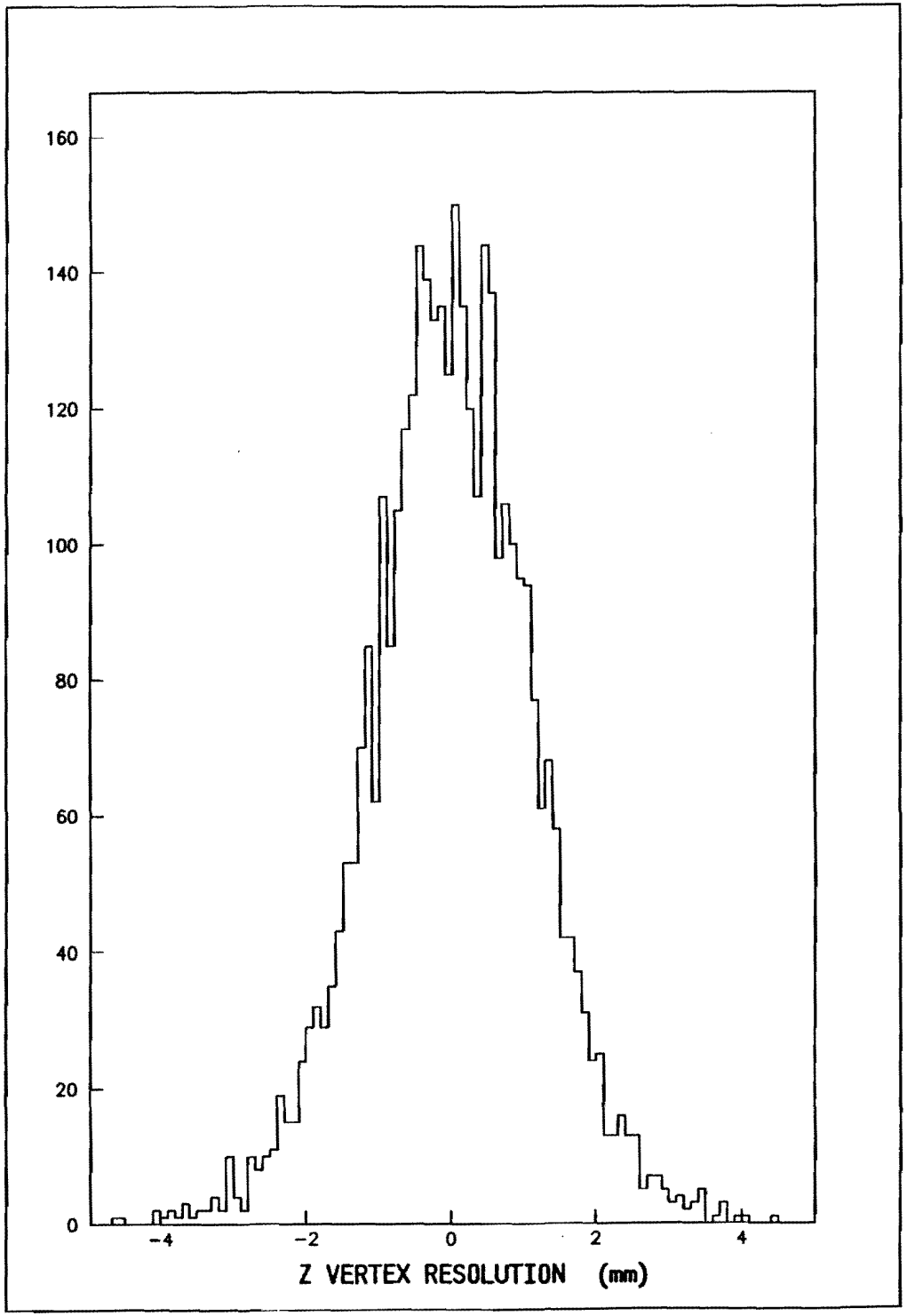

Figure 11(a).

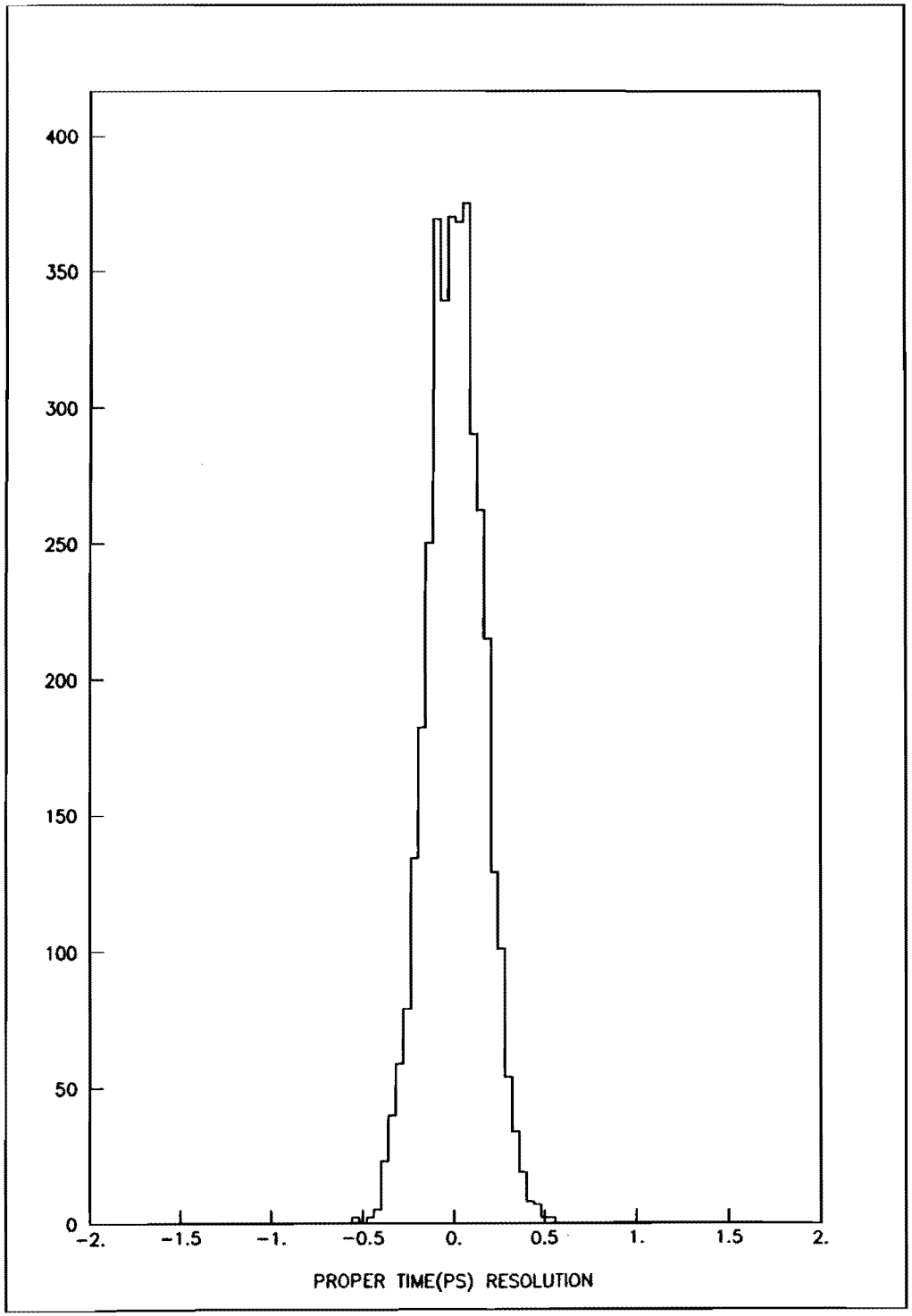
400
350
300
250
200
150
100
50
0
-2.
-1.5
-1.
-0.5
0.
0.5
1.
1.5
2.
PROPER TIME(PS) RESOLUTION

Figure 11(b).

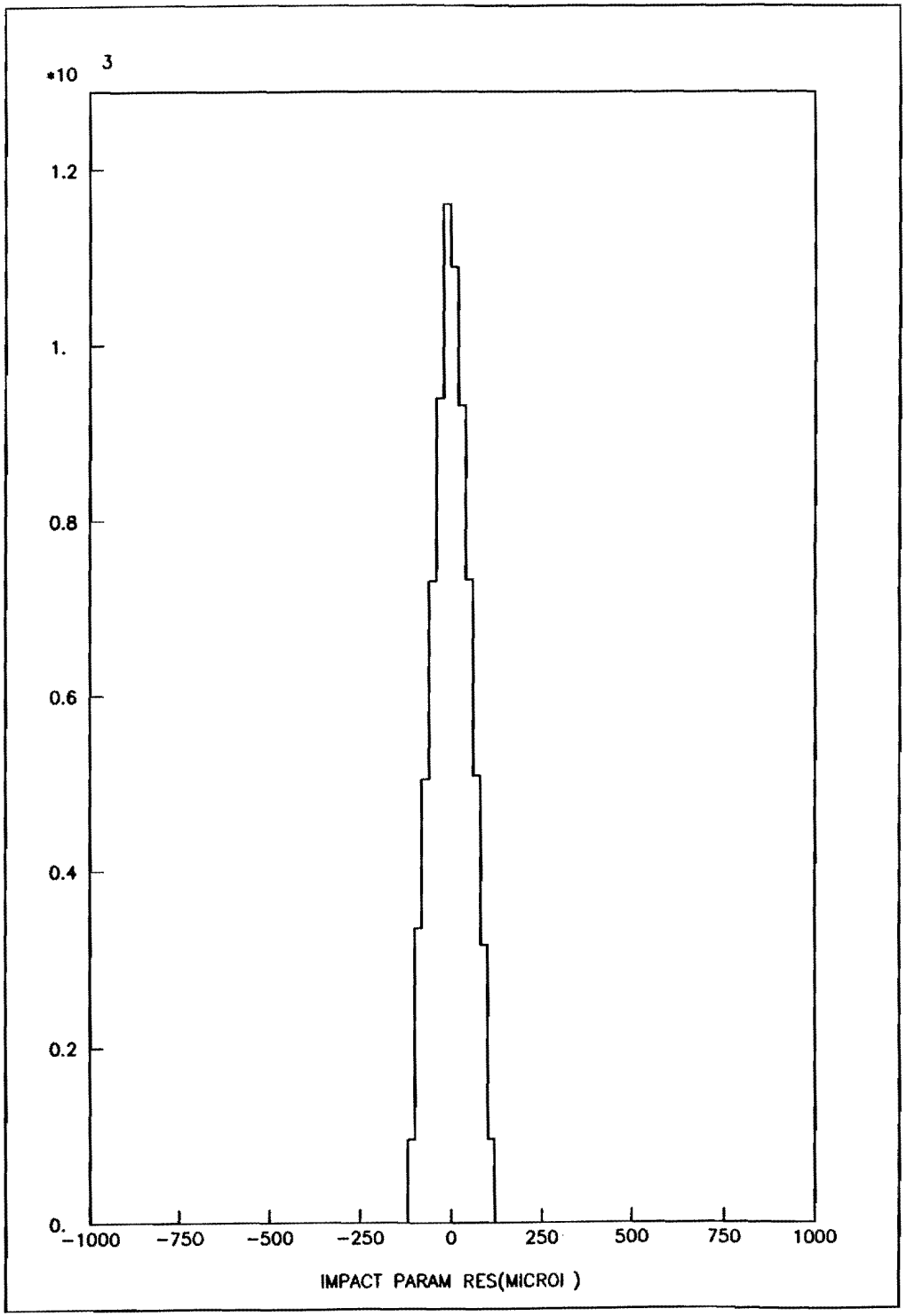
*10 3
1.2
1.
0.8
0.6
0.4
0.2
0.
-1000
-750
-500
-250
0
250
500
750
1000
IMPACT PARAM RES(MICROI)

Figure 11(c).

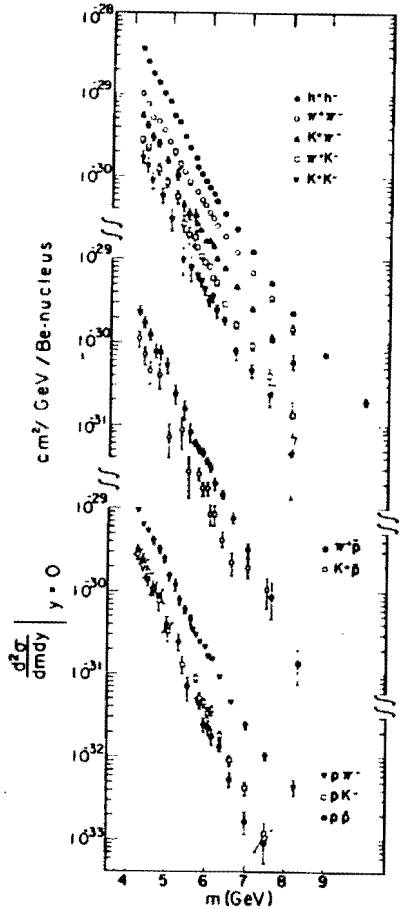

FIG. 2. The dihadron production cross sections $[d^2\sigma/dm\,dy]_{y=0}$ for hadrons and identified pairs of opposite charge vs mass m. The data are averaged over our rapidity acceptance which is peaked at $y \approx 0$ and includes the interval $-0.2 \leq y \leq 0.3$.

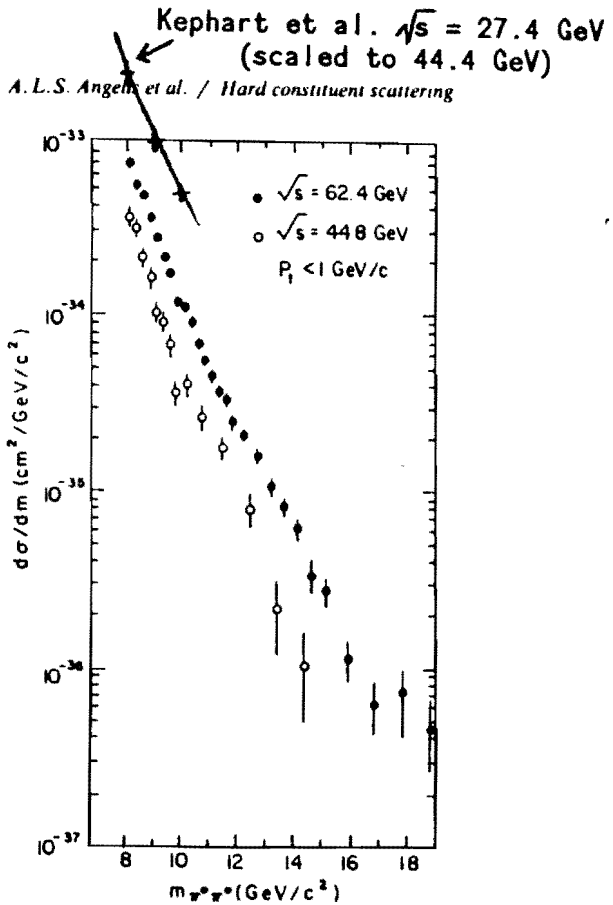

Fig. 5. $d\sigma/dm$ (as defined in eq. (1)) versus m for events with $P_T < 1.0$ GeV/c.

Figure 12.

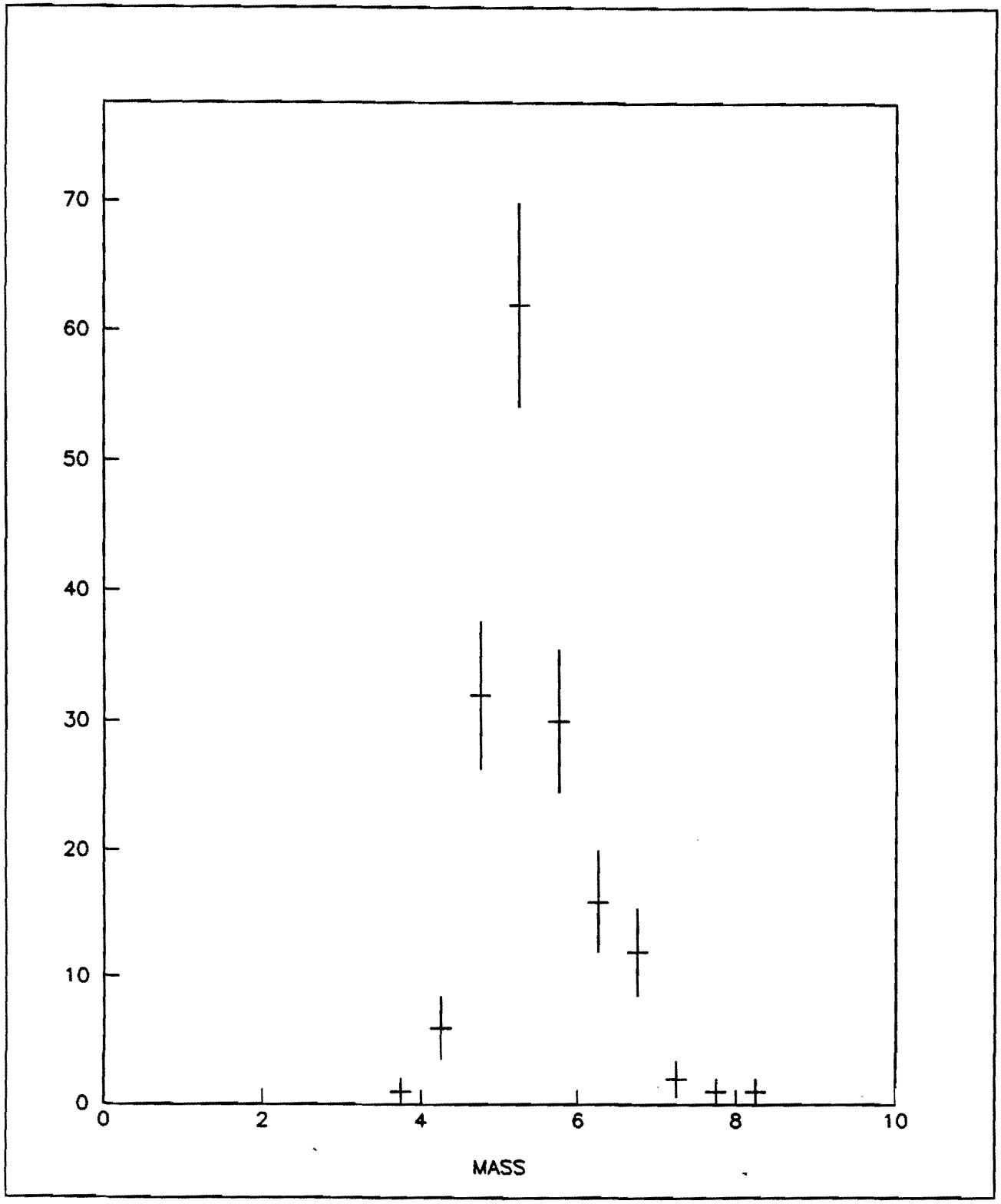

Figure 13.

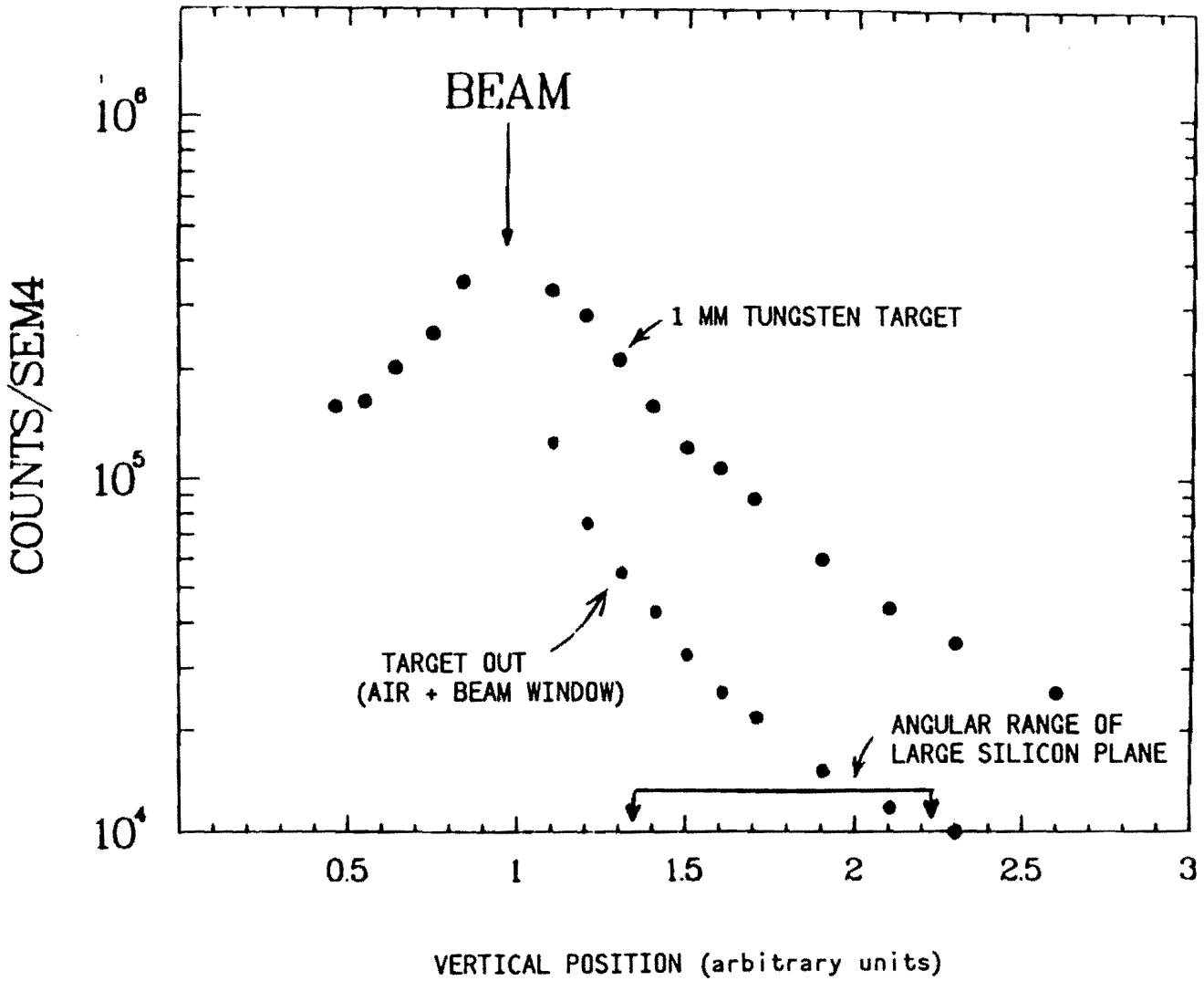
BEAM
1 MM TUNGSTEN TARGET
TARGET OUT
(AIR + BEAM WINDOW)
ANGULAR RANGE OF
LARGE SILICON PLANE
COUNTS/SEM4
10^6
10^5
10^4
0.5
1
1.5
2
2.5
3
VERTICAL POSITION (arbitrary units)

Figure 14.

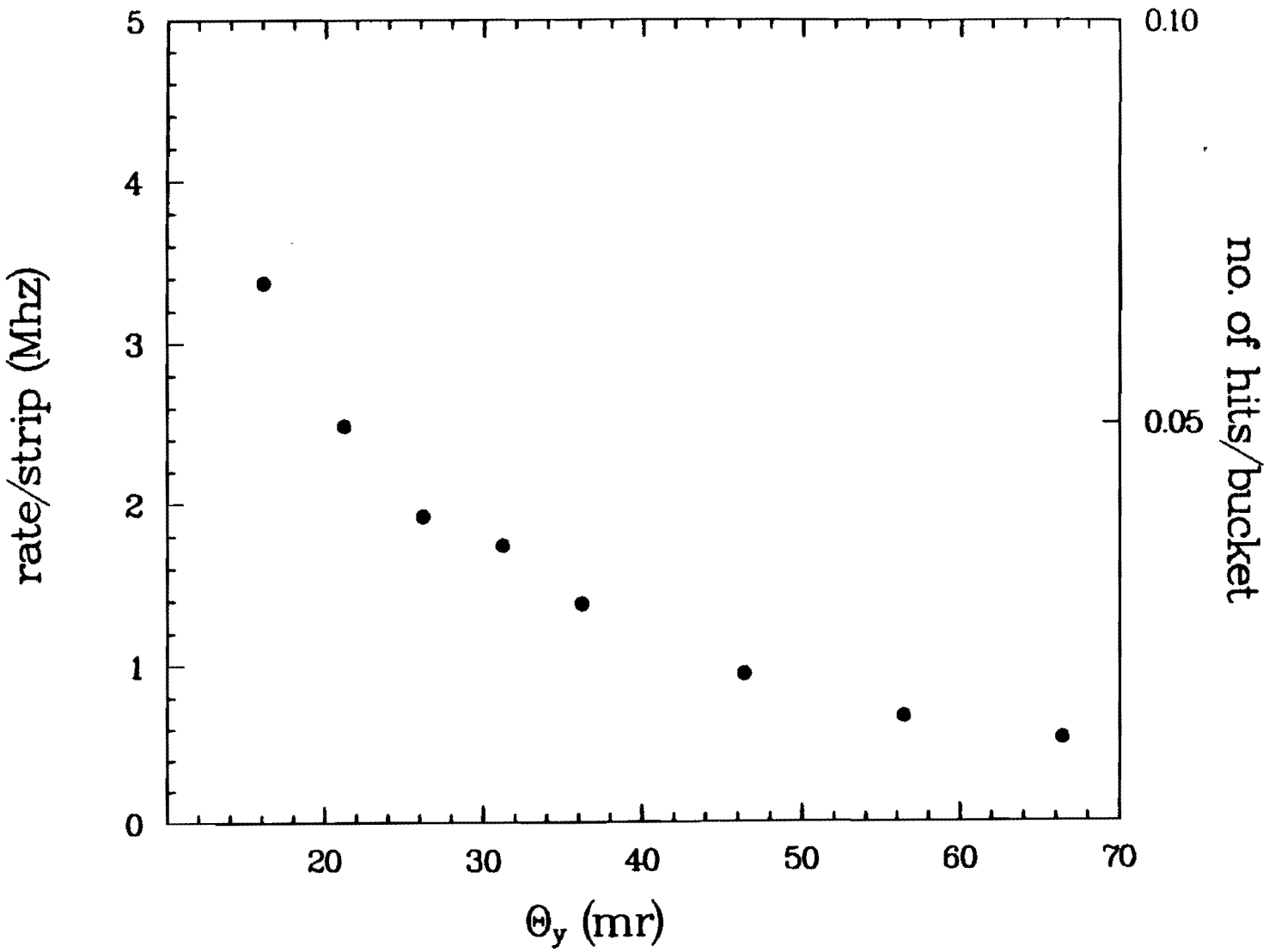
5
4
3
2
1
0
0.10
0.05
rate/strip (Mhz)
no. of hits/bucket
20
30
40
50
60
70
Θ_y (mr)

Figure 15.

APPPENDIX A

Backgrounds to P789 from D Decays

The backgrounds from the decays of a pair of D-mesons to fake a $B \rightarrow \pi^+\pi^-$ decay have been studied in an earlier report.[1] However, only two-body and three-body decays of $D^+ - D^-$ pairs have been considered. We have recently extended the Monte-Carlo codes to include four-body decays as well as decays from $D^\circ - \bar{D}^\circ$, $D^\pm - D^\circ$ pairs. The results of these calculations are presented in this note.

Table I lists the branching ratios for various decay channels of D-mesons we included in the Monte-Carlo code. The three-body and four-body decays have branching ratios several times greater than two-body decays. Furthermore, these branching ratios are weighted by a large combinational factor which accounts for the fact that any of the pions in the decay channels can participate in a "fake-B" pair. Table II lists the "effective branching ratios" for a pair of D mesons to produce a pair of pions in various combinations of decay channels. Table II shows that decay channels involving four bodies have significantly larger "effective branching ratios" than the other channels.

Some details of the Monte-Carlo codes used in the simulation of D-meson decay background were given in Ref. 1. The code used in the present calculations includes the following modification: (1) D mesons can decay to four-body final states with a momentum distribution of the pion given by phase space. (2) The different lifetimes of charged and neutral D mesons are taken into account. (3) The acceptance of the pion-pair in the spectrometer is calculated in a more realistic fashion than in Ref. 1. The results of the calculations are summarized in Table III which lists the probability for a pion-pair emitted in various D-pair decay channels to resemble a real B-meson decay. The criteria for an accepted pion-pair are (1) 5.3 GeV $<$ mass $<$ 5.305 GeV, (2) Z (vertex) $>$ 5 mm, (3) distance of closest approach between the two tracks is less than 100 μm, (4) both pions are accepted by the P789 spectrometer. The efficiency of these various requirements in rejecting the D-meson decay background is shown in Table IV. It is concluded that the mass cut and the spectrometer acceptance cut provide the most powerful rejection of the D-meson decay backgrounds. The extremely small spectrometer acceptance for the pion pair can be understood from Fig. 1 which shows the angular distribution of the pion in the rest frame of the di-pion system. In order to simulate a relatively heavy B-meson (5.3 GeV), the pion pairs in general consist of one pion with large longitudinal momentum and another pion with low longitudinal momentum. In order words, the polar angles of the pions with respect to the di-pion frame is strongly peaked at forward and backward directions. The acceptance of the P789 spectrometer, on the other hand, is centered around 90°. Therefore, the acceptance for the D-meson decay background is extremely small for the P789 experiment.

To find out the relative importance of the D-meson decay background in P789 with respect to the expected B-meson signals, we need to know the cross sections for D-meson pair production. The cross sections have been measured[2] at 400 GeV to be: $\sigma(D^+D^-) = 2.5 \pm 0.6\mu b$, $\sigma(D^+\bar{D}^\circ) = \sigma(D^-D^\circ) = 3.1 \pm 0.55\mu b$ and $\sigma(D^\circ\bar{D}^\circ) = 5.9 \pm 1.3\mu b$. These results imply that charged-D meson cross section is 11.2 μb. The measurements[3] at 800 GeV give $16.5 \pm 3.5\mu b$ as the charged D meson cross sections. We therefore scale the cross

section at 400 GeV by a factor of 16.5/11.2 to obtain the cross sections at 800 GeV for various D-meson pairs. Table V lists all the quantities we take into account to calculate the expected number of counts for the $B \rightarrow \pi^+\pi^-$ decays, the expected background from D-pair decay is between 0.05 and 0.10. We therefore conclude that the D-meson decay fackgrounds to not pose any problem for the experiment 789.

References

1. D. M. Kaplan, J. C. Peng, G. S. Abrams and I. E. Stockdale, Proceedings of the Workshop on Beauty Physics, Fermilab, 1987.
2. M. Aguilar-Benitez *et al.*, Phys. Letts. **189**, 476 (1987).
3. S. Rencroft, 6th International Conference on Physics in Collision, Chicago, 1986.

Table I. Branching ratios of D mesons decaying into two, three, and four body channels.

	D°	D^+
$K^-\pi^+$	5.4%	
$\bar{K}^\circ\pi^+$		4.1%
$K^-\pi^+\pi^\circ$	17.3%	
$\bar{K}^\circ\pi^+\pi^-$	8.5%	
$K^-\pi^+\pi^+$		11.4%
$\bar{K}^\circ\pi^+\pi^\circ$		13.4%
$K^-\pi^+\pi^+\pi^-$	10.9%	
$K^-\pi^+\pi^\circ\pi^\circ$	8%	
$\bar{K}^\circ\pi^+\pi^\circ\pi^-$	10.9%	
$K^-\pi^+\pi^+\pi^\circ$		6.4%
$\bar{K}^\circ\pi^+\pi^+\pi^-$		15.2%
$\bar{K}^\circ\pi^+\pi^\circ\pi^\circ$		15.2%

Table II. Effective branching ratios for D-mesons to produce two pions.

Decay Channels* (n,m)	D^+D^-	$D^\circ\bar{D}^\circ$	$D^\circ D^- + \bar{D}^\circ D^+$
(2,2)	0.17%	0.29%	0.44%
(3,3)	13.1%	7.39%	18.7%
(4,4)	36.4%	21.3%	54.2%
(2,3)	1.49%	1.4%	1.95%
(3,2)	1.49%	1.4%	1.06%
(2,4)	2.4%	2.2%	3.2%
(4,2)	2.4%	2.2%	1.7%
(3,4)	21.2%	12.3%	16.4%
(4,3)	21.2%	12.3%	14.7%

*(n,m) denote the number of particles in the decay channels of the first and second D meson.

Table III. Probability in unit of 10^{-10} for pion pair from D-mesons decay to simulate B-meson decay in P789 experiment.

Decay Channels (n,m)	D^+D^-	$D^\circ\bar{D}^\circ$	$D^\circ D^- + \bar{D}^\circ D^+$
(2,2)	0.0443	0.0139	0.0337
(3,3)	0.0036	0.00074	0.0024
(4,4)	<0.0012	<0.00010	<0.00057
(2,3)	0.022	0.0048	0.0154
(3,2)	0.022	0.0048	0.012
(2,4)	<0.0021	<0.00034	<0.00116
(4,2)	<0.0021	<0.00034	<0.00116
(3,4)	<0.0015	<0.00015	<0.00074
(4,3)	<0.0015	<0.00015	<0.00064

Table IV. Efficiency of various cuts for rejecting pion pairs from D^+D^- decay.

Decay Channels (n,m)	Events thrown	4.9 < M < 5.5 GeV	Mass cut and Z > 5mm	Mass cut and Z > 5mm and $\gamma_{close} < 0.1mm$	Mass cut and accepted by spectrometer
(2,2)	5×10^7	5.8×10^5	3.5×10^4	1.0×10^4	6
(3,3)	5×10^7	4.5×10^5	1.3×10^4	7.8×10^3	1
(4,4)	1×10^8	8.0×10^5	1.1×10^4	9.3×10^3	0
(2,3)	5×10^7	5.1×10^5	2.2×10^4	1.3×10^4	4
(2,4)	1×10^8	9.7×10^5	2.9×10^4	4.9×10^3	0
(3,4)	1×10^8	8.5×10^5	1.7×10^4	6.1×10^3	0

Table V. Expected Number of Events Accepted by Experiment P789.

	$B \to \pi^+\pi^-$	$\pi^+\pi^-$ from D decays
Interaction/pulse	10^{10}	10^{10}
Pulse/run	10^5	10^5
σ production	9 nb	x nb
$A^{0.29}$	4.5	4.5
$1/\sigma_T$	$2.5 \times 10^{-8} nb^{-1}$	$2.5 \times 10^{-8} nb^{-1}$
Effective B.R.	$0.3 \times 5 \times 10^{-5}$	y
Acceptance	$2\% \times 35\%$	$z \times 10^{-10}$
Total Events	100	$\Sigma\, x \times y \times z \times 0.0113$ $(0.10 > counts > 0.05)$

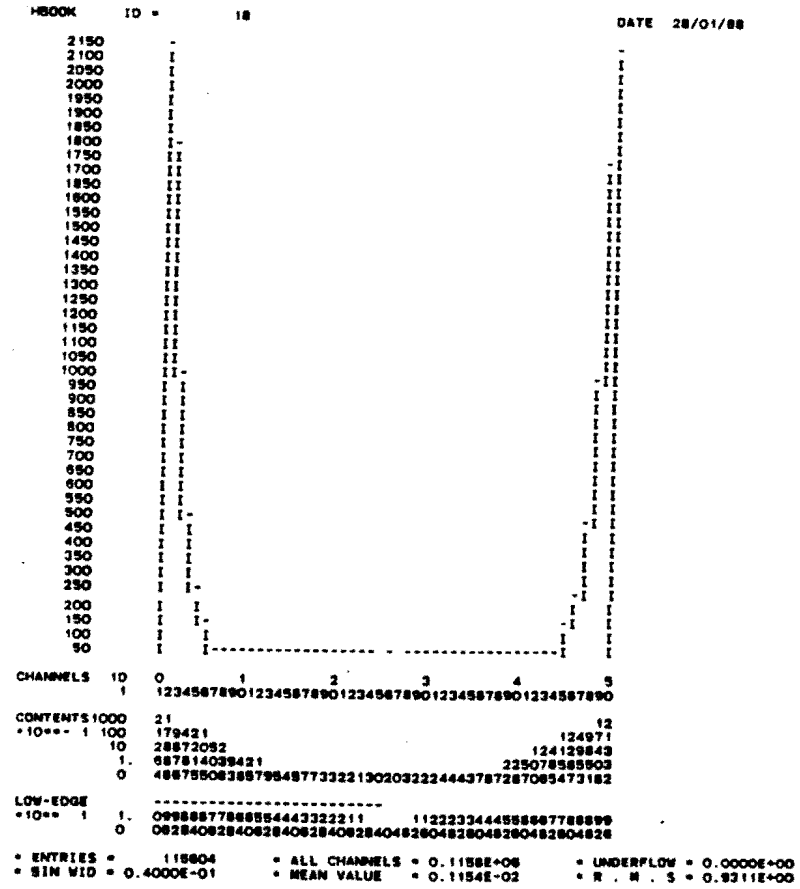

Fig. 1. Histogram for $cos\theta$, where θ is the polar angle of the pion with respect to the di-pion system.

APPENDIX B

Backgrounds to $B^\circ \to \pi^+\pi^-$ from $K^\circ\bar{K}^\circ \to \pi^+\pi^- X$ Decays

We consider here a source of background which contributes to the measurement of $B^\circ \to \pi^+\pi^-$ decays. Specifically, we consider the production of $K^\circ\bar{K}^\circ$ pair followed by the $K_s \to 2\pi$ decays. The K^+K^- pair cross section $d^2\sigma/dmdy$ at y=0 and 800 GeV beam energy can be parametrized as $ce^{-m/0.53GeV}$, where c = 6.0 x 10^{-27}/Gev/nucleon. (This represents the CFS cross section scaled down by a factor of 10 to agree with the CCOR and preliminary E605 data as discussed in the main text.)

In the Monte-Carlo simulation, we assume that the $K^\circ\bar{K}^\circ$ pair is produced with a Gaussian distribution in X_F ($\bar{X}_F$= 0.0, σ= 0.165) and a distribution in P_T as $e^{-P_T^2/7}$(< P_T >= 2.4 GeV). The $K^\circ\bar{K}^\circ$ pair then decays isotropically into $K^\circ, \bar{K}^\circ$, which subsequently decay into $\pi^+\pi^-$ isotropically.

The result of the Monte-Carlo simulation is shown in Table I. The various cuts are the following; Mass: 4.9 GeV< $M(\pi\pi)$ <5.5 GeV, Zcut: $0.5cm < Z < 2cm$, R(closest) cut:$R < 0.1mm$. Fig. 1 shows the $K^\circ\bar{K}^\circ$ mass distribution for the accepted events. A striking feature is the large acceptance of the P789 spectrometer for such background. Fig. 2 shows the angular distribution of the pion with respect to the di-pion frame. Contrary to the situation in the D-meson pair decays, the angular distribution is now nearly isotropic. An additional way to reject the background is to require that the summed momentum of the two pions point back to the target. By requiring $|\Delta y| \leq 2.5mm$, one gains an additional rejection factor of 4. Table II shows the expected yields for the $B \to \pi^+\pi^-$signal and the $K^\circ\bar{K}^\circ \to \pi^+\pi^- X$ background. The signal to background ratio is 25 to 1. We conclude that the $K^\circ\bar{K}^\circ$ background is more important than that from the D-meson pair decays, but still much smaller than the expected signal.

Table I. Efficiency of various cuts for rejecting pion pairs from $K^\circ\bar{K}^\circ$ decay.

Events thrown	4.9 < M < 5.5 GeV	Mass cut and Z > 5mm	Mass cut and Z > 5mm and $\gamma_{close} < 0.1mm$	Mass cut and accepted by spectrometer
1×10^6	9945	1107	22	442

Table II. Expected Number of Events Accepted by Experiment P789.

	$B \to \pi^+\pi^-$	$\pi^+\pi^-$ from $K^\circ\bar{K}^\circ$ decays
Interaction/pulse	10^{10}	10^{10}
Pulse/run	10^5	10^5
σ production	9 nb	260 nb
$A^{0.29}$	4.5	4.5
$1/\sigma_T$	$2.5 \times 10^{-8} nb^{-1}$	$2.5 \times 10^{-8} nb^{-1}$
Effective B.R.	$0.3 \times 5 \times 10^{-5}$	0.235
Acceptance	$2\% \times 35\%$	0.51×10^{-9}
Total Events	100	4

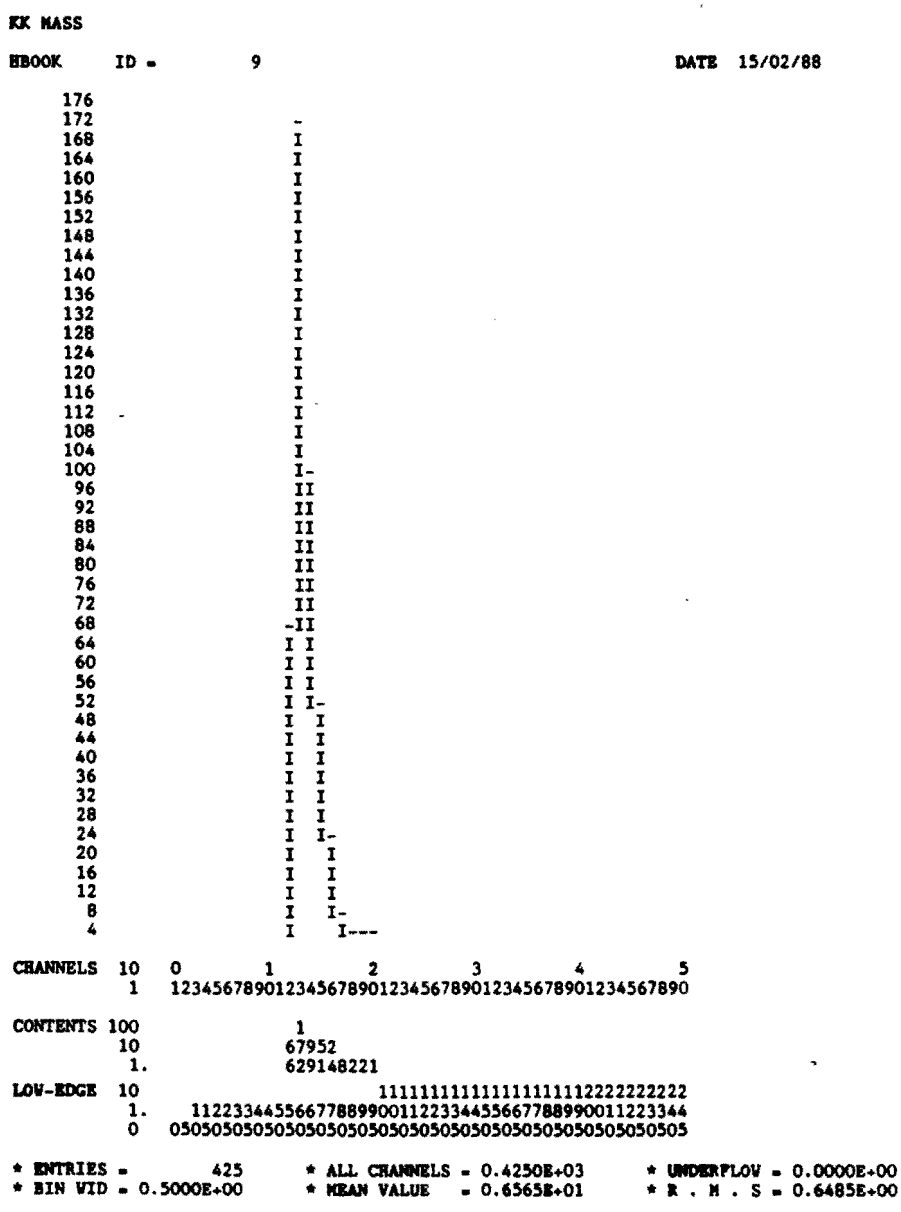

Fig. 1. Histogram for $K^\circ\bar{K}\circ$ pair mass in GeV

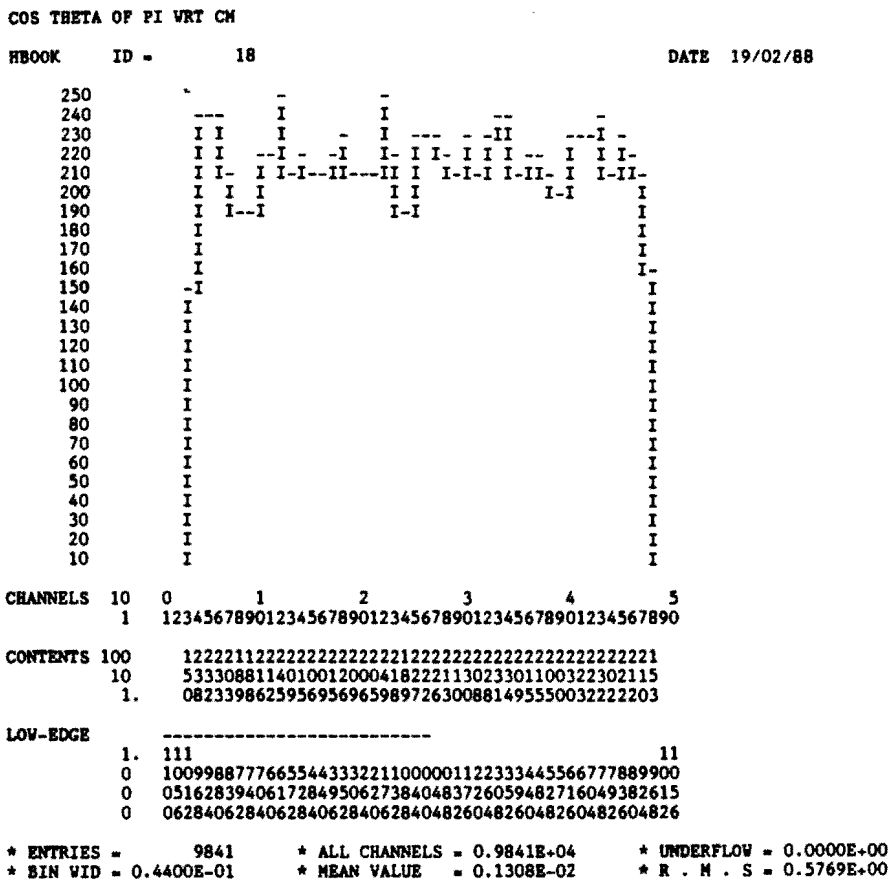

Fig. 2. Histogram for $cos\theta$, where θ is the polar angle of the pion with respect to the di-pion system.

REVISED FERMILAB PROPOSAL P-789

STUDY OF TWO-PRONG DECAYS OF NEUTRAL B MESONS AND Λ_b

Spokesmen: D. M. Kaplan and J. C. Peng

Participants: D. M. Alde, T. A. Carey, J. S. Kapustinsky, M. J. Leitch, J. W. Lillberg, P. L. McGaughey, C. S. Mishra, J. M. Moss, J. C. Peng,
Los Alamos National Laboratory

C. N. Brown, W. E. Cooper, Y. B. Hsiung, K. B. Luk,
Fermilab

D. M. Kaplan, R. S. Preston,
Northern Illinois University

F. T. Avignone, R. Childers, C. W. Darden,
University of South Carolina

M. L. Barlett,
University of Texas

September, 1988

EPITOME

We propose using an upgraded version of the E605/E772 spectrometer to measure two-body, two-prong decays of neutral b-quark hadrons.

The MEast beam, at an intensity of 3×10^{11} protons/spill, will be targeted on a 3 mm long $\times$ 0.2 mm high tungsten target. In a fixed-target run of 10^5 good spills, this will result in a luminosity of $1 \times 10^{41}\,\mathrm{cm}^{-2}$ and a yield of 10^9 $b\bar{b}$ pairs. This yield is based on the assumption of a 10 nb cross section for $b\bar{b}$ pair production and no heavy-target nuclear suppression of the cross section.

The E605/E772 spectrometer will be reconfigured to give a (model-dependent) acceptance of $\sim 2\%$ for $B(\bar{B}) \to h^+h^-$ decays. Assuming a hadronization probability of 0.3 to a particular B state having a branching ratio of 1×10^{-5}, 120 decays will be recorded in each such channel. An array of silicon microstrip detectors will be used to pinpoint the vertices of these two-body decays to ± 1 mm in z. The average decay distance for the B decays accepted by the downstream spectrometer is 1.0 cm for a 1.1×10^{-12} sec lifetime.

Extensive Monte Carlo simulations have indicated that a vertex cut 0.7 cm downstream of the target will retain 40 of the 120 decays and provide a suppression factor of $\geq 10^4$ against the copious dihadron pairs produced in the target. This suppression, combined with the excellent predicted mass resolution of 3 MeV at 5.3 GeV, will yield a flat background of less than 22 events per 3 MeV bin at 5.3 GeV in the worst-case channel ($\pi^+\pi^-$). The background in other channels is up to an order of magnitude smaller.

Simultaneously with the proposed search for $B_d, B_s, \Lambda_b \to (\pi^+\pi^-, K^+K^-, p\bar{p}, \pi^\pm K^\mp, p\pi^-, \bar{p}\pi^+, pK^-, \bar{p}K^+)$, we will be sensitive to other b-quark decays. Sensitivity will exist for $B_d, B_s \to \mu\mu, \mu e, ee$; $B \to J/\psi, \psi', \chi_0$; and $\eta_b, \Upsilon, \chi_b \to h^+h^-$. Information will be obtained on the mass, lifetime, and production dynamics of any state detected.

Tests of this proposed configuration of the spectrometer, performed after the completion of data acquisition for E772, yielded many of the numbers needed to predict the sensitivity of P789. With the exception of the silicon vertex array, only modest upgrades of the E605/E772 spectrometer and data acquisition systems are required.

TABLE OF CONTENTS

I. PHYSICS MOTIVATIONS

1. General

This proposal is motivated by two recent discoveries. First is the observation of large mixing in the $B^0\bar{B}^0$ meson system.[1,2] This suggests the possibility that CP-violation could be observed in a high-statistics study of B^0 meson decays. Second is the observation that the amplitude for $b \to u$ conversion might be large.[3] An analysis[4] of the charmless decays $B^+ \to \bar{p}p\pi^+$ and $B^0 \to \bar{p}p\pi^-\pi^+$ observed by the ARGUS Group yields $|V_{ub}/V_{cb}| \geq 0.07$. This suggests that the branching ratios for $B^0_{d,s} \to h^+h^-$ charmless decays could be of order 10^{-4} to 10^{-5}. The observation of charmless h^+h^- decays would contribute to the determination of V_{ub}. Such two-prong decays have not yet been observed.

At present there is conflict between ARGUS and recent results from CESR. With their larger data set, the CLEO Group[5] finds no evidence for the charmless decays seen by ARGUS. Additional channels have been examined by CLEO based on their 1987 high-statistics run. Their current upper limits[6] are summarized in Table II.1 below.

Even though the existing data on B meson production and decay originate almost exclusively from e^+e^- collider experiments, the luminosity at existing colliders severely limits the B production rate. Bjorken has suggested,[7] as an alternative, the detection of B decays in fixed-target experiments at FNAL, where the production rate of b-quark hadrons is orders of magnitude greater than that at current e^+e^- colliders. The crucial questions to be answered are: How many B's can be produced and detected, and to what extent can non-b-quark events be rejected from the data set? As the following sections demonstrate, significant information on charmless decays can be obtained at levels well below the ARGUS results. P789 will be sensitive to two-body decays with branching ratios in the 10^{-5} to 10^{-6} range.

2. Two-body Hadronic Decays

We propose that the existing E605/E772 spectrometer, characterized by its superb mass resolution and high-rate capability, is uniquely suitable for detecting the hadron pairs $(\pi^+\pi^-, K^+K^-, p\bar{p}, \pi^\pm K^\mp, p\pi^-, \bar{p}\pi^+, pK^-, \bar{p}K^+)$ emitted in the decay of neutral B mesons (B_d, B_s) and b-baryons $(\Lambda_b, \bar{\Lambda}_b)$. The key to these measurements is the addition of a vertex detector array to our spectrometer. Results from a test run in February '88 plus detailed Monte Carlo simulations of B decay events and various backgrounds show that we will be able to determine the mass and lifetime of any b-decay having a branching ratio $\geq 10^{-5}$.

3. Inclusive B Decays to Lepton Pairs

The E605/E772 spectrometer in closed aperture mode is noted for its high resolution $\mu^+\mu^-$ studies of the Υ region (Fig. 1a). More recently, during E772, we have obtained impressive results for the J/ψ and ψ' (Fig. 1b). During P789, the magnetic field configuration and hence acceptance will be further optimized to include $B \to J/\psi(\psi')X \to \ell^+\ell^- X$ decays. Predicted yields for $B \to J/\psi$ and ψ' are listed in Section IV.2.

Semileptonic decays of $B_u^{\pm}, B_d^0, \bar{B}_d^0$ and $B_s^0, \bar{B}_s^0$ yield a continuum of lepton pairs which may be separated from the Drell-Yan process via an impact parameter cut. Mixing of these states can be studied by measuring like-sign lepton pairs similarly to what has been done by the ARGUS collaboration.[2] Estimates of the continuum lepton-pair yields are given in Section IV.4.

4. Production Asymmetry, $B-\bar{B}$ Mixing, and CP Violation

It is interesting to examine the ramifications of observing an asymmetry, $A \equiv (B - \bar{B})/(B + \bar{B})$, in B and $\bar{B}$ yields. It is straightforward to derive[8]

$$\Gamma(B_{d,s}^{neutral} \to K^-\pi^+) \quad \propto \quad e^{-\Gamma_{d,s}t}\left[\frac{1}{2}(1 + e^{-\Delta\Gamma_{d,s}t}) - A\cos\Delta m_{d,s}t\right] \qquad (1).$$

Equation (1) shows that even without flavor tagging, it is possible to observe an oscillatory component in the time evolution of this decay. Such an observation could lead to the determination of Δm and A. Unfortunately, it is difficult to predict the best kinematic region for a large production asymmetry.

The asymmetry in $B^0(\bar{B}^0) \to K^{\mp}\pi^{\pm}$ decays is sensitive to CP-violation. Bigi and Stech[8] show

$$\frac{\text{Yield}(K^-\pi^+)_B}{\text{Yield}(K^+\pi^-)_B} = \frac{1 + A\,f(t)}{1 - A\,f(t)} \cdot \frac{|\text{Ampl}(\bar{B}^0 \to K^-\pi^+)|^2}{|\text{Ampl}(B^0 \to K^+\pi^-)|^2} \qquad (2)$$

where $f(t) = 2\,e^{-1/2\Delta\Gamma t}/(1 + e^{-\Delta\Gamma t})\cos\Delta mt$. CP-violation is established if the second factor in Eq. (2) is different from unity. For $B_d(\bar{B}_d) \to K^{\mp}\pi^{\pm}$ decays the CP-asymmetry in Eq. (2) might be as large as 20%.[8] Again, Eq. (2) assumes no tagging.

Although P789 is not sensitive to CP-violation, determination of $B \to h^+h^-$ branching ratios is nevertheless important for identifying promising avenues for future studies of CP-violation in b-systems.

II. PROPOSED MEASUREMENTS

The goals of this experiment are to :

- Determine the values (or upper limits) of the branching ratios for a variety of b-particle dihadronic decays.
- Search for B_s and Λ_b.
- Measure the lifetimes and masses of B_d, B_s, and Λ_b.
- Measure the $B \to J/\psi X, \chi_0 X,$ and$\psi' X$ inclusive decays.
- Search for exclusive dilepton decays $B \to \mu^+\mu^-$, e^+e^-, $\mu^\pm e^\mp$.
- Study inclusive dilepton decays of $B-\bar{B}$ pairs.
- Search for the η_b and for dihadron decays of Υ and χ_b states.

1. b-particle Dihadron Decays

The main goal of the proposed experiment is to determine values (or upper limits) for the branching ratios of:

(a) $B_d(\bar{B}_d) \to \pi^+\pi^-, K^+K^-, p\bar{p}, \pi^\pm K^\mp$;
(b) $B_s(\bar{B}_s) \to \pi^+\pi^-, K^+K^-, p\bar{p}, \pi^\pm K^\mp$;
(c) $\Lambda_b \to p\pi^-, pK^-$;
(d) $\bar{\Lambda}_b \to \bar{p}\pi^+, \bar{p}K^+$.

Table II.1 summarizes our current knowledge concerning these decays.

These branching ratios provide important constraints for determining the K-M matrix element V_{ub}. Using the spectator model for B decays, Bigi and Stech obtain the (model-dependent) result[8]

$$\mathrm{BR}(B_d \to \pi^+\pi^-) \simeq \mathrm{BR}(B_s \to K^-\pi^+) \simeq 2 \times 10^{-3}|V_{ub}/V_{cb}|^2.$$

The uncertainty for deducing V_{ub} from these decays is expected to be smaller than from the $B \to p\bar{p}\pi^+\pi^-$ decays (which involve the extra complication of baryon-pair production). These branching ratios are intimately connected to the dynamics underlying heavy-flavor decay. E.g., the large spread in the theoretical predictions for the $B_d \to K^+\pi^-$ and $B_s \to K^+K^-$ branching ratios shown in Table II.1 can be attributed to the uncertainties of penguin diagram contributions.[8,9]

Determination of the branching ratios of $B \to h^+h^-$ decays will be an important first step in choosing the most suitable channels for pursuing CP-violation. As shown in Table II.1, the Standard model predicts that asymmetries of $B^0 \to h^+h^-$ versus $\bar{B}^0 \to h^+h^-$ could be as large as $\sim$0.2.

TABLE II.1. Theoretical and Experimental Status of $B^0, \Lambda_b \to h^+h^-$ Decays

Decay Mode	BR (Expt.)	BR (Theory)	CP-asym(Theory)
$B_d \to \pi^+\pi^-$	$< 0.9 \times 10^{-4}$ [a]	0.8×10^{-4} [b]	$0.1 - 0.3$ [c]
$B_d \to K^+\pi^-$	$< 0.9 \times 10^{-4}$ [a]	0.64×10^{-5} [b] 1×10^{-4} [c] 0.7×10^{-4} [d]	0.2 [c]
$B_d \to K^+K^-$		small [b]	
$B_d \to p\bar{p}$	$< 1.3 \times 10^{-4}$ [e] $< 0.4 \times 10^{-4}$ [a]	$\sim 0.4 \times 10^{-5}$ [b]	
$B_s \to \pi^+\pi^-$		small [b]	
$B_s \to K^-\pi^+$		0.8×10^{-4} [b] 1×10^{-4} [c]	2×10^{-2} [c]
$B_s \to K^+K^-$		0.64×10^{-5} [b] 1×10^{-4} [c]	$0.2 - 0.4$ [c]
$B_s \to p\bar{p}$		small [b]	
$\Lambda_b \to p\pi^-$		1.2×10^{-4} [b]	
$\Lambda_b \to pK^-$		0.92×10^{-5} [b]	

[a] Ref. 6; [b] Ref. 8,with $|V_{ub}/V_{cb}| = 0.2$; [c] Ref. 9; [d] Ref. 10; [e] Ref. 3

2. Searches for B_s and Λ_b

This experiment could lead to the first observation of these particles. Table II.1 indicates that $B_s \to K^-\pi^+$ and $\Lambda_b \to p\pi^-$ are expected to have favorable branching ratios and should be the most suitable decay channels for these searches.

3. Measurement of the B_d, B_s and Λ_b Lifetimes and Masses

Except for a single event observed in an emulsion experiment at CERN,[11] all existing data[12] on b-particle lifetimes comes from e^+e^- storage rings (see Table II.2). Notably, none of these experiments distinguishes between different beauty mesons or baryons, because no exclusive b-particle decays have been reconstructed in these experiments.

TABLE II.2. Experimental Status of b-particle Lifetimes[12]

	MARK II	MAC	DELCO	HRS	JADE	TASSO
lifetime (psec)	0.98	1.24	1.17	1.02	1.46	1.39
Statistical Error	±0.12	±0.20	+0.27 -0.22	+0.42 -0.39	±0.19	±0.10
Systematic Error	±0.13	±0.17	+0.17 -0.16	±0.30	±0.25	

The only lifetime data for individual B mesons comes from the CLEO collaboration.[13] They deduce $0.4 < \tau(B^0)/\tau(B^+) < 2.0$ from the number of dileptons observed in $\Upsilon(4S)$ decay. Using the measured semi-leptonic branching ratio of B mesons and the average B lifetime, one obtains[12]

$$0.5|V_{cb}|^2 + |V_{ub}|^2 = (1.13 \pm 0.14\,(stat) \pm 0.30\,(sys)) \times 10^{-3}.$$

Both the statistical and theoretical uncertainties can be reduced through accurate measurement of individual b-particle lifetimes.

In the simple spectator model of heavy-quark decay, the lifetimes of all b-particles are equal, but this model fails to account for the observed spread in charm-particle lifetimes. Soni has predicted $0.56 < \tau(B^0)/\tau(B^+) < 0.71$ after considering nonspectator diagrams.[14] Tests of theoretical models for B-decay dynamics clearly require better measurements of individual b-particle lifetimes.

Because P789 will accurately determine the decay vertices of *exclusive* $B, \Lambda_b \to h^+h^-$ decays, knowledge of beauty-particle lifetimes will be considerably enhanced. The most promising channels are $B_d \to \pi^+\pi^-$, $B_s \to \pi^+K^-$ and $\Lambda_b \to p\pi^-$. Here we expect $\delta z_{\rm vertex} = 0.84\,{\rm mm}$ and $\delta\tau = 0.13\,{\rm psec}$. Also, since B_s is expected to be $\simeq$ 120 MeV heavier and $\Lambda_b \simeq 300$ Mev heavier than B_d,[15] our mass resolution of $\delta m \simeq 3\,{\rm MeV}$ near $m \simeq 5\,{\rm GeV}$ will provide accurate measurements of $[m(B_s) - m(B_d)]$ and $[m(\Lambda_b) - m(B_d)]$.

4. Measurement of $B \to J/\psi X$, $B \to \psi' X$, $B \to \chi_0 X$ Inclusive Decays

Measurements at e^+e^- experiments[16] yield branching ratios for these inclusive decays of $(1.2 \pm 0.3)\%$ for $B \to J/\psi X$ and $(0.46 \pm 0.3)\%$ for $B \to \psi' X$. Lifetime information was not extracted because the B mesons were produced at rest on the $\Upsilon(4S)$ resonance.

No observation of such decays has been reported in hadron-collision experiments. With the impact parameter and z_{vertex} cuts on the lepton pairs from $J/\psi, \psi' \rightarrow \ell^+\ell^-$ decays, P789 will provide additional new information on the lifetimes of b-particles. Also, since the branching ratios (BR) are already known for the $B \rightarrow J/\psi X$ and $B \rightarrow \psi' X$ decays, measurements of $[\sigma \cdot \text{BR}]$ for these decays will yield the corresponding b-particle production cross sections (σ).

P789 will also be sensitive to $B \rightarrow \chi_0 X$ inclusive decay, through detection of $\chi_0 \rightarrow \pi^+\pi^-, K^+K^-$ (BR $\simeq 0.8\%$). Such decays have not yet been reported.

Finally, because the lepton-detection properties of the downstream spectrometer are well known, the J/ψ and ψ' measurements will provide a tool for commissioning the silicon vertex array and optimizing the mass resolution without requiring the RICH detector at the outset of P789.

5. Search for Exclusive Dilepton Decays $B \rightarrow \mu^+\mu^-, e^+e^-, \mu^\pm e^\mp$

Table II.3 lists the current upper limits for these decays from the ARGUS and CLEO collaborations.[6,17] The e^+e^- and $\mu^+\mu^-$ branching ratios are predicted to be very small in the Standard Model (about 10^{-12} and 10^{-8}, respectively).[18] The μe decay mode is forbidden by lepton number conservation.

TABLE II.3. Upper Limits for Exclusive Dilepton Decays

Decay Channel	ARGUS ($\times 10^{-5}$)	CLEO ($\times 10^{-5}$)
$B_d \rightarrow e^+e^-$	8.5	3.0
$B_d \rightarrow \mu^+\mu^-$	5.0	4.0
$B_d \rightarrow \mu^\pm e^\mp$	5.0	3.0

Because the silicon vertex array allows rejection of the Drell-Yan continuum background (which originates from the target), the sensitivity of P789 to these decays will be at the 10^{-6} level. Furthermore, unlike the ARGUS and CLEO experiments, we are also sensitive to $B_s \rightarrow \ell^\pm\ell^\mp$ decays.

6. Inclusive Dilepton Decays of $B\bar{B}$ pairs, and $B-\bar{B}$ Mixing

Evidence for $B-\bar{B}$ mixing has been reported in three experiments measuring like-sign dileptons (Table II.4; $R \equiv \Gamma(B^0 \to \bar{B}^0 \to x)/\Gamma(B^0 \to x')$). The primary semileptonic decays $b \to \ell^- \bar{\nu}_\ell c$ and $\bar{b} \to \ell^+ \nu_\ell \bar{c}$ normally yield a pair of leptons with opposite charges. Through mixing, a B^0 meson can transform into its anti-particle and decay as $\bar{B}^0$, signalled by the appearance of like-sign lepton pairs.

TABLE II.4. Experimental Results on $B-\bar{B}$ Mixing

Experiment	Number of Like-Sign Dileptons	Number of Unlike-Sign Dileptons	Mixing Parameter R
UA1 [1]	15	98	0.121 ± 0.047
ARGUS [2]	$24.8 \pm 7.6 \pm 3.8$	$270 \pm 19.4 \pm 5.0$	$0.22 \pm 0.09 \pm 0.04$
MAC [19]	5	7	$0.21^{+0.29}_{-0.15}$

Compared to the existing measurements, P789 will have less contamination from non-B-decay background, because of the rejection provided by the impact parameter cut from the silicon vertex array. Complementing ARGUS, our measurements will be sensitive to the possibly larger[20] $B_s-\bar{B}_s$ mixing in addition to $B_d-\bar{B}_d$ mixing, with better statistics than UA1, MAC, and ARGUS in each case.

7. Search for η_b and Dihadron Decays of $b\bar{b}$ States

The improved mass resolution of the upgraded E605/E772 spectrometer will facilitate sensitive searches for new resonances through their two-body decays. E.g., the branching ratio for $\eta_c \to p\bar{p}$ has been measured[21] to be $(1.2 \pm 0.6) \times 10^{-3}$. Although the branching ratio for $\eta_b \to p\bar{p}$ is expected to be smaller, with $\delta m \sim 8$ MeV for $m \sim 10$ GeV, P789 offers new opportunities for locating the η_b quarkonium state through this channel.

Dihadron decays of $c\bar{c}$ quarkonium states are known to have reasonably large branching ratios;[21] $BR(J/\psi \to p\bar{p}) = (2.2 \pm 0.1) \times 10^{-3}$ and $BR(\chi_0 \to \pi^+\pi^-) = (0.8 \pm 0.2) \times 10^{-2}$. It is thus also interesting to search for the dihadron decays of known $b\bar{b}$ states, such as $\Upsilon, \Upsilon', \Upsilon'' \to (\pi^+\pi^-, K^+K^-, p\bar{p})$ and $\chi_b, \chi_b' \to (\pi^+\pi^-, K^+K^-)$. No upper limits on the branching ratios for these decays have yet been reported.[21] P789 will be able to search for these decays at the $\sim 10^{-4}$ level, without extra spectrometer settings.

III. EXPERIMENTAL SETUP

A schematic diagram of the E605/E772 spectrometer is shown in Figure 2. The large magnets SM12 (p_t kick $\sim$ 4 GeV) and SM3 (p_t kick $\sim$ 1 GeV) provide excellent momentum resolution. Figure 1a shows the well-separated peaks of the Υ states in the dimuon mass spectrum obtained in E605. This spectrometer was also used (by the present collaboration) in the 1987 E772 fixed-target run (cf. Figure 1b). Several modifications are required for P789.

1. Target

We will employ a tungsten target 3 mm long $\times$ 0.2 mm high $\times$ 10 mm wide. The short length and small height of the target will facilitate an impact parameter separation between primary and decay vertices. The small height will further help to reject those background tracks whose 3-momenta point back to the target and will provide an additional cut on the 3-momenta of dihadrons, which will be required to point to the target.

2. Aperture

The spectrometer will be used in the open-aperture configuration. The aperture will be collimated at the downstream end of the first analysis magnet in order to optimize the acceptance for a mass of 5.3 GeV while minimizing spectrometer singles rates. Results of a February 1988 test run under the approximate conditions of P789 are described in Appendix II.

3. Silicon Microstrip Detectors

These detectors are required for reconstructing the B-decay vertex. We propose a total of 16 planes of Si microstrip detectors, placed between 60 and 125 cm downstream of the target, and covering the range 18 mr $\leq |\theta_y| \leq$ 68 mr and -26 mr $\leq \theta_x \leq$26 mr. The proposed locations and specifications of these detectors are detailed in Table III.1 and Figure 3. The February '88 test run showed that these detectors will perform adequately despite the high particle rates at their locations (see Appendix II).

The proposed silicon detector configuration is based on careful simulations of vertex reconstruction in the presence of multiple low-energy pions (see Appendix I). We are continuing to investigate alternative configurations, including the possible addition of more silicon planes.

TABLE III.1. Si Microstrip Detector Configuration

Plane	z (cm)	Size (x cm $\times$ y cm) (horiz $\times$ vert)	No. of Strips Instrumented	Spacing (μm)
Y1	60	4.2 $\times$ 4.0	600	50
U1	65	4.2 $\times$ 4.0	820	50
V2	75	4.2 $\times$ 4.0	948	50
Y2	80	4.2 $\times$ 4.0	800	50
Y3	105	6.5 $\times$ 6.3	524	100
U3	110	6.5 $\times$ 6.3	696	100
V4	120	6.5 $\times$ 6.3	760	100
Y4	125	6.5 $\times$ 6.3	624	100

Total number of channels = 5772 $\times$ 2 = 11544

4. Analysis Magnets

The sensitivity of the proposed experiment depends critically on the mass resolution one can achieve. A mass resolution of $\delta m \simeq 30\,\mathrm{MeV}$ at $m \simeq 9.5\,\mathrm{GeV}$ was obtained in E605 with closed aperture and an extended target.[22] The use of silicon microstrip detectors, a short target, and an open-aperture configuration lead to excellent vertex determination and improved mass resolution. Monte Carlo simulation of the expected mass resolution (Section IV) yields $\delta m \simeq 3\,\mathrm{MeV}$ at $m = 5.3\,\mathrm{GeV}$. In order to achieve this, the magnetic field in the SM12 magnet will have to be carefully mapped at the chosen setting. E772 data on NMR probes located in the analysis magnets confirm 0.01% stability of the magnetic fields. This is more than sufficient for the predicted resolution.

5. Drift Chambers

We propose replacing the existing Station 1 MWPC's with high-rate drift chambers to obtain better position resolution there. This will improve our ability to associate downstream spectrometer tracks with tracks in the silicon vertex array. The proposed dimensions of these new drift chambers are listed in Table III.2.

6. Hodoscope Scintillators

For the proposed spectrometer setting, the profile of accepted 5.3-GeV-mass events at Station 1 is about half the vertical size of the existing Station 1 hodoscopes. We propose to rebuild the Station 1 hodoscopes with the same number of scintillators but half the current vertical size. This will improve the hodoscope trigger matrix definition at the

TABLE III.2. New Station 1 Drift Chambers

Chamber	Size (cm × cm) (horiz × vert)	No. of channels	Cell size (cm)
Y1	110 × 72	72	1
Y1′	110 × 72	72	1
U1	110 × 72	96	1
U1′	110 × 72	96	1
V1	110 × 72	96	1
V1′	110 × 72	96	1

lowest trigger level.

7. Cherenkov Detector

The ring-imaging-Cherenkov detector (RICH), used in the 1982 and 1984 E605 runs, was not used in the 1985 E605 and 1987 E772 runs. The present proposal requires that the RICH detector be made operational again for particle identification.

IV. PREDICTED YIELDS

The expected number of events is given by

$$N_{det} = N_{beam} \times N_{targ} \times \sigma \times \epsilon \times BR \times Acc \times Eff. \quad (5)$$

Assuming a fixed-target run of 10^5 spills at 3×10^{11} protons/spill, the total number of incident protons is $N_{beam} = 3 \times 10^{16}$. A 3 mm-long W target (3% interaction length) gives $N_{targ} = 3.5 \times 10^{24}$ nucleon/cm^2. Berger predicts[23] the 800-GeV production cross section $\sigma(pp \to b\bar{b}X)$ to be in the range 9–19 nb; we use 10 nb in this proposal. Bjorken has estimated[7] the probability that produced $b, \bar{b}$ quarks will hadronize into particular B mesons or b-baryons to be $\epsilon(b \to B_d) \simeq 30\%$, $\epsilon(b \to B_s) \simeq 15\%$, and $\epsilon(b \to \Lambda_b) \simeq 15\%$. BR is the expected branching ratio for a specific b-hadron decay. The spectrometer acceptance Acc for two-prong decays is calculated to be $\sim 2\%$ for a 5.3 GeV mass. Eff is the efficiency of the various background-rejection cuts (mainly on mass and z_{vertex}); we estimate Eff to be $\sim 30\%$. The following sections list the yields expected for the various decay channels we propose to study.

1. $B^0, \Lambda_b \to h^+h^-$

The dynamics of heavy quark production in hadron interactions was recently investigated by E. Berger.[23] His model reproduces the existing data from the LEBC[25] and WA78[26] experiments. Figure 4 shows the predicted x_F and p_t distributions for b-quark production in p + nucleus and π + nucleus collisions. We assume similar distributions for B-meson production in our Monte Carlo simulations (x_F distribution $\propto e^{-x_F^2/2\sigma^2}$, with $\sigma = 0.17$; p_t distribution $\propto e^{-(p_t^2/7\mathrm{GeV}^2)}$). Figures 5a,b show the acceptance of the spectrometer as a function of SM12 current and target location, respectively. The choices SM12 = 1800 amps and $z_{targ} = -80$ inches are used throughout this proposal. Results from the February '88 test run corroborate that these are the optimal choices for $B^0, \Lambda_b \to h^+h^-$ events.

Figures 6a,b show the spectrometer acceptance as a function of the x_F, p_t of the B meson. The acceptance as a function of dihadron mass is shown in Figure 6c. Note that the acceptance for m $\sim$ 9.5 GeV is reasonably large. Hence searching for η_b, Υ, χ_b decays does not require additional spectrometer settings. Figures 7a,b show the x_F, p_t dependences of the acceptance folded with Berger's production model; the distribution with p_z is shown in Figure 8a. Due to the 800-GeV beam energy, the accepted B mesons have $< p_z > \simeq 165$ GeV. This implies that the average distance between the primary production vertex and secondary decay vertex is $\sim$1.0 cm (Figure 8b).

To simulate the mass resolution of the spectrometer, multiple-scattering in the various materials and the finite position resolutions of the chambers are taken into account. Figure 9 shows the spectrum of reconstructed mass for B meson decays. The large p_t kick of the SM12 magnet and the precise vertex determination by the silicon microstrip array are responsible for $\delta m/m \simeq 0.6 \times 10^{-3}$.

Table IV.1 lists the number of $B^0, \Lambda_b \to h^+h^-$ events predicted for various decay channels after all cuts have been applied. For purposes of illustration we here assume $\sigma(pp \to b\bar{b}X) = 10\,\text{nb}$ and $\text{BR} = 1 \times 10^{-5}$ for each decay mode. The background estimate is based on the dihadron yield measured in the February '88 test run, and assumes a vertex rejection factor of 10^4. Extensive simulations demonstrate that this is a conservative assumption. Backgrounds and their rejection are discussed in detail in Section V and Appendix I.

TABLE IV.1. Predicted Yields (per 10^{15} interactions, for $\text{BR} = 1 \times 10^{-5}$)

Decay Mode	No. of Events	Background (per 3 MeV)	Significance ($\times\sigma$)
$B_d, \bar{B}_d \to \pi^+\pi^-$	40	22	3.5
$B_d, \bar{B}_d \to K^+K^-$	40	3	5.5
$B_d, \bar{B}_d \to p\bar{p}$	40	4	5.
$B_d \to K^+\pi^-$	20	10	2.5
$\bar{B}_d \to K^-\pi^+$	20	6	3.
$B_s, \bar{B}_s \to \pi^+\pi^-$	20	22	2.
$B_s, \bar{B}_s \to K^+K^-$	20	3	3.5
$B_s, \bar{B}_s \to p\bar{p}$	20	4	3.
$B_s \to K^-\pi^+$	10	6	2.
$\bar{B}_s \to K^+\pi^-$	10	10	1.5
$\Lambda_b \to p\pi^-$	10	16	1.
$\Lambda_b \to pK^-$	10	4	2.
$\bar{\Lambda}_b \to \bar{p}\pi^+$	10	3	2.
$\bar{\Lambda}_b \to \bar{p}K^+$	10	1.5	2.5

We recognize that the $b\bar{b}$ cross-section might be smaller and/or the background larger than assumed. The main cause of background is confusion of the pattern-recognition in the silicon detectors due to large soft-pion multiplicities (see Appendix I), an effect

exhibiting strong rate dependence. If the rates in the silicon are a factor of two larger than assumed, we will need to decrease the beam intensity by the same factor to maintain the same background rejection. If the cross-section is also a factor of two smaller than Berger predicts, we will then have sensitivity to dihadron branching ratios of: 0.8×10^{-5} for $B_d, \bar{B}_d \to \pi^+\pi^-$; 0.5×10^{-5} for $B_d, \bar{B}_d \to K^+K^-$; 1.5×10^{-5} for $B_s, \bar{B}_s \to K^\mp\pi^\pm$; and 2×10^{-5} for $\bar{\Lambda}_b \to \bar{p}\pi^+$ or $\bar{p}K^+$. These are 90% c.l. upper limits assuming 10^4 vertex rejection. Even in this pessimistic scenario we retain a sensitivity unrivaled by any other experiment. Should we achieve 10^5 vertex rejection as our simulations suggest, we will observe ≤ 1 background event per bin in each channel, and the sensitivities will all be better than 1×10^{-5}.

2. $B \to J/\psi X$, $B \to \psi' X$, $B \to \chi_0 X$ Inclusive Decays

We assume B production cross sections and spectrometer settings identical to those of Section IV.1 to calculate the acceptance for these events. The branching ratios are[21]

$$\mathrm{BR}(B \to J/\psi X) = 1.2 \pm 0.3\%, \qquad \mathrm{BR}(B \to \psi' X) = 0.46 \pm 0.3\%,$$
$$\mathrm{BR}(J/\psi \to \ell^+\ell^-) = 13.8 \pm 1.8\%, \qquad \mathrm{BR}(\psi' \to \ell^+\ell^-) = 1.8 \pm 0.3\%.$$

The momentum distributions of the J/ψ and ψ' from these inclusive decays are unknown. We make the simple assumption that $B \to J/\psi K$ and $B \to \psi' K$ decays approximate them. Simulations then yield 400 J/ψ and 160 ψ' events, compared to 320 and 30 (respectively) background events (cf. Appendix I.2.a).

Similar estimates were made for $B \to \chi_0 X$. Assuming BR $\simeq$ 1% for these inclusive decays, we expect 130 $\chi_0 \to \pi^+\pi^-$ events and 110 $\chi_0 \to K^+K^-$ events, compared to 230 and 200 (respectively) background events.

3. $B \to e^+e^-, \mu^+\mu^-, \mu^\pm e^\mp$ Rare Decays

The spectrometer acceptance for these decays is identical to that for $B \to h^+h^-$. If no events are seen in these channels and also no background (cf. Appendix I.2.b), then an upper limit of 6×10^{-7} for B_d and 1.2×10^{-6} for B_s will be established in each channel (90% c.l.).

4. $B\bar{B} \to$ Lepton-Pair Inclusive Decays

We have calculated the acceptance for a pair of leptons produced in semileptonic decays of a pair of $B, \bar{B}$ mesons, where B can be B_u, B_d, or B_s. Figure 10 shows the inclusive lepton momentum spectrum obtained by the CLEO collaboration.[27] The dotted

curve represents the predicted shape of the primary decay $B \to \ell\nu X$, while the dashed curve corresponds to the secondary decay $B \to D \to \ell\nu X$. Our Monte Carlo utilizes the measured[27] value $11.0 \pm 0.8\%$ for the primary decay branching ratio and the ARGUS[2] value 0.21 for the mixing parameter $R \equiv \Gamma(B_d^0 \to \bar{B}_d^0 \to x)/\Gamma(B_d^0 \to x')$. The mixing parameter for B_s is unknown but is predicted to be larger than that for B_d^0, since the associated $\Delta m/\Gamma$ is expected to be ~ 5 times larger.[20] We therefore assumed $R = 0.5$ for $B_s - \bar{B}_s$ mixing.

The yield of inclusive lepton pairs is most sensitive to the assumed correlations between the produced B and $\bar{B}$. For no correlation, 3700 unlike-sign and 1700 like-sign pairs are expected. For a pure back-to-back correlation of the B's in the $B\bar{B}$ center of mass, 8700 unlike-sign and 70 like-sign pairs are predicted. Backgrounds are negligible (cf. Appendix I.2.c).

5. Two-body Decays of η_b, Υ, χ_b Quarkonium States

E605 measured a 44 pb/nucleon cross section $(d\sigma/dy)_{y=0}$ for Υ production in 800-GeV p + nucleus collisions.[28] The η_b and χ_b productions are estimated to be ~ 2.5 times larger than this, based on the ratio $\sigma(\chi_0)/\sigma(J/\psi)$ measured at the ISR.[44] Assuming a p_t distribution $\propto e^{-0.37 p_t^2}$ and an x_F distribution $\propto e^{-18 x_F^2}$ (cf. Ref. 29), we have estimated the P789 spectrometer acceptance and the expected number of events for various dihadron decays of b quarkonium states (Table IV.2). The backgrounds (cf. Appendix I.2.d) in the $p\bar{p}$ and K^+K^- channels are sufficiently small to permit searches for these decays at the BR $\sim 1 \times 10^{-4}$ level.

TABLE IV.2. Predicted Yields (per 10^{15} interactions, for BR $= 1 \times 10^{-4}$)

Decay Mode	No. of Events	Background
$\eta_b \to p\bar{p}$	70	40
$\Upsilon \to p\bar{p}$	30	40
$\chi_b \to K^+K^-$	60	30
$\chi_b \to \pi^+\pi^-$	60	1700

N.B. $\sigma_{\rm prod}(\eta_b), \sigma_{\rm prod}(\chi_b)$ assumed to be $2.5 \times \sigma_{\rm prod}(\Upsilon)$

V. BACKGROUNDS

There are two major types of background for P789. The first derives from particles produced directly in the target. The second arises from pairs of produced particles at least one of which is relatively long-lived and decays downstream of the target. Estimates of these backgrounds are given below. Appendix I provides a detailed description of our background simulations.

1. Backgrounds for B, $\Lambda_b \to h^+h^-$

a. Backgrounds from Direct Hadron-pair Production

Parton-parton scattering at high energies produces pairs of high-p_t hadrons. This background affects the proposed experiment in two ways. First, it sets a lower limit on the trigger rate. Second, it determines the ultimate sensitivity of the off-line analysis. This is because some of these particles will, when combined with the high rate of soft pion tracks in the silicon detectors, lead to fake vertices more than 7 mm downstream from the target.

The cross sections for hadron-pair production were measured directly in the P789 test run in February 1988 (see Appendix II and IV for details). The trigger rate due to target dihadrons will be 4×10^3 events per spill, a rate well within the capabilities of our (upgraded) data acquisition system. The off-line rejection of these direct dihadrons via vertex cuts will be better than 10^4 (see Appendix I). Table IV.1 summarizes the background from this source.

b. Backgrounds from Hadron Decay

Background from decays of K_s, D, and B mesons downstream of the target was also simulated (see Appendix I). The sum of contributions to each final state is < 0.2 events per 3 MeV mass bin at 5.3 GeV.

2. Backgrounds for Other Two-prong Decays

Appendix I also details considerations of backgrounds from:

a) $B \to J/\psi X, B \to \psi' X, B \to \chi_0 X$;

b) $B \to e^+e^-, \mu^+\mu^-, \mu^\pm e^\mp$ rare decays;

c) $B\bar{B} \to$ inclusive lepton pairs;

d) η_b, Υ, χ_b dihadron decays.

Backgrounds for cases b) and c) are found to be negligible. Backgrounds for cases a) and d) have been cited in Section IV above.

VI. COST ESTIMATES

A number of changes to the E605/772 spectrometer are required for P789. These include: installation of a silicon vertex detector, a new Station 1 drift chamber, construction of an aperture wall in the SM12 magnet, rehabilitation of the RICH detector, upgrades to the data acquisition system including a vertex processor, and rebuilding of two hodoscope planes. The total estimated cost is $980K. This is based primarily on the P789 impact statement written by D. Christian dated November 29, 1987 and assumes that the existing E605/772 MWPC latching system will be used with new MECL10K latches for the silicon vertex detector readout. The breakdown of costs is as follows:

1) Silicon Detectors		
Silicon (16 planes + spares)	$150K	
Mounts	35K	
Preamps (12K channels)	120K	
Amps and Latches(12K channels)	300K	
A/C & RF shielding	30K	
Re-shielding target cave	30K	
Total		$665K
2) New Station 1 Drift Chamber		
Mechanical	$ 40K	
Readout electronics	10K	
Total		$ 50K
3) Partially Open Magnet Aperture		
Machining and rigging	$ 50K	
Total		$ 50K
4) RICH Detector		
Readout electronics (2000 chan.)	$120K	
Misc. rehabilitation	$ 20K	
Total		$140K
5) DAQ Upgrade		
Megamemory replacement	$ 30K	
Si vertex processor	$ 25K	
Addt'l TRANSPORT modules	$ 10K	
Total		$ 65K
6) Hodoscope rebuild		
Rebuild 2 planes - mechanical	$ 10K	
Total		$ 10K
Total Estimated Cost		$980K

VII. PROPOSED SCHEDULE

OCT '88	Approval by PAC.
NOV '88	Finalize magnet aperture. Finalize silicon configuration, order silicon microstrip detectors.
DEC '88 – JAN '89	Design collimator inserts. Order silicon electronics. Finalize Station 1 drift chamber and order parts. Order electronics for RICH detector.
FEB '89 – APR '89	Rebuild Station 1 hodoscope planes. Begin upgrades to buffer memory/readout subsystem. Begin construction of Station 1 drift chambers. Build collimator wall in SM12 magnet.
MAY '89 – AUG '89	Build silicon detector system & electronics. Debug in LAMPF test beam. Re-equip RICH detector. Install Station 1 drift chambers. Complete upgrades to buffer memory/readout subsystem.
SEP '89	Install silicon detector system at FNAL.
OCT '89 – JUL '90	First run of E789. Tune mass and vertex resolution on $J/\psi, \psi', \Upsilon$'s. Take first production data.
SEP '90 – SEP '91	Use data from 1st run to finalize vertex processor design. Upgrade silicon array as necessary. Re-map magnet fields.
OCT '91	Second run of E789. Push sensitivity limits with optimized spectrometer.

VIII. SUMMARY

We propose to reconfigure the E605/E772 spectrometer to study the two-body, two-prong decay modes of neutral B mesons and baryons. The superb mass resolution and high-rate capability of this instrument are uniquely suited to this objective. Based upon plausible assumptions for cross sections, a sample of a few hundred b-decays can be obtained even if their branching ratios are as small as 1×10^{-5}. These data could provide first measurements of the masses, lifetimes and branching ratios for a variety of charmless decays into pions, kaons, and protons. While some upgrades to the spectrometer are required, the anticipated cost ($980K) and level of effort involved are reasonable in light of the potential physics insight that can be obtained.

REFERENCES

1. C. Albajar *et al.*, Phys. Lett. **186B**, 247 (1987).
2. H. Albrecht *et al.*, Phys. Lett. **192B**, 245 (1987).
3. H. Albrecht *et al.*, Phys. Lett. **209B**, 119 (1988).
4. W. Schmidt Parzefall, Proceedings of the 1987 International Symposium on Lepton and Photon Interactions at High Energies, Hamburg, W. Germany, July 27-31, 1987.
5. C. Bebek *et al.*, CESR Preprint No. CBX-88-34, July 1988.
6. P. Baringer *et al.*, CESR Preprint No. CBX-88-26, July 1988.
7. J. D. Bjorken, Invited talk at the International Symposium for the Fourth Family of Quarks and Leptons, UCLA, Los Angeles, California, February 26–28, 1987.
8. I. I. Bigi and B. Stech, in *Proceedings of the Workshop on High Sensitivity Beauty Physics at Fermilab, Fermilab, Illinois, November 11–14, 1987*, edited by A. J. Slaughter, N. Lockyer, and M. Schmidt (FNAL, 1988).
9. L. L. Chau and H. Y. Cheng, Phys. Rev. Lett. **59**, 958 (1987).
10. M. B. Gavela *et al.*, Phys. Lett. **154B**, 425 (1985).
11. J. P. Albanese *et al.*, Phys. Lett. **158B**, 186 (1985).
12. V. Lüth, SLAC Preprint No. SLAC-PUB-4552, 1988.
13. A. Bean *et al.*, Phys. Rev. Lett. **58**, 183 (1987).
14. A. Soni, Phys. Rev. Lett. **53**, 1407 (1984).
15. K. Berkelman, Rep. Prog. Phys. **49**, 1 (1986).
    A. Martin and J. M. Richard, Phys. Lett. **185**, 426 (1987).
16. Particle Data Group, *Review of Particle Properties*, April 1988.
17. H. Albrecht *et al.*, Phys. Lett. **199**, 451 (1987).
18. Report of the Working Group on CP violation and rare decays, in Proceedings of the 1984 Snowmass Summer Study.
19. H. R. Band, Phys. Lett. **200**, 221 (1988).
20. F. J. Gilman, in *Proceeding of the Workshop on High Sensitivity Beauty Physics at Fermilab, Fermilab, Illinois, November 11–14, 1987*, edited by A. J. Slaughter, N. Lockyer, and M. Schmidt (FNAL, 1988).
21. Particle Data Group, Phys. Lett. **170B**, 74 (1986).
22. FNAL E605 Collaboration (to be published).

23. E. L. Berger, Invited paper at the XXII Rencontre de Moriond, Les Arcs, France, March 15-21, 1987; E. L. Berger, Argonne National Laboratory preprint ANL-HEP-CP-88-26, 1988.

24. J. D. Bjorken (private communication).

25. M. Aguilar-Benitez *et al.*, Phys. Lett. **135B**, 237 (1984); Phys. Lett. **189B**, 476 (1987).

26. M. G. Catanesi *et al.*, Phys. Lett. **187B**, 431 (1987).

27. S. Behrends, Phys. Rev. Lett. **59**, 407 (1987).

28. T. Yoshida, Ph. D. Thesis, Kyoto University, 1986.

29. W-Y. P. Hwang, J. M. Moss, and J. C. Peng, Los Alamos National Laboratory Preprint No. LAUR-88-862, 1988.

30. R. D. Kephart *et al.*, Phys. Rev. Lett. **39**, 1440 (1977).

31. H. Jöstlein *et al.*, Phys. Rev. **D20**, 53 (1979).

32. A. L. S. Angelis *et al.*, Nucl. Phys. **B209**, 284 (1982).

33. W. Thomé *et al.*, Nucl. Phys. **B129**, 365 (1977).

34. S. Reucroft, "Hadroproduction Characteristics of Charm and Beauty," Sixth International Conference on Physics in Collision, Chicago, Illinois, 1986.

35. V. Barger *et al.*, Phys. Lett. **91B**, 253 (1980).

36. E. J. Suskind *et al.*, Phys. Rev. **D21**, 628 (1980).

37. E. Eichten *et al.*, Rev. Mod. Phys. **56**, 579 (1984).

38. I. R. Kenyon, Rep. Prog. Phys. **45**, 1261 (1982).

39. P. Borgeaud *et al.*, Nucl. Instrum. Methods **211**, 363 (1983).

40. M. Campanella *et al.*, Nucl. Instrum. Methods **A243**, 93 (1986).

41. H. Deitl *et al.*, Nucl. Instrum. Methods **A253**, 460 (1987).

42. T. Ohsugi *et al.*, Nucl. Instrum. Methods **A265**, 105 (1988).

43. J. P. Raymond and E. L. Peterson, IEEE Trans. Nucl. Sci. **NS-34**, No. 6, 1622 (1987).

44. C. Kourkoumelis *et al.*, Phys. Lett. **81B**, 405 (1979).

45. B. C. Brown *et al.*, Fermilab preprint FERMILAB-77/54-EXP (1977).

46. P. L. McGaughey, (private communication, E772 preliminary result).

APPENDIX I. DETAILS OF BACKGROUND ESTIMATES

1. Backgrounds for $B, \Lambda_b \to h^+h^-$

a. Backgrounds from Direct Dihadron Production

Dihadron production in the target is the most important source of background. The cross sections for hadron-pair production have been measured both in a fixed-target experiment by the CFS group[30,31] and in the CCOR experiment at the ISR,[32] but the literature on the subject is confusing. Figure 11 reproduces the CFS and CCOR results. Also indicated is the CFS cross section extrapolated to ISR energy via the CFS scaling fit. The two experiments disagree by an order of magnitude.

The dihadron yield at 800 GeV beam energy had not been published prior to our February '88 test run (see Appendix II). We have now completed a careful analysis of the test run data, the results of which will soon be submitted for publication. (A draft of this paper is attached as Appendix IV.) The cross-section $d^2\sigma/dmdy$ per nucleon is given in Figure 12. Our results show that the cross-section at the mass of the B is an order of magnitude below that published by CFS. To compute backgrounds for P789 we use our observed event yield per incident proton, corrected for the small differences between the test run apparatus and the proposed P789 configuration. (This calculation is insensitive to the production-model uncertainties which can have a strong effect on $d^2\sigma/dm\,dy$.) We observed $(3.7 \pm 0.2) \times 10^{-9}$ dihadrons per proton incident on a 3-mm-thick tungsten target. The acceptance $\times$ trigger efficiency will be larger for P789 by factors of 1.7 due to a looser trigger requirement (no left-right coincidence required, see Appendix II) and 1.2 due to an optimization of the collimator geometry. In addition, we will be sensitive to $\sim 70\%$ higher dihadron yield with the magnets set for 10% lower mass. We thus multiply the observed dihadron rate by 3.5, giving 4×10^3 dihadrons per beam spill at the proposed beam intensity.

The background to observation of a b decay in any channel is obtained from the observed yield per incident proton per 3-MeV mass bin at the B mass: $(7.6 \pm 1.0) \times 10^{-12}$. This we scale by 1.7 (for the looser trigger) $\times$ 1.2 (collimator) $\times$ 1.5 (increase in acceptance at the B mass due to the lower magnet setting), giving a total of $(6.8 \pm 0.9) \times 10^5$ events per fixed-target run. A vertex rejection factor of 10^4 leaves 68 events divided among the various pion, kaon, and proton pair final states, as shown in Table IV.1. We use the pair species ratios of Kephart *et al.*[30]

In principle all of these target dihadrons can be rejected in the off-line analysis using

vertex information from the silicon microstrip array. In practice, the $z_{\rm vertex}$ resolution, due to multiple-scattering in the silicon detectors and ambiguities in the track reconstruction, limits the rejection efficiency. Detailed Monte Carlo simulations show that we can achieve a rejection factor better than 10^4.

The Monte Carlo first generates dihadron background events which satisfy the downstream spectrometer. Following the cross-section shapes measured in Kephart *et al.*,[30] we parameterize the hadron-pair-p_t distribution as $Ed^3\sigma/dp^3 \propto e^{-7p_t^2}$, and we take the distributions in rapidity and decay cosine to be flat over the small ranges in those variables covered by our acceptance. The dihadron tracks are traced forward with multiple scattering at each detector plane and the resolutions of all downstream detectors included.

Additional hits on the silicon detectors are generated to account for the soft pion background. We have used two different parametrizations of this background, both of which are consistent with the rates measured in our February test. We find that our results are insensitive to which parametrization we choose. The first utilizes the θ_y distribution we measured in February '88, an *ad hoc* θ_x distribution given by $dN/d\theta_x \propto (2-|\theta_x|/30\,\mathrm{mrad})$, and the hadron rapidity distribution measured by Thomé *et al.*[33] at the ISR. The second parametrization uses our measured θ_y distribution along with the well-known $Ed^3\sigma/dp^3 \propto e^{-6p_t}$ characteristic of low-p_t hadron production.

The dihadron tracks are then traced back upstream to the silicon vertex spectrometer and are used to define narrow roads for the silicon trackfinding. Candidate tracks in the silicon planes are next subjected to χ^2 quality cuts and impact parameter cuts (0.15 mm on each track). Final cuts on the pair track quality (overall goodness of fit and at least 15 of 16 planes participating) and pair vertex (including decay volume and distance of closest approach) complete the rejection. We impose a $z_{\rm vertex}$ cut of 0.7 cm. Many silicon detector and target configurations were investigated. Of those, the configuration given in Section III gives the best vertex rejection factor.

The strong dependence of the rejection factor on the assumed soft-pion multiplicity is indicated in Table AI.1. For our anticipated pion multiplicity of 25 (Appendix II) and the proposed silicon array (Section III), a rejection factor of $\geq 10^5$ (3 events accepted for 500,000 thrown) is obtained for the prompt-dihadron background. The vertex cuts also reduce the acceptance for B decay events. Table AI.2 shows that $\sim 30\%$ of the B decays survive these cuts. We obtain the the prompt-dihadron background yields listed in Table IV.1 under the conservative assumption of a vertex rejection factor of 10^4.

We have also included the effect of noise in the silicon detectors by throwing 5 random

TABLE AI.1. Acceptance of Prompt Dihadrons Accompanied by Soft Pions

Soft Pion Multiplicity	Events Thrown	Events Accepted	Rejection Factor
5	10^5	0	$> 10^5$
15	10^5	0	$> 10^5$
25	5×10^5	3	$\sim 2 \times 10^5$
35	10^5	0	$> 10^5$
45	5×10^4	3	$\sim 2 \times 10^4$
55	5×10^4	7	$\sim 7 \times 10^3$

TABLE AI.2. Acceptance of $B \to h^+h^-$ Events Accompanied by Soft Pions

Soft Pion Multiplicity	Events Thrown	Events Accepted
5	1000	329
15	1000	311
25	1000	308
35	1000	325
45	1000	340

hits on each silicon plane in addition to the soft-pion tracks. This corresponds to a noise rate of 500 kHz per strip. Based on discussions with D. Christian and our own tests (see Appendix II), the actual noise rate will be well below this level. Within statistics, the rejection factors are the same as those without noise hits. This result confirms the expectation that prompt pion tracks, especially the more energetic ones, are responsible for confusing the pattern recognition in the silicon array.

Table AI.1 indicates that we lose an order of magnitude in prompt-dihadron rejection for each doubling of the effective background pion rate. Higher instantaneous rates could originate from either higher beam intensity or worse spill duty cycle. In our February '88 test run we observed an average rate corresponding to 14 pions per detector plane. On our 1987 E772 data tapes we find a 55% average duty factor, based on the measured rate of chance coincidences in two uncorrelated counters. In this proposal we assume that the Tevatron will continue to run with a 55% duty cycle, leading to the 25 soft pions per plane per event assumed above.

Given the deterioration of the vertex discrimination shown in Table AI.1 for high rates, it is clear that single-bucket resolution is important to P789. Appendix III details

how we will achieve this time resolution.

b. Rejection of Delayed Dihadron Background

In addition to the prompt dihadron background discussed above, there are potential backgrounds involving delayed decays of K_s, D, and B mesons. The ones listed below can specifically contribute to the backgrounds in $B \to \pi\pi$ and $B \to K\pi$ searches. We separate these backgrounds into two categories, depending on whether they contribute to the $\pi\pi$ or to the πK modes. Note that some of these reactions (a–c, f, g) represent two delayed decays and so produce two downstream vertices. Others (d, e, h, i) arise from the coincidence of a delayed decay with a prompt track, and so produce one downstream vertex. We expect smaller rejection factors in the first case than in the second; in particular, the vertex cut rejection in the second case should be roughly the square of that in the first.

Reactions contributing to $\pi\pi$ mode:

a) $DD \to \pi\pi X$,
b) $K_sK_s \to \pi\pi X$,
c) $BB \to \pi\pi X$,
d) $K_s\pi \to \pi\pi X$,
e) $D\pi \to \pi\pi X$.

Reactions contributing to πK mode:

f) $DD \to \pi KX$,
g) $BB \to \pi KX$,
h) $K_sK \to \pi KX$,
i) $DK \to \pi KX$.

We parameterize their production and decay distributions as follows:

a,f) Independent production of D pairs according to production distributions measured by Reucroft *et al.*[34]; decay to $K\pi$ according to two-body kinematics, which results in the hardest (i.e., most conservative) p_t distribution (however, we normalize the result using effective branching ratios which include the 3- and 4-body $K\pi\pi$ and $K\pi\pi\pi$ combinatorics).

b,d,h) Correlated production of hadron pairs according to production distributions measured by Kephart *et al.*[30]

c,g) Independent B production according to $dN/dp_t^2 \propto e^{-p_t^2/7}$; π or K decay momentum distribution from Berkelman,[15] fit as $dN/dp \propto (p/2.6\text{GeV})(1-p/2.6\text{GeV})^{5.5}$.

e,i) D as in a,f); π or K following single-hadron scaling fit of Jõstlein *et al.*[31]

Table AI.3 lists the vertex rejection factors for these backgrounds, calculated for a range of soft pion multiplicities which bracket the expected running conditions and for a coarser-grained version of the silicon array. The column labeled "Rejection Factor" gives the value for 25 soft pions per spectrometer arm. As anticipated, the reactions fall into two groups distinguished by prompt hadron count, with $\sim 10^2$ rejection if neither hadron is prompt and $\sim 10^4$ if one is prompt.

TABLE AI.3. Vertex Rejection Factors for Delayed Backgrounds

Reaction	Events Thrown	Events Accepted*	Rejection Factor†
a), f)	10^4	27, 53, 91	$\sim 2 \times 10^2$
b)	5×10^5	12, 21, 24	$\sim 2 \times 10^4$
c), g)	10^4	17, 38, 61	$\sim 3 \times 10^2$
d), h)	10^5	0, 3, 8	$\sim 3 \times 10^4$
e), i)	10^5	0, 17, 57	$\sim 6 \times 10^3$

*Soft pion multiplicity = 5, 25, 45
†For soft pion multiplicity = 25

The rejection for $DD \to \pi(\pi \text{ or } K)X$ and $BB \to \pi(\pi \text{ or } K)X$ stems mainly from the fact that the accepted pairs can only fake the mass of a B if both members are emitted along a direction near that of the parent hadron. The reconstructed vertex then tends towards the target rather than the secondary decay vertex. Large decay angles require correspondingly larger transverse momenta of the parent and so are strongly suppressed. The $K_s K_s \to \pi\pi X$ background is trivially rejected because most of the K_s decay downstream of the silicon detectors.

When we apply additional invariant mass and acceptance cuts from the downstream spectrometer and include known production cross sections and branching ratios for these reactions, we obtain the results of Table AI.4. The backgrounds from delayed decay are clearly much smaller than those from prompt dihadron production (compare Table IV.1). Again, this table was compiled for a coarser-grained version of the silicon array (FNAL Proposal P789, April 1988). With the improved configuration of Table III.1 and Figure 3 these backgrounds will be even more insignificant than indicated here.

TABLE AI.4. Background per 3-MeV Mass Bin from Delayed Decay

Reaction	Number of Events*
$DD \to \pi\pi X$	~ 0.05
$K_s K_s \to \pi\pi X$	~ 0.01
$BB \to \pi\pi X$	~ 0.03
$\pi K_s \to \pi\pi X$	~ 0.05
$D\pi \to \pi\pi X$	~ 0.03
$DD \to \pi K X$	~ 0.01
$BB \to \pi K X$	~ 0.01
$DK \to \pi K X$	~ 0.003

*In a 10^5-spill fixed-target run, and for soft pion mulitplicity = 25

2. Backgrounds for Other Two-prong Decays

a. Background for $B \to J/\psi X, B \to \psi' X, B \to \chi_0 X$

The dominant background comes from prompt J/ψ and ψ' production. For J/ψ production at 800 GeV, $(d\sigma/dy)_{y=0} \times \mathrm{BR}_{\mu\mu} = 10\,\mathrm{nb}$.[35] Using the x_F distribution measured at 400 GeV[36] we deduce $\sigma(pp \to J/\psi X) \simeq 0.4\,\mu\mathrm{b}$ at 800 GeV. For ψ' production the corresponding $[\sigma \cdot \mathrm{BR}]$ is measured[45] to be $\sim 2\%$ of that for the J/ψ, implying a 56 nb production cross section. Folding these cross sections with the spectrometer acceptance, and using a target A-dependence[46] $\propto \mathrm{A}^{0.84}$ and a vertex rejection factor of 10^4, gives 320 background events for $B \to J/\psi X$ and 30 background events in the ψ' channel. With $\sigma(pp \to \chi_0 X)/\sigma(pp \to J/\psi X) = 2.5$ from the ISR,[44] we similarly estimate 230 background events for $B \to \chi_0 X \to \pi^+\pi^- X$ and 200 background events for $B \to \chi_0 X \to K^+K^- X$.

b. Background for $B \to e^+e^-, \mu^+\mu^-, \mu^\pm e^\mp$ Rare Decays

Unlike-sign dileptons can be produced by the Drell-Yan process. Using the EHLQ structure functions[37] and a K-factor of 2 implies a Drell-Yan cross section of 11.4 pb/GeV at $m = 5.3\,\mathrm{GeV}$. A 2% spectrometer acceptance then yields 70 Drell-Yan events per 3 MeV mass bin in this region. These events are completely suppressed with a vertex rejection factor of 10^4.

c. Background for $B\bar{B} \to$ Inclusive Lepton Pairs

Pairs of leptons from semileptonic B decay form a continuous mass spectrum. To estimate the background of Drell-Yan dileptons we fold the Drell-Yan yield with the spec-

trometer acceptance. This gives 1.5×10^5 Drell-Yan pairs detected over our full mass range. A 10^4 rejection factor passes 15 total $\ell^+\ell^-$ background events.

The like-sign dilepton background is more difficult to estimate. Previous dilepton experiments[38] have measured a like-sign yield at least a factor of 5 lower than that for unlike-sign pairs in this mass region. Given our silicon vertex array, channels involving like-sign pairs should therefore have totally negligible background.

d. Background for η_b, Υ, and χ_b Two-prong Decays

The background for these decays is expected to come mainly from direct dihadron production in the target. Figure 10 of Appendix IV indicates that the dihadron rate at 10 GeV mass is a factor 700 smaller than that at 5 GeV. We have used this result and the extrapolated species ratios of Kephart *et al.*[30] to estimate these backgrounds. The p_t and x_F distributions of these dihadrons are also presumed identical to those from Υ production. The resulting backgrounds predicted for a 8-MeV mass bin are summarized in Table IV.2.

Note that vertex rejection is not applicable for these decays, since the signals and backgrounds all come from the target region.

APPENDIX II. RESULTS FROM TEST RUN

In January and February 1988, after the completion of Experiment 772, we performed several tests to evaluate the spectrometer configuration proposed for P789. The major goals of these tests were to:

1. Check the singles rates in various detectors in the proposed open-aperture configuration.
2. Measure the rate of charged-particle production from the interaction of an 800-GeV proton beam with a 3-mm-thick tungsten target. The neutron flux was also measured. These measurements are crucial for evaluating the silicon microstrip singles rates and radiation damage.
3. Measure trigger rates.

For these tests we removed the SM0 magnet and the hadron absorber wall used for E772. The SM12(SM3) current was set at 2000(-4250) amps. The exit of SM12 was collimated to 50 cm high $\times$ 70 cm wide. Both 1-mm and 3-mm-thick W targets were used, with beam intensities in the range of a few $\times 10^{10}$ to a few $\times 10^{11}$ per spill. We present results normalized to the proposed 3 mm W target and 3×10^{11} protons/spill.

1. Singles Rates at Hodoscopes and Wire Chambers

Table AII.1 lists the singles rates observed at the various hodoscope stations. The maximum is ~ 6 MHz, well within the capabilities of these counters. The currents drawn by the wire chambers at Stations 1, 2, and 3 were 50, 100, and 300 μamps, respectively. The hit multiplicities on these stations for reconstructed dihadron events were 12, 10, and 15. These chamber currents and multiplicities are similar to or less than those tolerated during E605.

2. Si Microstrip Detector Rates

We installed a 5 cm $\times$ 5 cm 50 μm-pitch Si strip detector 150 cm downstream of the target. Three adjacent strips of this detector were read out. The preamp outputs exhibited a clear minimum-ionization band. Measurements were taken with the Si detector at two different heights, corresponding to $\theta_y = 50$ mr and $\theta_y = 96.5$ mr. Additionally, a 7-cm-wide $\times$ 0.3-cm-high $\times$ 0.3-cm-thick finger scintillator was mounted on a motor-driven frame 125 cm downstream of the target. Its phototube output also showed a clear minimum-ionization band. Data were obtained for vertical positions of this scintillator spanning a range corresponding to $6\,\text{mr} \leq |\theta_y| \leq 90\,\text{mr}$. Figure 13 shows the observed scintintillator

TABLE AII.1. Maximum Hodoscope Rates

Plane [a]	Rate (MHz) [b]
X1R	3.0
Y1R	2.4
Y2R	1.6
X3R	4.4
Y3R	6.5
X4R	0.25
Y4R	0.10

[a] X1R,Y1R rates normalized to proposed reduced-size planes
[b] 3×10^{11} protons/spill on 3 mm W

count rates as a function of vertical position, along with target-out rates. The rates measured in the Si detector are in agreement with these scintillator rates to within a factor of two.

These data determine the rates in the proposed Si strip detectors (cf. Table III.1). Table AII.2 and Figure 14 show the predicted rate/strip on various strips of the Y1 plane as a function of θ_y, as well as the flux per cm^2 into Y1 and Y4 integrated over one fixed-target running period. The average rate/strip is 1.4 MHz and the average number of hits per RF bucket is ~14. Recent results on annealing (cf. Appendix III) suggest a radiation damage limit in excess of 10^{14} minimum-ionizing particles/cm^2, so we expect the upstream Si detectors to last for at least several months. (We anticipate that these upstream planes can be replaced midway through the run, if necessary, for ~$7K per silicon wafer.)

Table AII.2. Si detector count rate/strip (3×10^{11} proton/spill on 3mm W)

θ_y(mr)	Rate (MHz) (per Y1 strip)	Hits/RF bucket (per Y1 strip)	Integrated flux/cm^2 (per 10^{15} interactions) into Y1	into Y4
18.1	2.50	0.059	2.8×10^{14}	0.63×10^{14}
21.2	2.08	0.050	2.3×10^{14}	0.53×10^{14}
26.2	1.60	0.038	1.8×10^{14}	0.41×10^{14}
31.2	1.45	0.035	1.5×10^{14}	0.37×10^{14}
36.2	1.15	0.028	1.2×10^{14}	0.28×10^{14}
46.4	0.79	0.019	0.86×10^{14}	0.20×10^{14}
56.4	0.57	0.014	0.61×10^{14}	0.14×10^{14}

To estimate the overall radiation damage to the silicon detectors and their preamplifiers, the neutron flux in the target cave was also measured (behind a few inches of concrete shielding). The observed neutron rates were lower than the direct charged-particle rates from the target. With a modest amount of shielding, the neutron dose $\sim 1/2$ m east and west of the beam axis (where the preamplifiers will be located) can be reduced to <50 krad for 10^5 spills. D. Christian has informed us that the new generation of preamplifiers should not experience problems at this level of irradiation. Finally, the neutron rates on axis will cause less damage to the silicon wafers than the charged particle rates.

3. Trigger Rate Studies

Several tapes of dihadron test data were recorded using a variety of hodoscope- and calorimeter-based triggers under various beam and target conditions (see Table AII.3). The trigger conditions applied were:

$(3/4L\cdot R) \equiv$ a hodoscope coincidence requiring good hits in 3 out of 4 hodoscope planes on both the left and right sides of the apparatus;

$E_{tot} \equiv$ total energy deposition in the calorimeter of at least 70 GeV;

$(h^+h^-) \equiv$ a 6-fold hodoscope trigger-matrix hit pattern consistent with two oppositely charged particles originating from the target.

They were all implemented with our existing low-level trigger matrix and logic subsystems.

TABLE AII.3. Results of Trigger Rate Study with 3 mm W Target

Trigger	Target	Protons/spill	Triggers/spill
$(3/4L\cdot R)\cdot E_{tot}$	In	3.4×10^{10}	1.9×10^4
$(3/4L\cdot R)\cdot E_{tot}$	Out	3.6×10^{10}	1.2×10^4
$(3/4L\cdot R)\cdot E_{tot}$	In	9.8×10^{10}	7.5×10^4
$(3/4L\cdot R)\cdot E_{tot}$	Out	1.4×10^{11}	7.0×10^4
$(3/4L\cdot R)\cdot E_{tot}\cdot(h^+h^-)$	In	2.6×10^{10}	1.2×10^3
$(3/4L\cdot R)\cdot E_{tot}\cdot(h^+h^-)$	Out	2.1×10^{10}	5.2×10^2
$(3/4L\cdot R)\cdot E_{tot}\cdot(h^+h^-)$	In	1.4×10^{11}	1.2×10^4
$(3/4L\cdot R)\cdot E_{tot}\cdot(h^+h^-)$	Out	1.3×10^{11}	6.7×10^3

We expect that the raw trigger rate of 1.2×10^4 per spill observed at 1.4×10^{11} protons/spill will increase to about 3×10^4 at 3×10^{11} incident protons/spill. Table AII.3 in-

dicates that about half of this rate is due to particles coming from the beam dump. They will be more efficiently rejected by the trigger matrix when the new, finer-grained Y1 hodoscope is installed (cf. Section III.6). We can also easily require two energy "clusters" in the calorimeter to remove the dominant background of high-energy single hadrons. But this rate is *already* well within the bandwith of our parallel, pipelined trigger processor, which requires only 10–20 μsec per event. In past running this processor has provided trigger rate reductions of 5–10 by utilizing the higher resolution wire chamber information to find pairs of oppositely charged tracks originating near the target. This will place the number of events per spill safely inside the anticipated capacity of the upgraded data buffer. If necessary, the processor is also capable of imposing tight mass cuts on these target-track pairs to reduce the data rate still further.

We are also planning to augment our data acquisition system with a silicon vertex track processor, mainly to reduce the amount of tapewriting and also the off-line computing load. The existing trigger processor architecture provides a natural avenue for one possible implementation. However, it is not anticipated that this information will be used in the trigger during the first run of P789. Rather, experience gained from this run will allow an optimal silicon vertex processor to be developed before the second run.

APPENDIX III. SILICON MICROSTRIP DETECTORS

1. Tests of Timing Resolution

To investigate the feasibility of latching a silicon microstrip array with one-RF-bucket time resolution, a detector was borrowed from the FNAL E761 Group and was equipped with 12 channels of LSI preamplifier recently developed by the FNAL Research Division. Tests in a LAMPF pion beam are currently underway. In preceding bench tests these preamps gave 24 mV outputs into a 130Ω stripline for pulser inputs simulating charge collection from minimum ionizing particles (4 fC). The output pulses had 8 ns risetime and returned to zero in 24 ns. They were subsequently amplified to ~2.2 V with a hybrid fast-timing amplifier (cf. ESN FTA 410/810), which provided additional shaping and shortened the time for return to baseline to < 20 ns (see Figure 15). A second pulse arriving 20 ns after an immediately preceding pulse efficiently refires the preamp-plus-amplifier. The MECL10K coincidence latches used for the E605/E772 hodoscopes have a coincidence resolution of 8 ns. Hence, there now appears to be a straightforward approach to single-bucket sensitivity for the silicon vertex array.

2. Radiation Damage of Silicon Detectors

Since P789 was first proposed we have uncovered more information germane to potential radiation damage of silicon detectors in our proposed high-rate environment. Several recent reports describe both radiation damage and subsequent annealing in silicon strip detectors.[39-42] The published damage factors and annealing rates agree within a factor of four. In November 1987, we placed a silicon strip detector near the beam in MEast, and exposed it to a total fluence of 2×10^{13} charged particles/cm^2. The observed noise levels and leakage currents versus exposure are in good agreement with the literature and support our assumptions concerning both the damage and annealing rates of silicon. In the following discussion we assume the worst-case reported damage constant ($\alpha = 9 \times 10^{-8}$ nA/cm).

The observation of annealing suggests that radiation damage may be substantially less serious than previously assumed. The published studies derive mainly from brief exposures to high-intensity beams over periods of several hours, while the irradiation of our detectors will be stretched over months. Furthermore, the room-temperature annealing results of Ohsugi *et al.*[42] imply that significant annealing will occur even while the irradiation takes place. During the course of the run there will also be scheduled and unscheduled "down times" during which the beam will be off and substantial annealing will occur. According

to Ohsugi *et al.*,[42] we can expect the radiation-induced leakage current to recover by $\sim 17\%$ during a 24-hour beam-off period. Recovery can be accelerated by elevating the temperature of the silicon during this time. It is thus quite possible that we will not have to replace any silicon wafers.

The associated leakage current leads mainly to a DC offset of the signal. The expected levels of DC-offset current ($\sim$ several $\times 10^{-7}$ A/strip) will not affect the performance of the preamp electronics, which will be AC-coupled with a small time constant. The rate at which high-frequency fluctuations of this offset current cause noise counts is small compared to the MHz per strip signal rate. Also, if necessary, the ambient leakage current can be reduced by an order of magnitude by cooling the silicon to 0°C.

Potential radiation damage of the preamps also requires consideration. Use of LSI technology in the preamp design (as opposed to the hybrid technology generally used in the past) reduces the area and therefore the particle fluence per device on the chip. The transistors will not be exposed to fluxes above the damage threshold for bipolar devices during the proposed P789 running period.[43]

APPENDIX IV. P-NUCLEUS DIHADRON CROSS SECTIONS

The dihadron yields from our February '88 test run have been combined with a careful Monte Carlo simulation of the corresponding spectrometer configuration to yield absolute cross sections. These cross sections compare very reasonably with information available on dihadron yields at other energies. We felt that confusion arising from apparent incompatibility of Figures 2 and 3 of Kephart *et al.*[30] warranted dissemination of our test measurements. A draft version of a paper on our results (to be submitted for publication) is included below. We now know the absolute dihadron yield at 800 GeV to better than a factor of two. Since the singles rates, trigger rates, and dihadron yields relevant to P789 were measured in a configuration similar to that proposed, the uncertainty in those rates is even less.

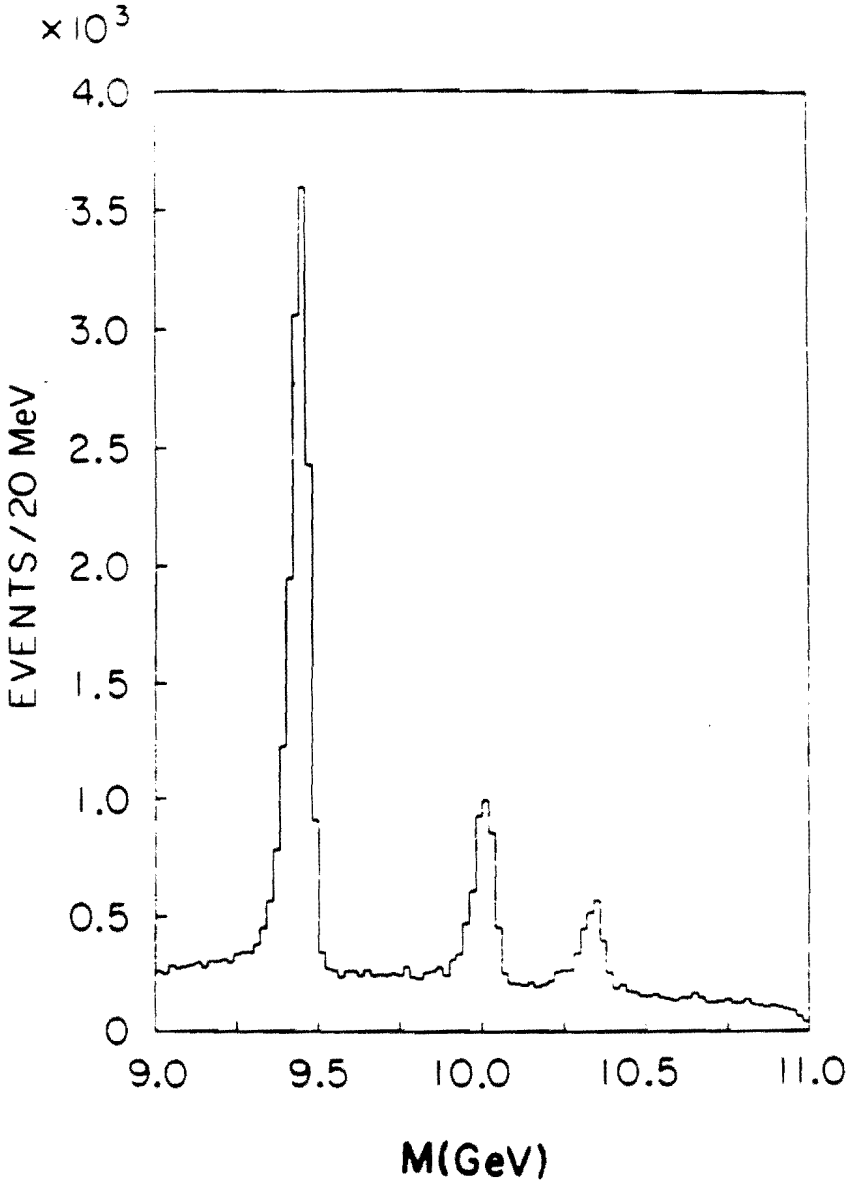

FIG. 1a. Dimuon mass spectrum from E605.

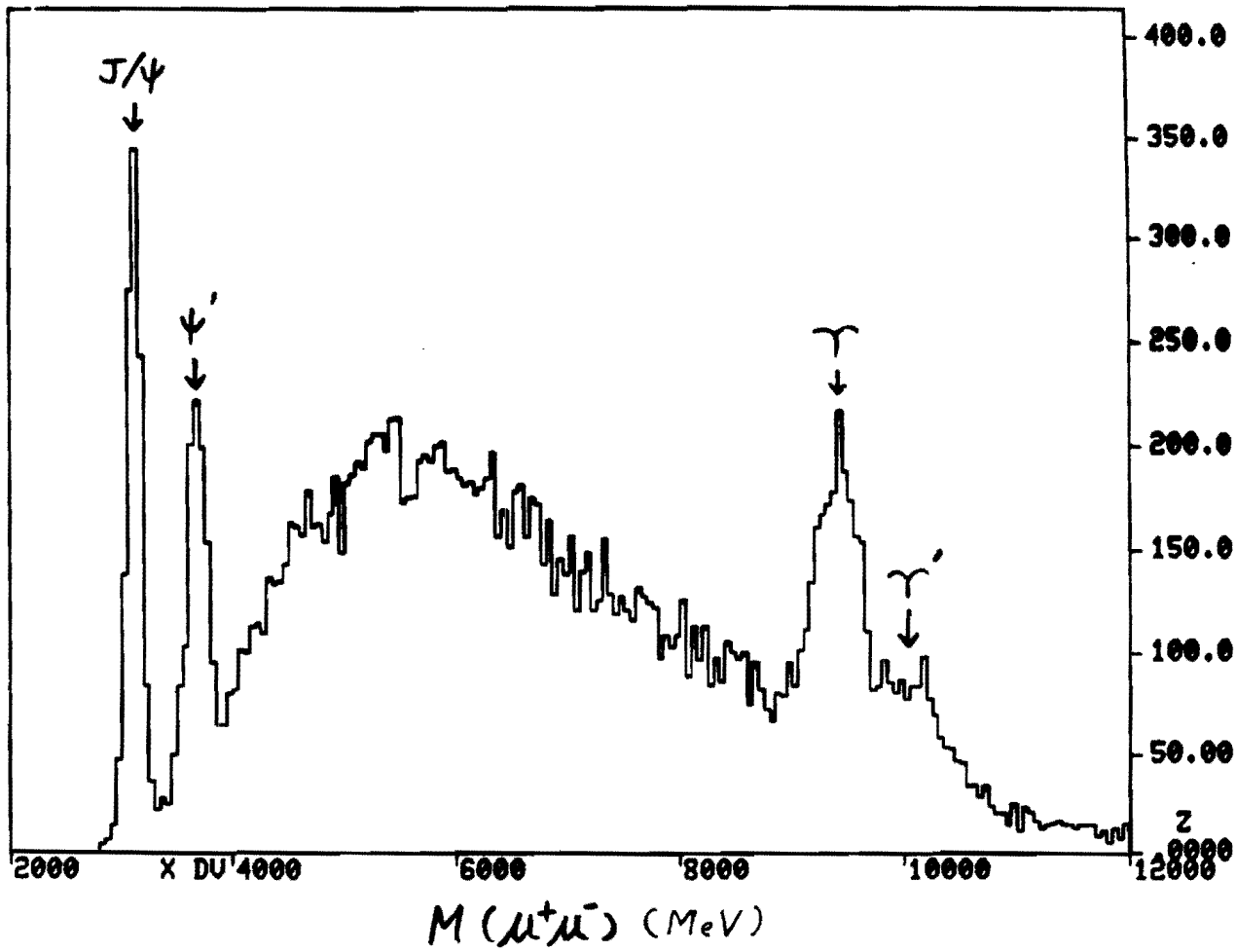

FIG. 1b. Dimuon mass spectrum for E772.

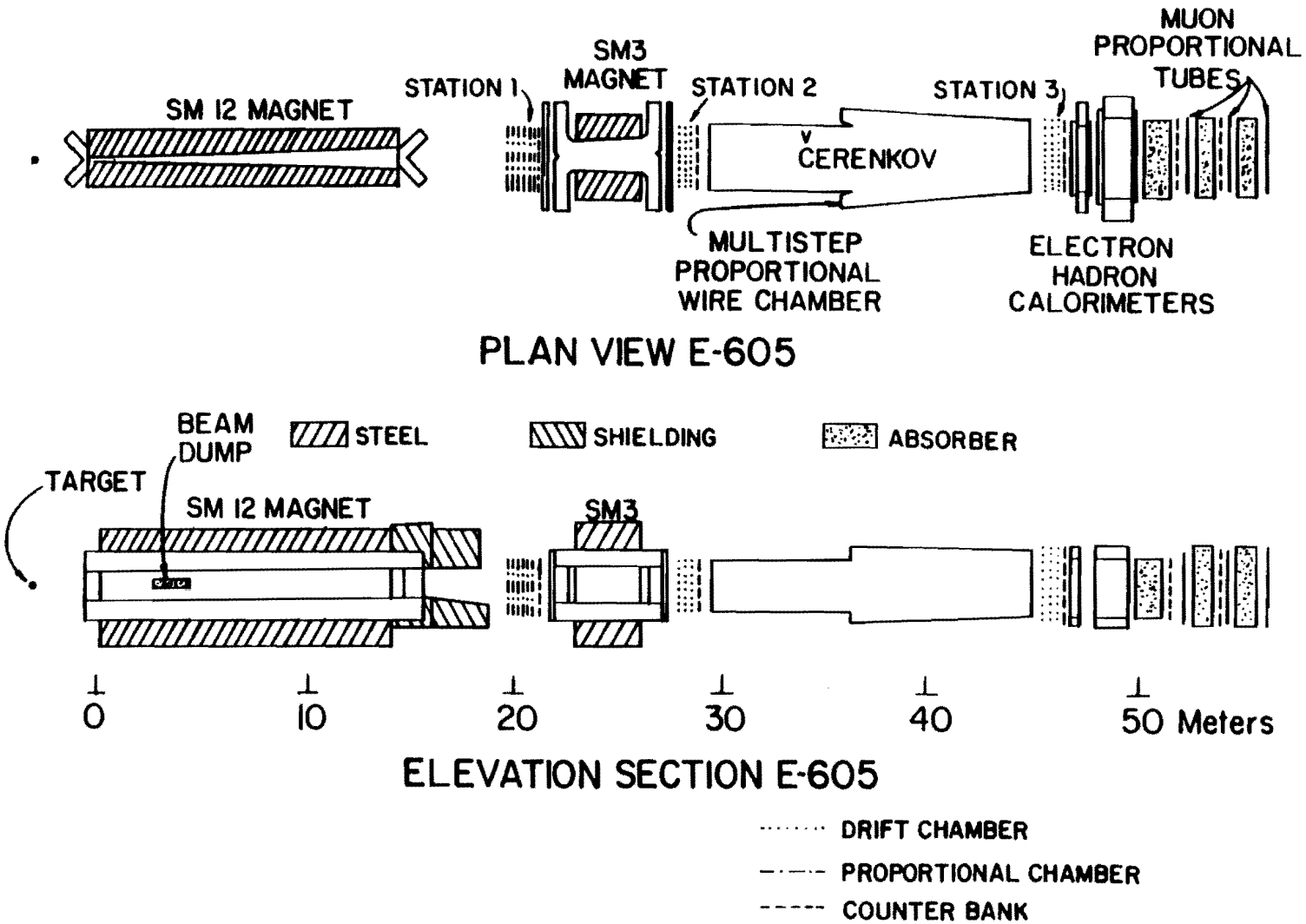

FIG. 2. Schematic diagram of E605/E772 spectrometer.

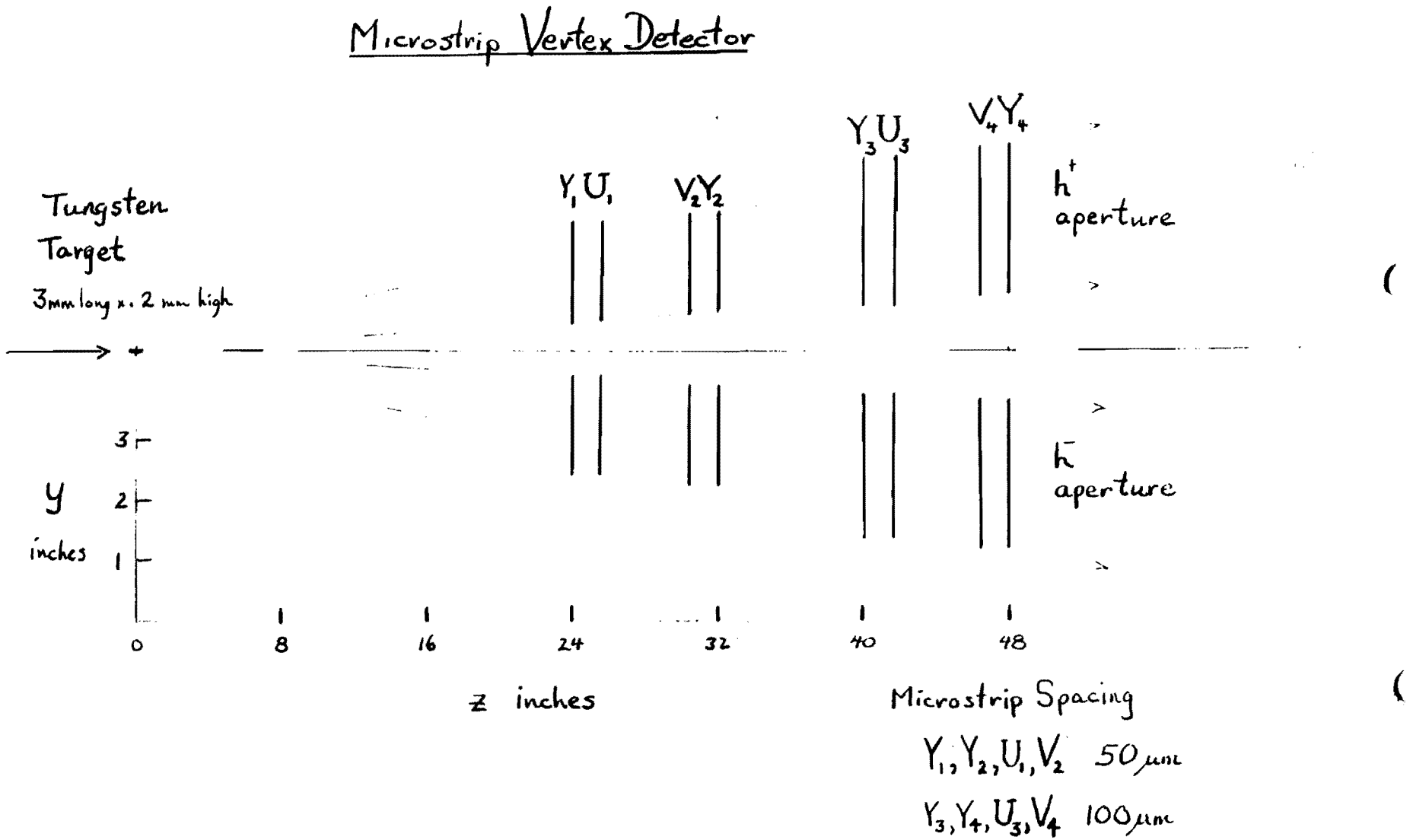

FIG. 3. Proposed configuration of silicon detectors.

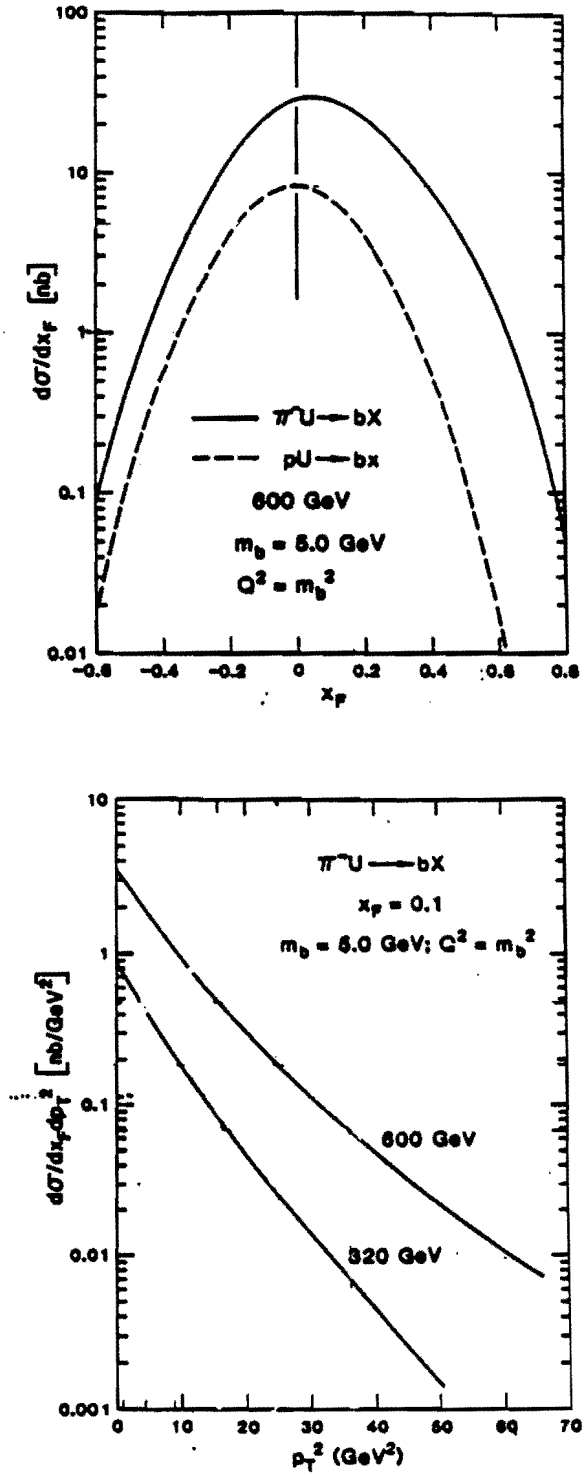

FIG. 4. Predicted x_F and p_t distributions for b production (Ref. 23).

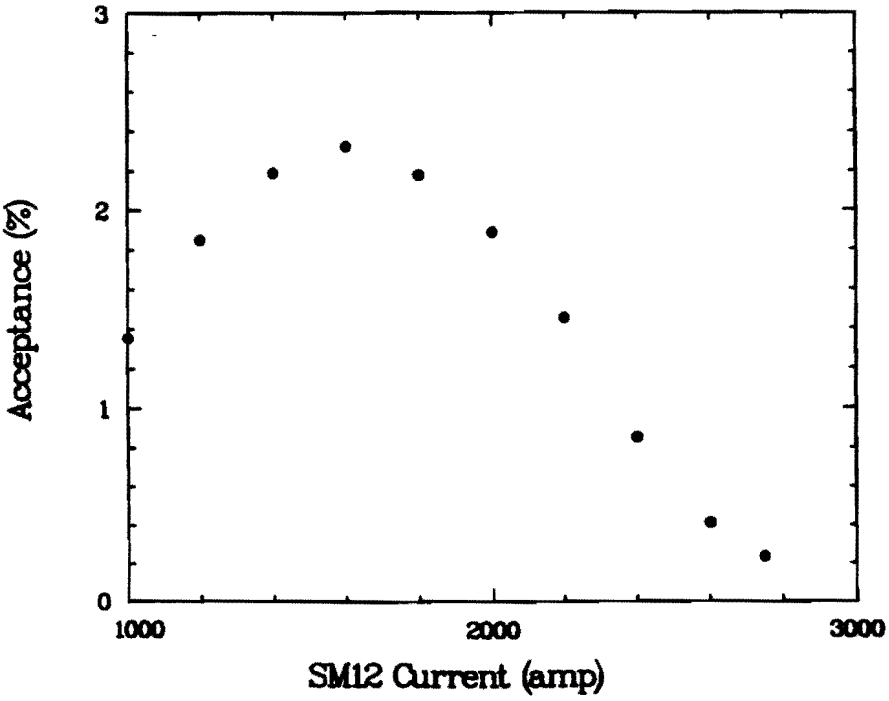

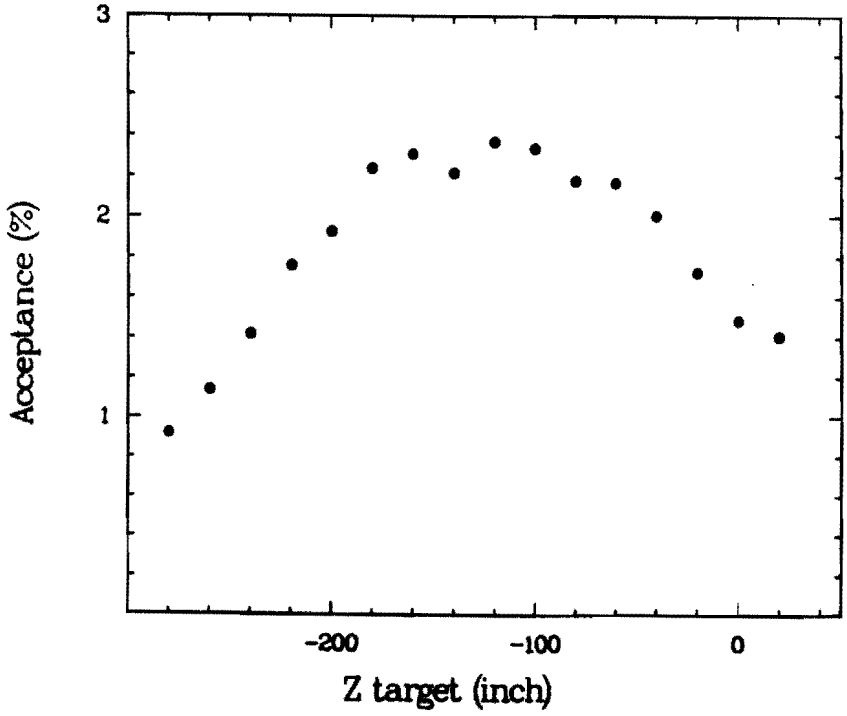

FIG. 5. Spectrometer acceptance as a function of (a) SM12 current, (b) target location.

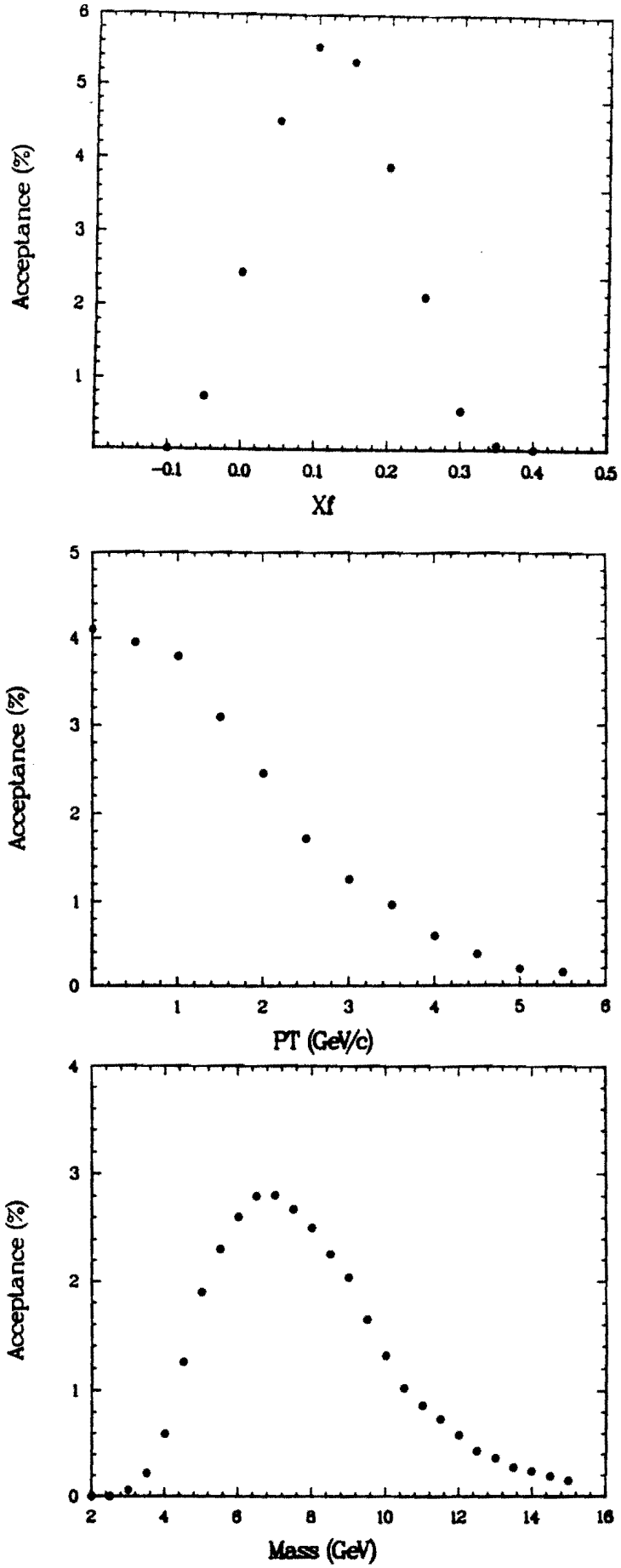

FIG. 6. Spectrometer acceptance as a function of (a) x_F, (b) p_t, and (c) dihadron mass.

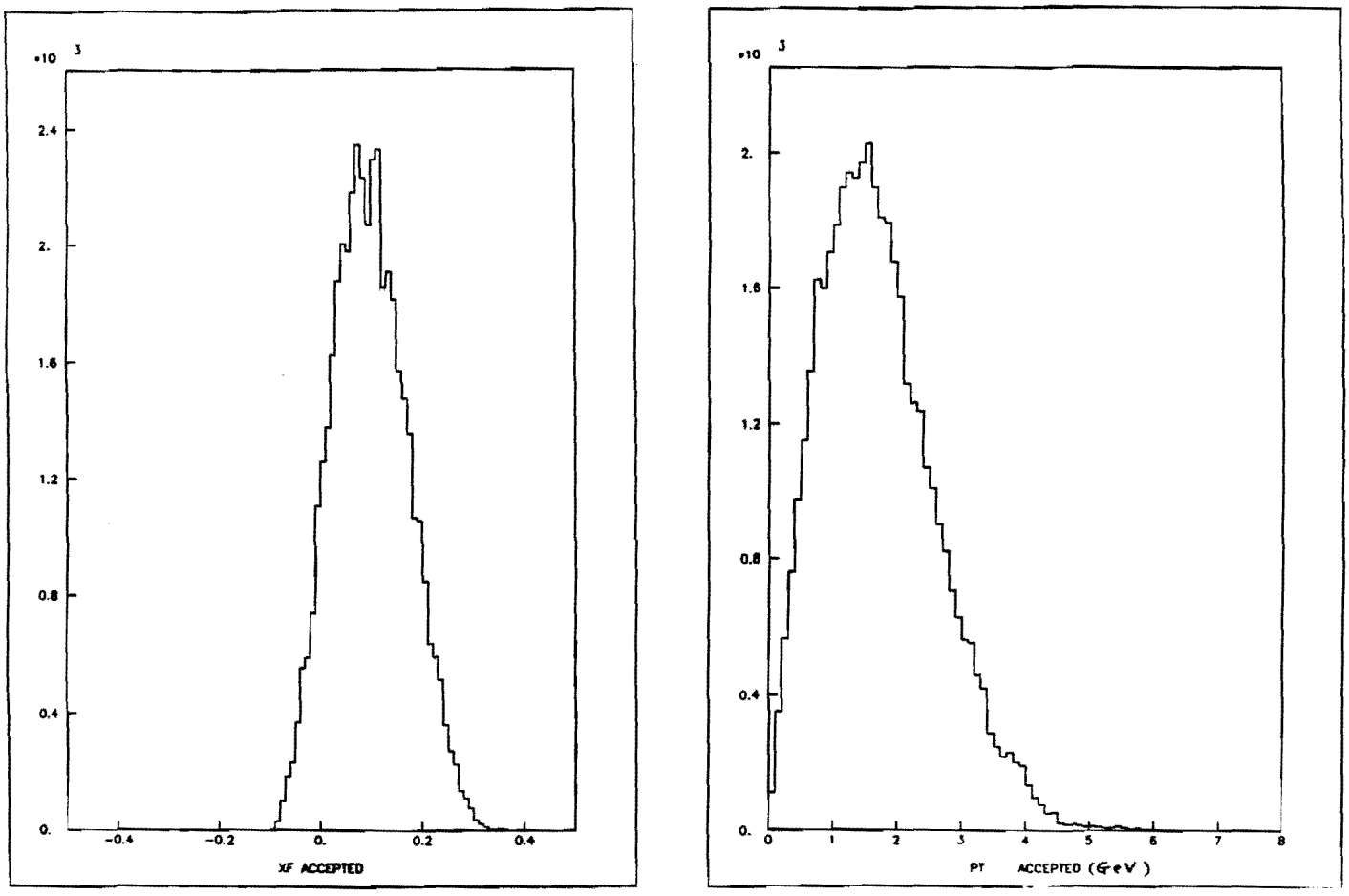

FIG. 7. Distribution of accepted B events vs. (a) x_F and (b) p_t.

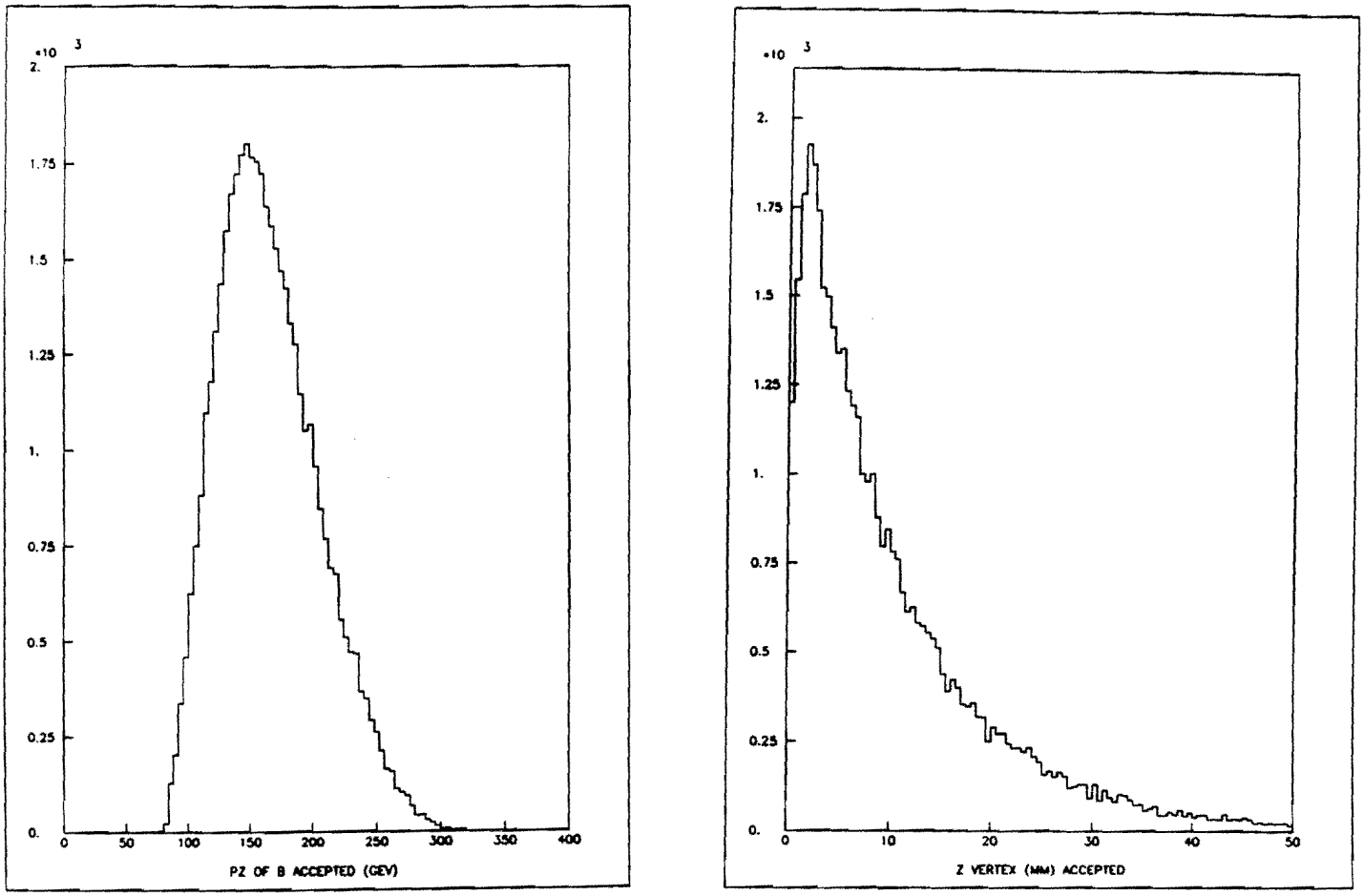

FIG. 8. Distribution of accepted B events vs. (a) P_z and (b) decay z_{vertex}.

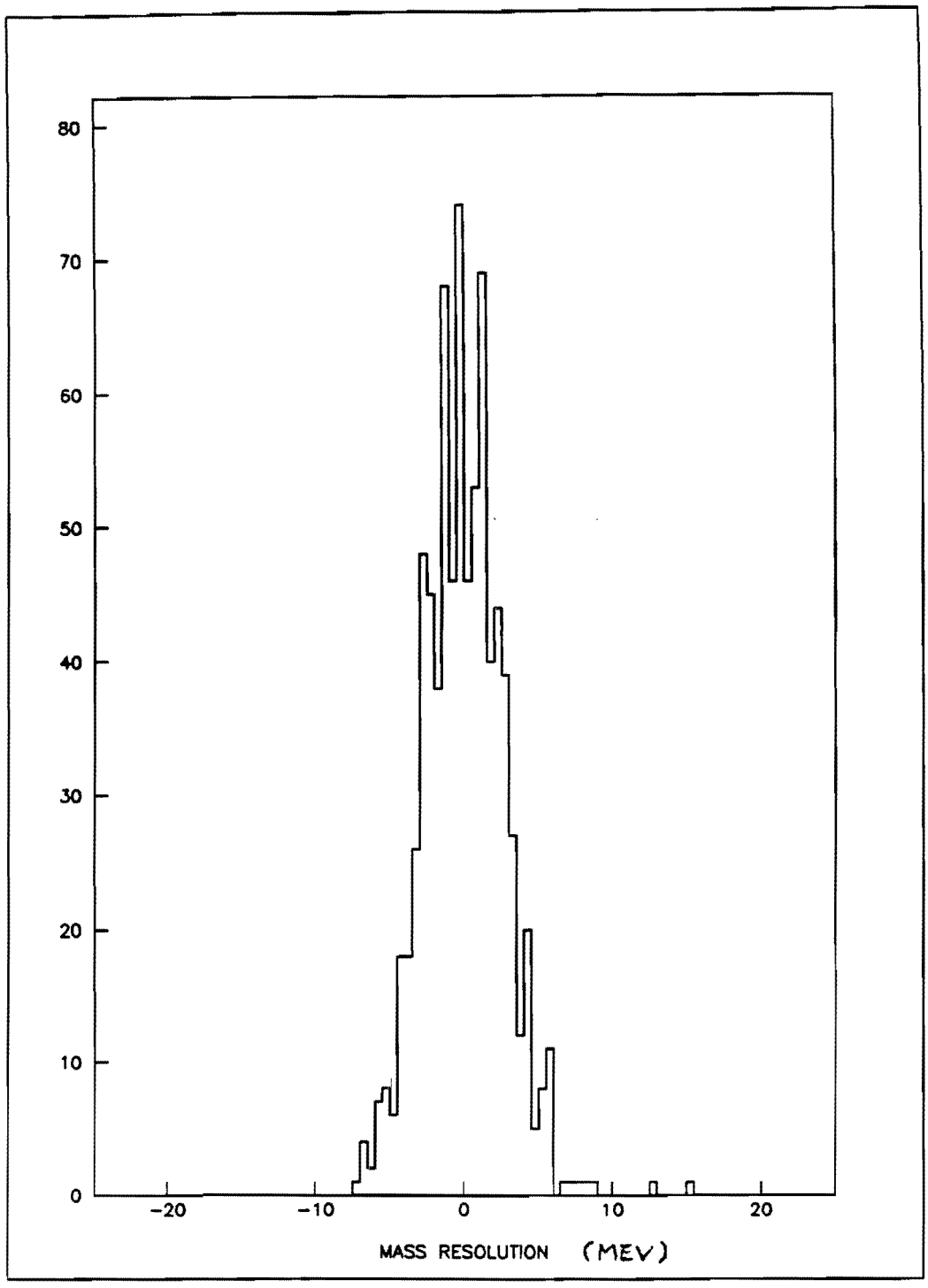

FIG. 9. Mass resolution for accepted B events.

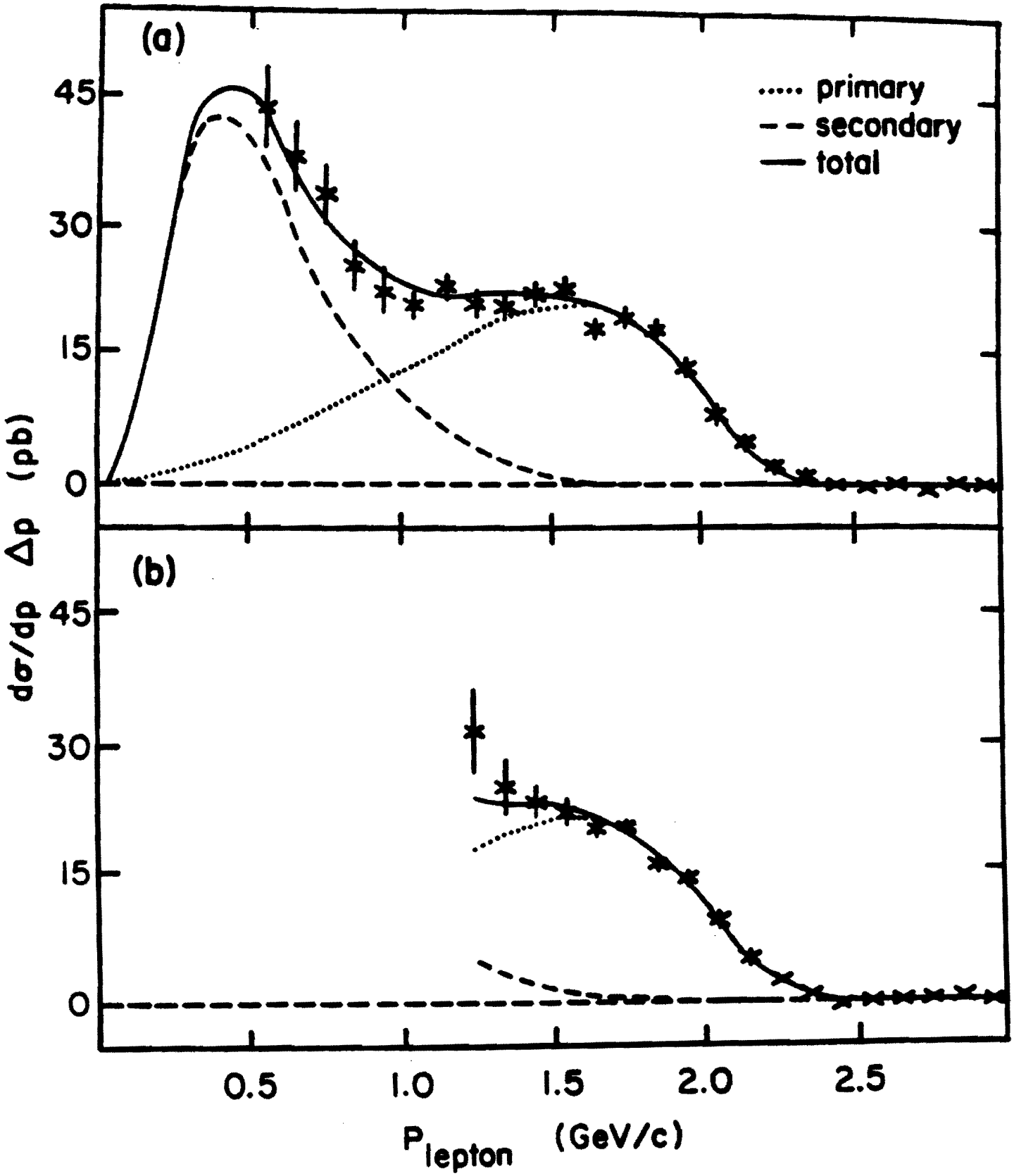

FIG. 10. Inclusive lepton spectrum for (a) electrons and (b) muons from the CLEO Collaboration (Ref. 27).

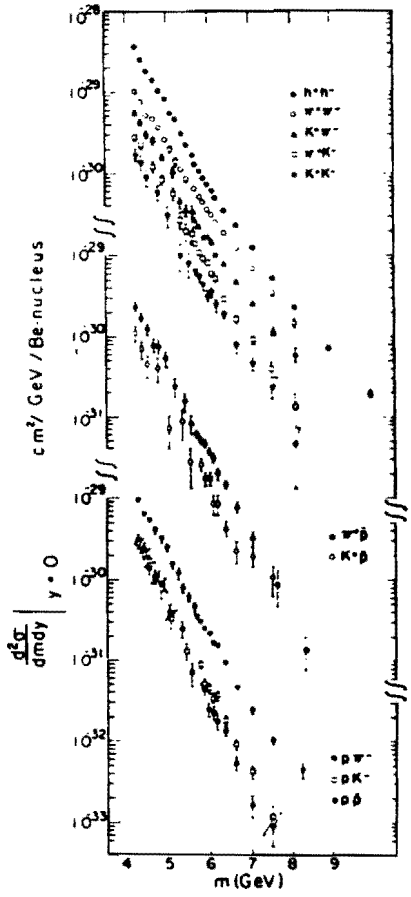

FIG. 2. The dihadron production cross sections $d^2\sigma/dm\,dy|_{y=0}$ for hadrons and identified pairs of opposite charge vs mass m. The data are averaged over their rapidity acceptance which is peaked at $y \approx 0$ and includes the interval $-0.2 \leq y \leq 0.3$.

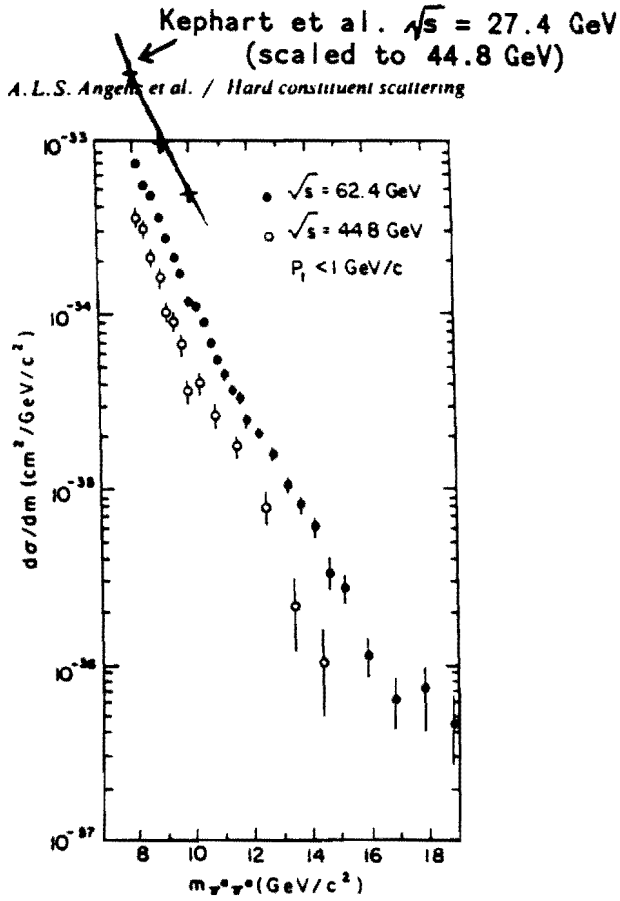

Fig. 5. $d\sigma/dm$ (as defined in eq. (1)) versus m for events with $P_T < 1.0$ GeV/c.

FIG. 11. Dihadron cross sections measured at FNAL (Refs. 30,31) and ISR (Ref. 32).

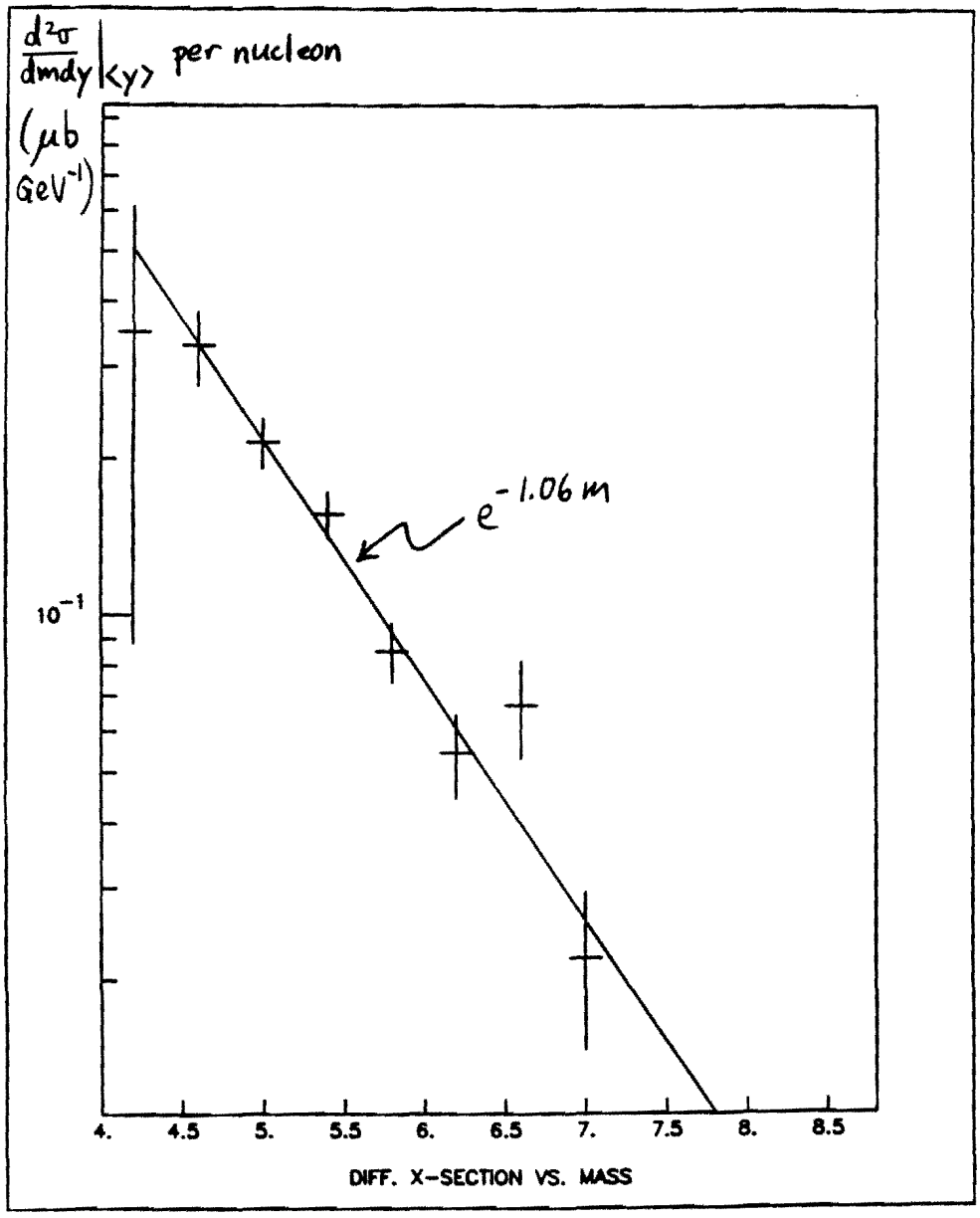

FIG. 12. Dihadron cross section measured in our February '88 test run.

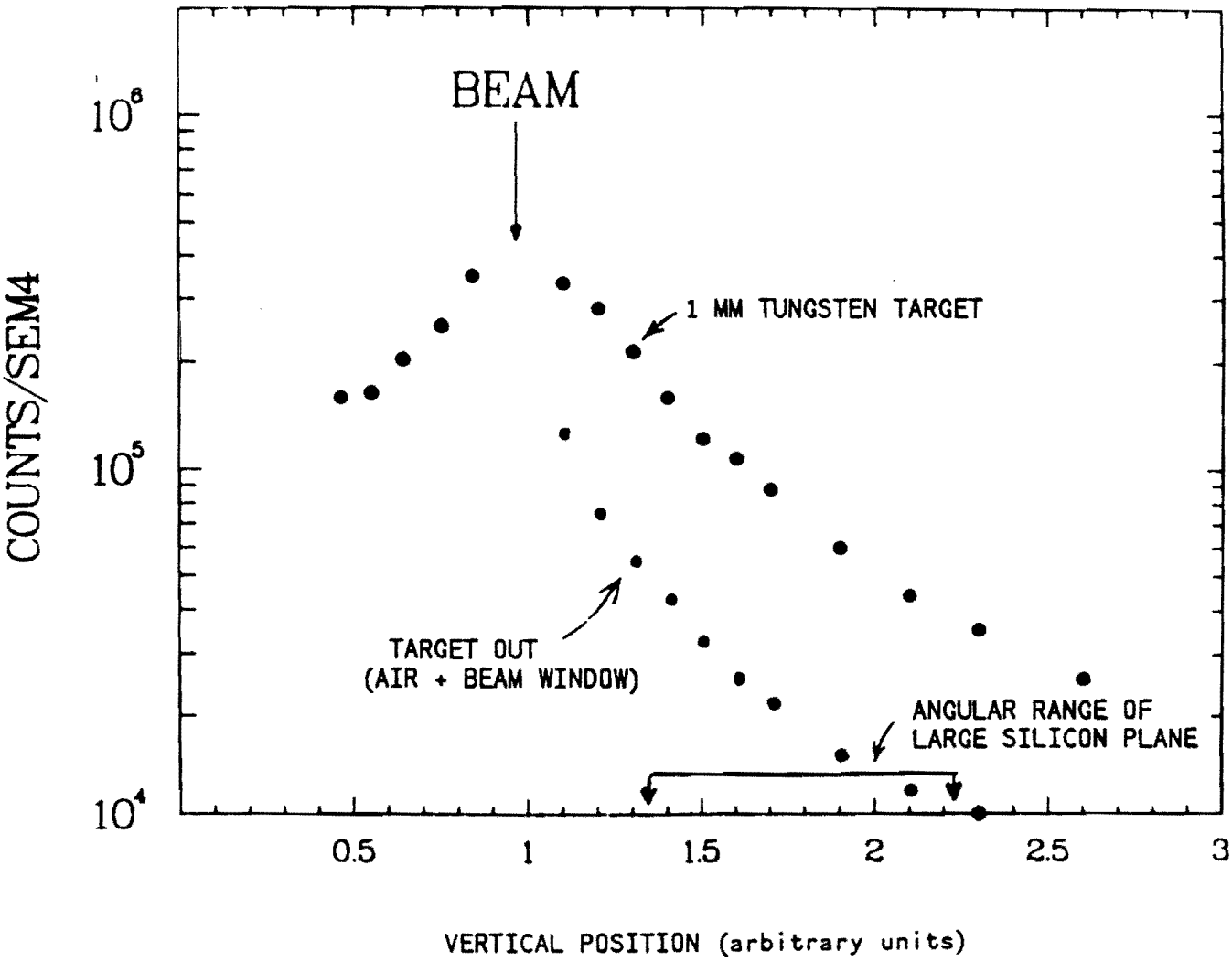

FIG. 13. Count rate in finger scintillator as a function of its vertical position.

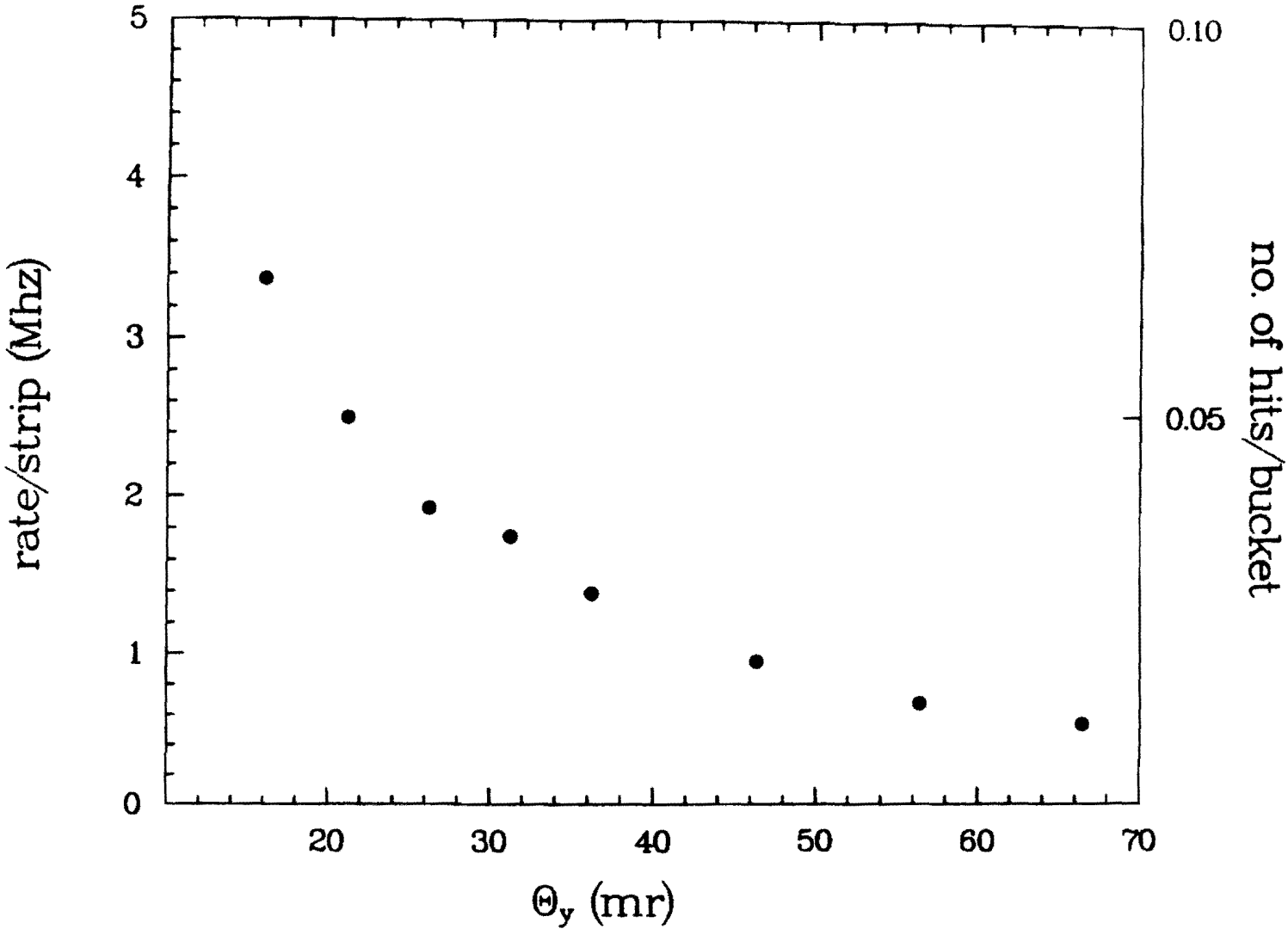

FIG. 14. Estimated rate/Si strip as a function of vertical angle θ_y.

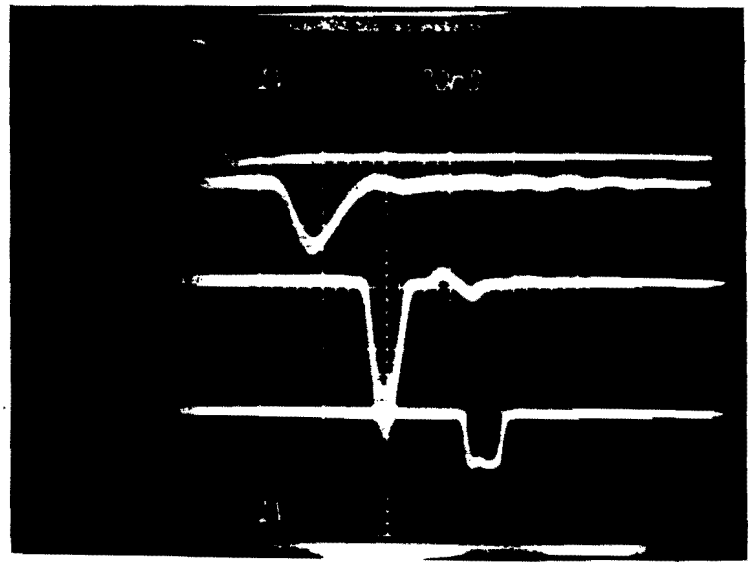

FIG. 15. Silicon detector preamplifier and amplifier output pulses, from pulser tests with an injected charge approximating minimum ionizing particles. (a) single pulse, (b) two pulses, 20 nsec apart.

DRAFT 9/26/88

Comment on Scaling of the Massive-Dihadron Cross-Section

D. M. Kaplan, R. Guo
Northern Illinois University

C. N. Brown, W. E. Cooper
Fermi National Accelerator Laboratory

M. J. Wang
Case Western Reserve University

T. A. Carey, M. J. Leitch, P. L. McGaughey
C. S. Mishra, J. M. Moss, J. C. Peng
Los Alamos National Laboratory

M. L. Barlett, G. W. Hoffmann
University of Texas

In the late 1970's, the Columbia-Fermilab-Stony Brook (CFS) group studied the production of pairs of high-transverse-momentum hadrons in collisions of 200-, 300-, and 400-GeV protons with beryllium and tungsten targets,[1-4] and the Columbia-CERN-Oxford-Rockefeller (CCOR) group studied production of π^0 pairs at the ISR.[5] Recently, in the process of designing an experiment to measure B-meson decays for which the dihadron continuum constituted an important background, we have taken additional dihadron data using 800-GeV protons incident on a tungsten target. We here compare these new data with the lower-energy CFS and higher-energy CCOR samples. We find that the CFS scaling relationship is borne out at the higher energy, but that one of the CFS publications[1] contains a misleading figure.

We utilized the Fermilab E605/772 spectrometer (Figure 1), the details of which have been published previously[6]. For this test run, we added a collimator at the exit of the "SM12" analyzing magnet, composed of 24" of copper followed by 48" of borated polyethylene, that restricted the vertical aperture to ± 10". 2.5×10^{10} protons per 20s beam pulse were incident on the face of a tungsten-disk target of thickness 3mm and diameter 3". Since the diameter of the target was much larger than the size of the beam, the targetting efficiency was 100%.

The beam flux was monitored by means of a secondary emission monitor (SEM) located in the beam line upstream of the target. The SEM has been calibrated several times in the last five years by comparing the SEM rate to the rate of production of ^{24}Na in copper foils; the calibration is found to be stable within $\pm 5\%$. Integrated proton fluxes are derived using a cross-section[7] per Cu nucleus of 3.9 mb for the production of ^{24}Na. Note that the published CFS cross-sections were based on a 10% lower value measured at

Brookhaven[8], since measurements at Fermilab energies were not then available. We use this older value when comparing our results to those of CFS.

Events satisfying a trigger condition were written to tape. The trigger required at least 60 GeV of energy-deposition in the hadron calorimeter and coincident hits in three out of four hodoscope planes both on the left and right sides of the vertical centerline of the spectrometer.

For 1.2×10^{11} incident protons and 43,922 events written to tape, 3404 were found to contain two oppositely-charged hadron tracks after track reconstruction. These tracks were traced back through the magnetic field of SM12, and fiducial cuts were imposed to eliminate tracks passing too close to shielding material. 2516 pair events survived these fiducial cuts. Additional cuts were made on the vertical and horizontal positions at the target, to eliminate events due to upstream vacuum windows or the downstream beam dump. 448 events survived these target cuts. For each track pair, the point of intersection was then computed in the y-z (magnetic bend) view and the x-z (non-bend) view. Figure 2 shows the distribution of these points along the z axis (incident beam direction) in the two views. The target is seen clearly in both views. Figure 3 shows the mass and pair-p_t distributions of these events, and Figure 4 shows the pair-p_t distribution in two bins of mass: 5-6 GeV and 6-7 GeV.

Our efficiencies for recording and reconstructing these events are all high. Electronic dead time caused a 13.7% loss of beam. The trigger allowed any one of four hodoscope elements to be missing on each of the right and left sides, and the hodoscope counter efficiencies were all over 95%, so we make no correction for trigger counter efficiency. The calorimeter energy threshhold was well below the geometric turnon of the magnetic spectrometer acceptance (the lowest observed total momentum of a target-originated hadron pair was 90 GeV), so we make no correction for calorimeter trigger efficiency. The track reconstruction allowed up to seven of the 18 chamber planes to be missing (not more than three at any one of the three measurement stations), and the chamber efficiencies were all over 90%. The most likely number of planes per track was observed to be 17 and the measured reconstruction efficiency was 0.997 per track. We make no correction for tracking efficiency. At an early stage of analysis, events containing more than two tracks were eliminated from the data sample, amounting to 6% of events having two or more tracks. Since many of these events were probably not of target origin, we correct our cross-sections upwards by 3% and assign a $\pm 3\%$ error contribution on the overall normalization to this source.

We compute the spectrometer acceptance by Monte Carlo simulation, using a dihadron production model which has been iterated to agree with the observed distributions. To convert these distributions into cross-sections nevertheless requires some knowledge of the production distributions in regions not covered by our spectrometer. Figure 5 shows the spectrometer acceptance vs. mass, pair-p_t, rapidity, and dihadron-rest-frame polar angle. Like the CFS spectrometer, the E605/772 spectrometer covers only narrow regions in

rapidity and polar angle, and its acceptance falls rapidly with increasing pair-p_t. We therefore follow the CFS convention and report cross-sections averaged over our rapidity interval, and we make the conventional assumption, appropriate to the production and decay into dihadrons of a hypothetical resonance, of isotropic distribution in dihadron polar angle. Since the acceptance vs. mass depends on the assumed p_t production distribution (larger for a narrow p_t distribution and smaller for a broad one), we consider first the invariant differential dihadron cross-section vs. pair-p_t, which does not suffer from this model-dependence. Figure 6a shows this cross-section in two bins of mass.

To compare with 400-GeV CFS cross-sections per beryllium nucleus, we scale according to the linear nucleon-number (A) dependence which CFS observed.[2,4] We correct for our higher beam energy according to the CFS fit to the beam-energy dependence[4] $\sigma \propto (1 - m/\sqrt{s})^{13.0 \pm 0.4}$. Figure 7 compares the resulting cross-sections with those of Reference 1, Figure 3. The agreement is quite good, verifying the p_t dependence observed by CFS as well as the s and A dependences.

We use a parametrization[9] of the observed CFS p_t dependence to compute the acceptance vs. mass (Figure 5). Figure 6b gives the cross-section $d^2\sigma/dmdy$, averaged over our rapidity interval $-0.26 < y < 0.46$. In Figure 8, we compare this cross-section, scaled as above for the s and A dependence, with that of Reference 1, Figure 2. The scaled 800-GeV data are in substantial disagreement with the CFS 400-GeV cross-section (lower by a factor ranging from 10 at low mass to 3 at high mass).

We also compare these results to those of the CCOR group.[5] They measured the production of pairs of π^0's in proton-proton collisions at $\sqrt{s} = 44.8$ and 62.4 GeV at the ISR. They report a cross-section differential in mass and rapidity and integrated over the range $p_t < 1.0$ GeV, $-0.4 < \cos\theta^* < 0.4$. Their observed $\cos\theta^*$ dependence is parametrized as $dN/d\cos\theta^* \propto (1 - \cos\theta^*)^{-a} + (1 + \cos\theta^*)^{-a}$, with $a = 2.97 \pm 0.05$, independent of mass and $\sqrt{s}$. We use this fit to extrapolate our cross-section to their $\cos\theta^*$ range. The result is shown in Figure 9, plotted in the CCOR scaling form $m^{6.5} d^2\sigma/dmdy$, along with the CCOR data. The agreement is reasonably good, considering the differing initial and final states and center-of-mass energies involved.

Finally, we compare our data with preliminary results from Fermilab E711.[10] Figure 10 shows that the agreement with their data is quite reasonable, and in addition shows impressive agreement with the leading-log QCD calculation of Duke and Owens.[11]

The new data confirm that the dihadron cross-section near $y = 0$ and $p_t = 0$ shows a simple scaling behavior with energy. The results differential in pair-p_t should have the smallest systematic normalization uncertainty, which we estimate to be $\pm 20\%$. Attempts to integrate this cross-section over pair-p_t are sensitive to regions of large p_t not yet measured experimentally, which may help to explain the large discrepancy seen in Figure 8.

References

1. R. D. Kephart *et al.*, Phys. Rev. Lett. 39, 1440 (1977).

2. R. L. McCarthy *et al.*, Phys. Rev. Lett. 40, 213 (1978).

3. R. J. Fisk *et al.*, Phys. Rev. Lett. 40, 984 (1978).

4. H. Jöstlein *et al.*, Phys. Rev. D 20, 53 (1979).

5. A. L. S. Angelis *et al.*, Nucl. Phys. B209, 284 (1982).

6. Y. B. Hsiung *et al.*, Phys. Rev. Lett. 55 457, (1985); J. A. Crittenden *et al.*, Phys. Rev. D 34 2584, (1986) ; D. M. Kaplan, "Production of Hadrons and Leptons at High p_t and Pairs at High Mass", in **Proceedings of the Seventh Vanderbilt Conference on High Energy Physics**, Nashville, TN, May 1986.

7. S. Baker *et al.*, Nucl. Instr. Meth. 222, 467 (1984).

8. J. Hudis *et al.*, Phys. Rev. 129, 434 (1963) and J. B. Cumming *et al.*, Phys. Rev. C 14, 1554 (1976).

9. $dN/dp_t \propto p_t\ e^{-[p_t^2/b(m)]}$, $b(m) = 1.27(0.16m^2 - 1.23m + 3.48)^2$.

10. K. Turner *et al.*, 1988 APS-DPF Meeting, Storrs, CT, August 1988.

11. D. W. Duke and J. F. Owens, Phys. Rev. D 30, 49 (1984).

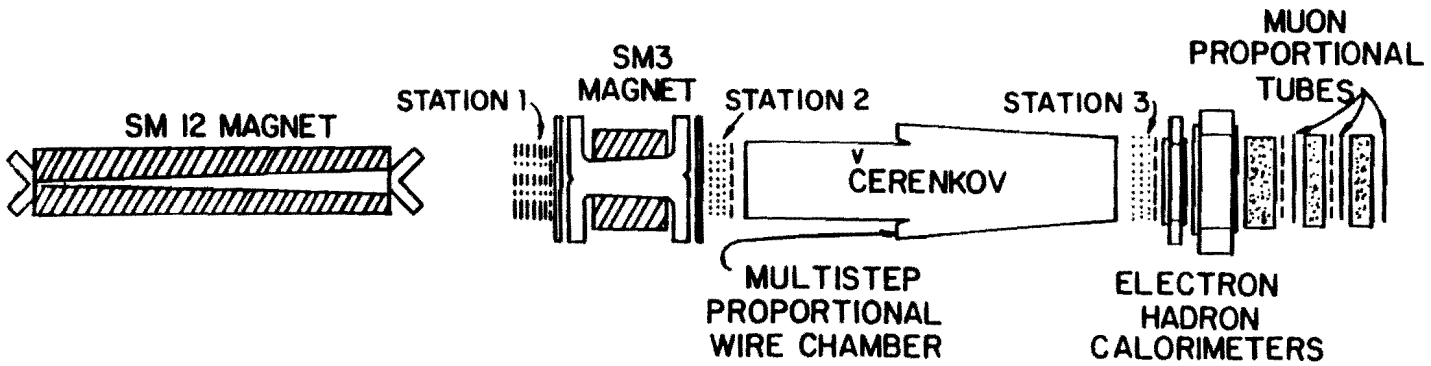

PLAN VIEW E-605

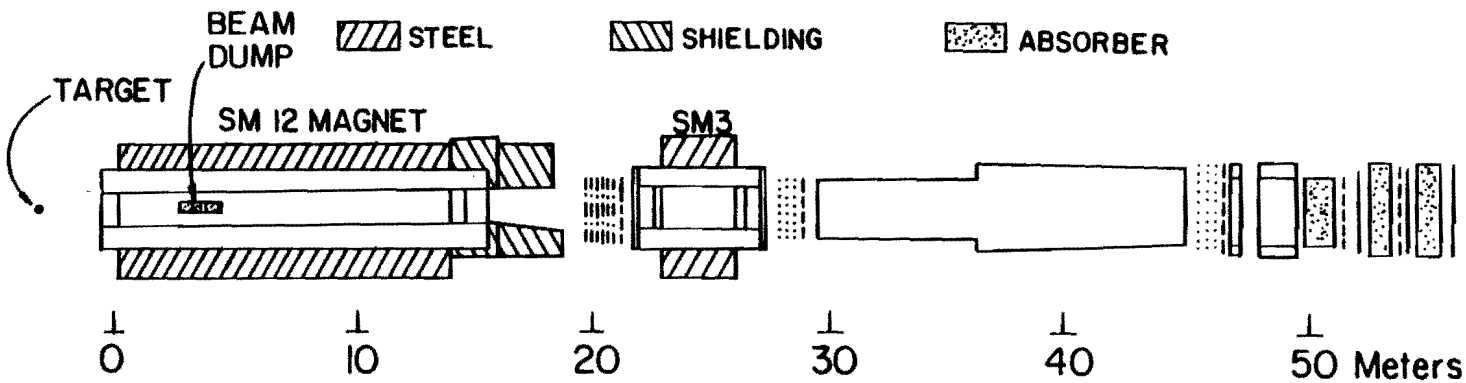

ELEVATION SECTION E-605

····· DRIFT CHAMBER

-·-·- PROPORTIONAL CHAMBER

----- COUNTER BANK

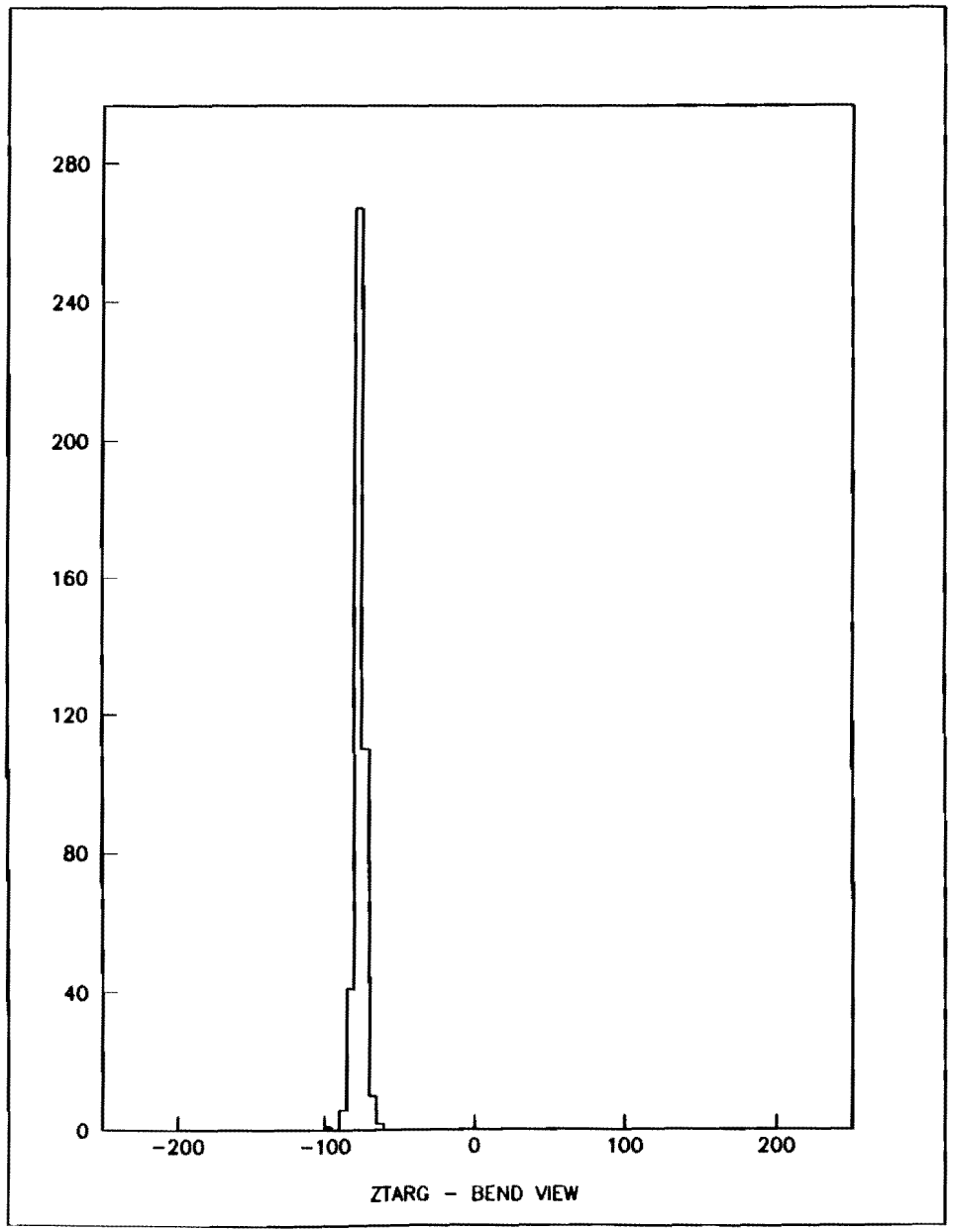

Fig. 2a

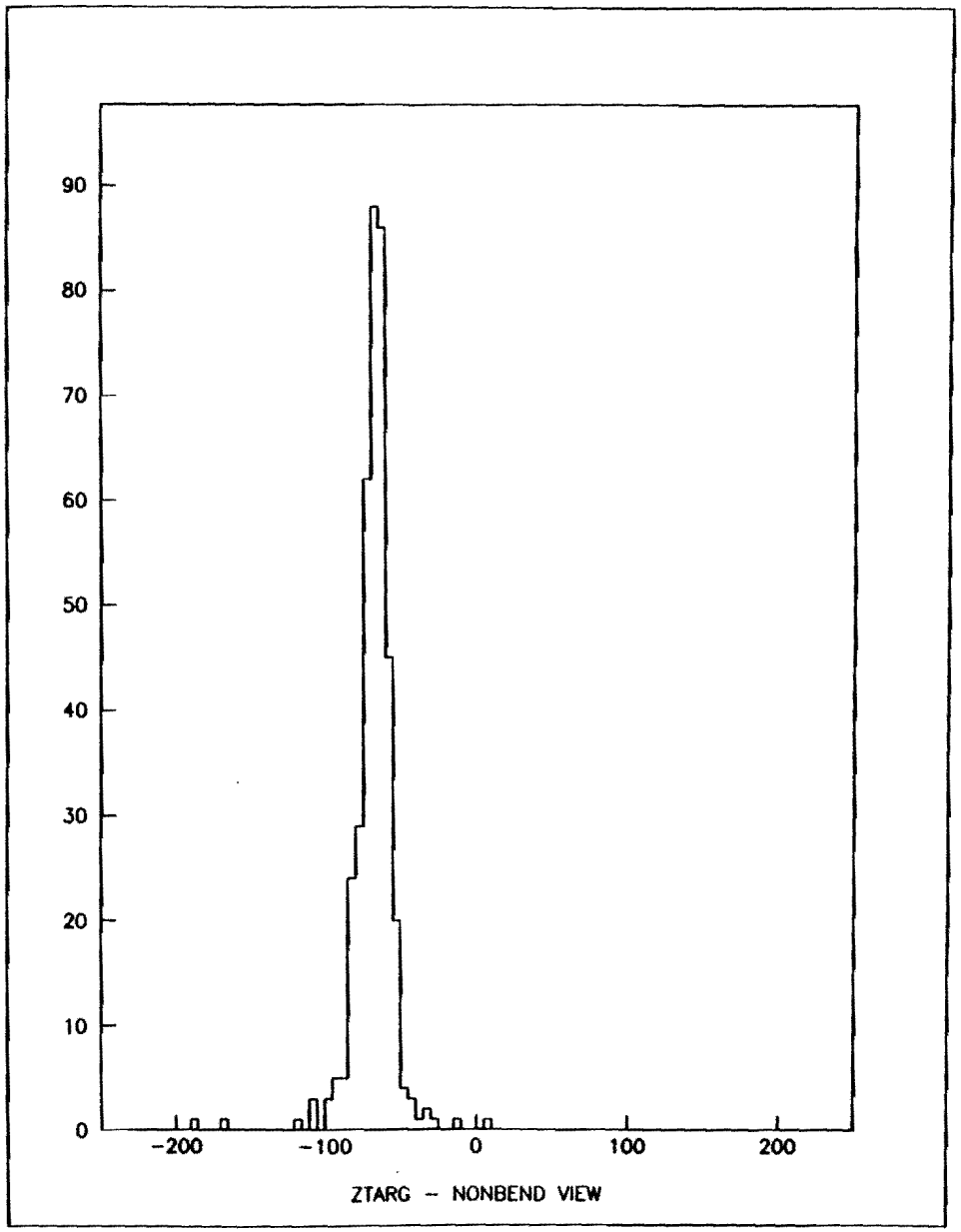

Fig. 2b

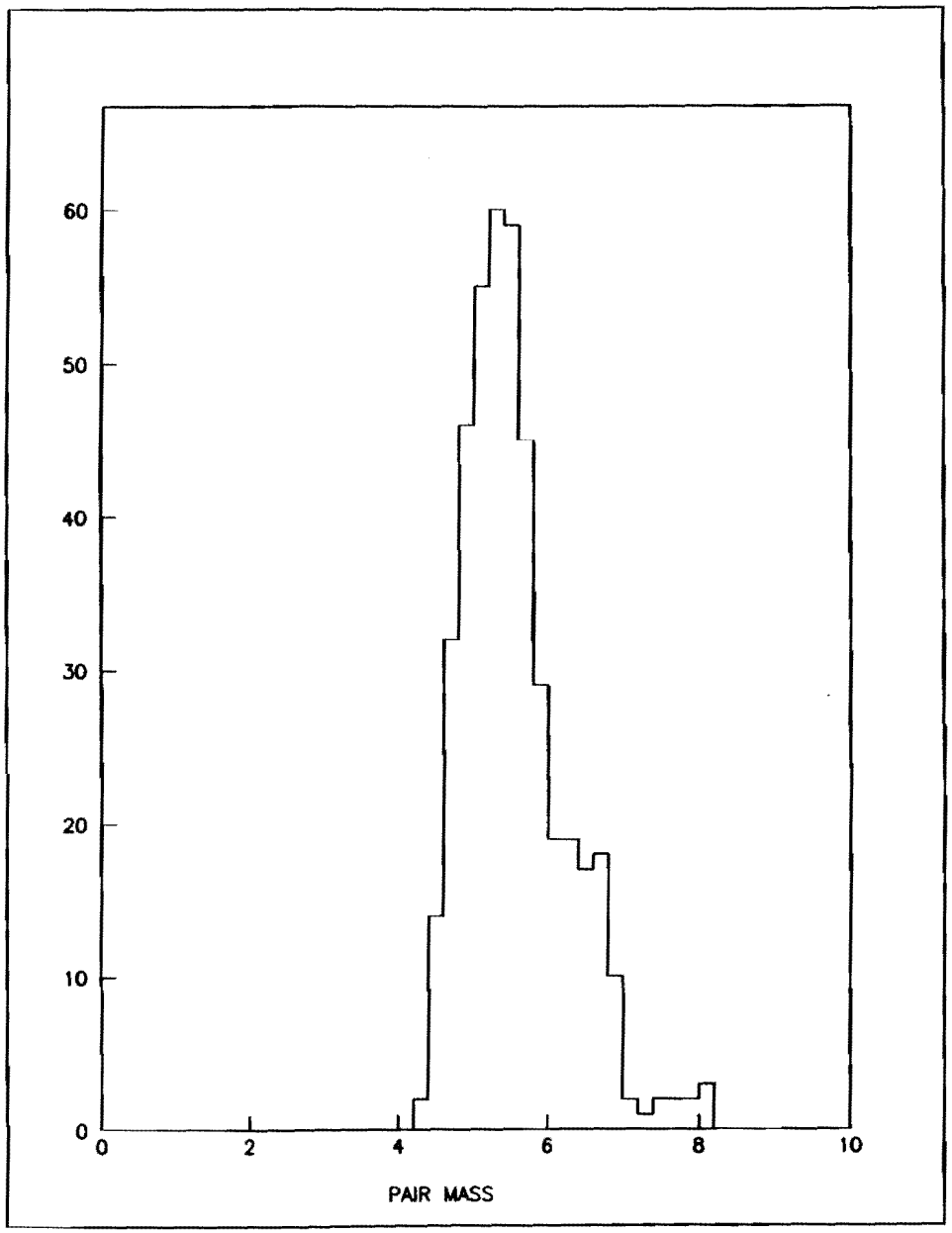

Fig 3a

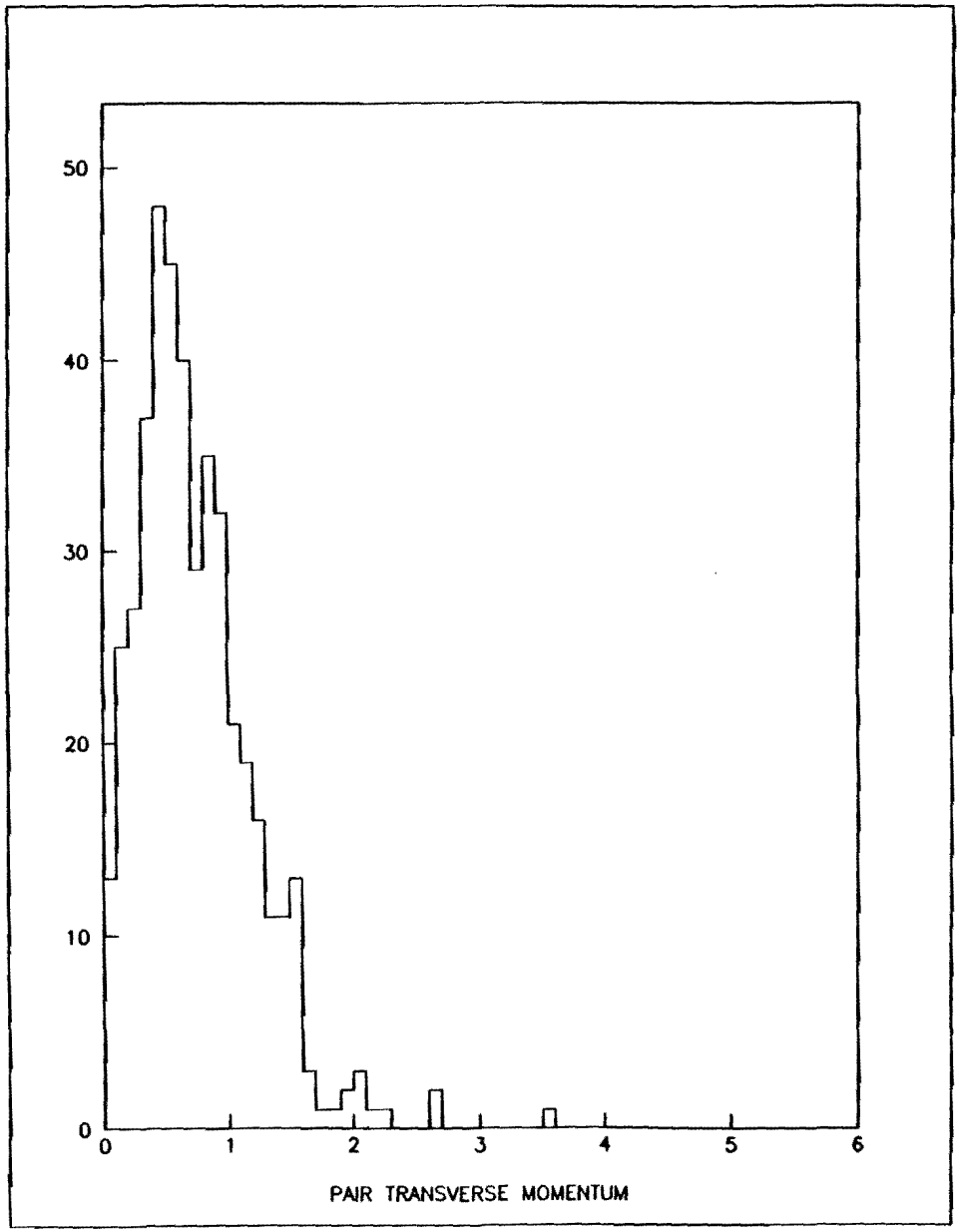

Fig 3b

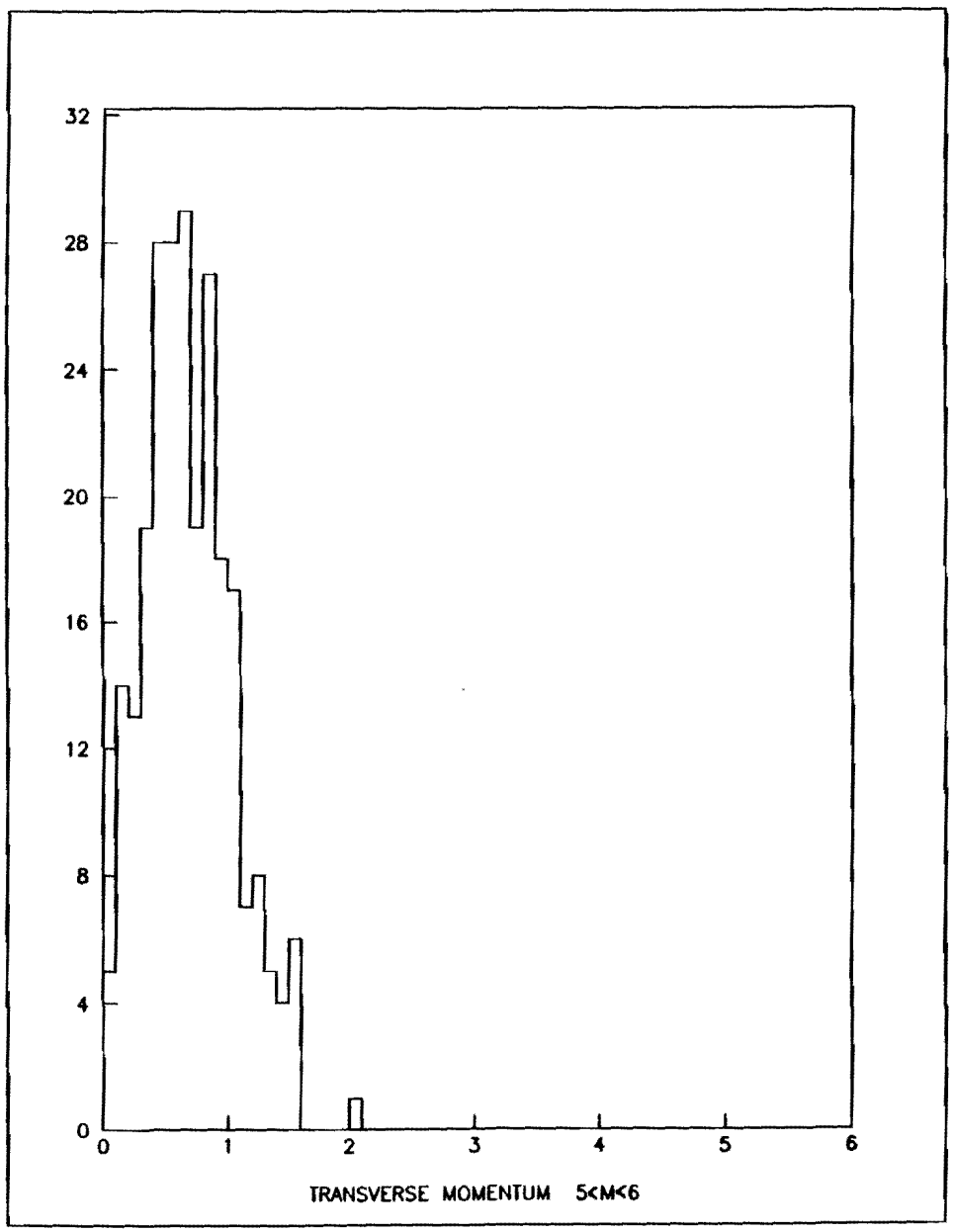

Fig 4a

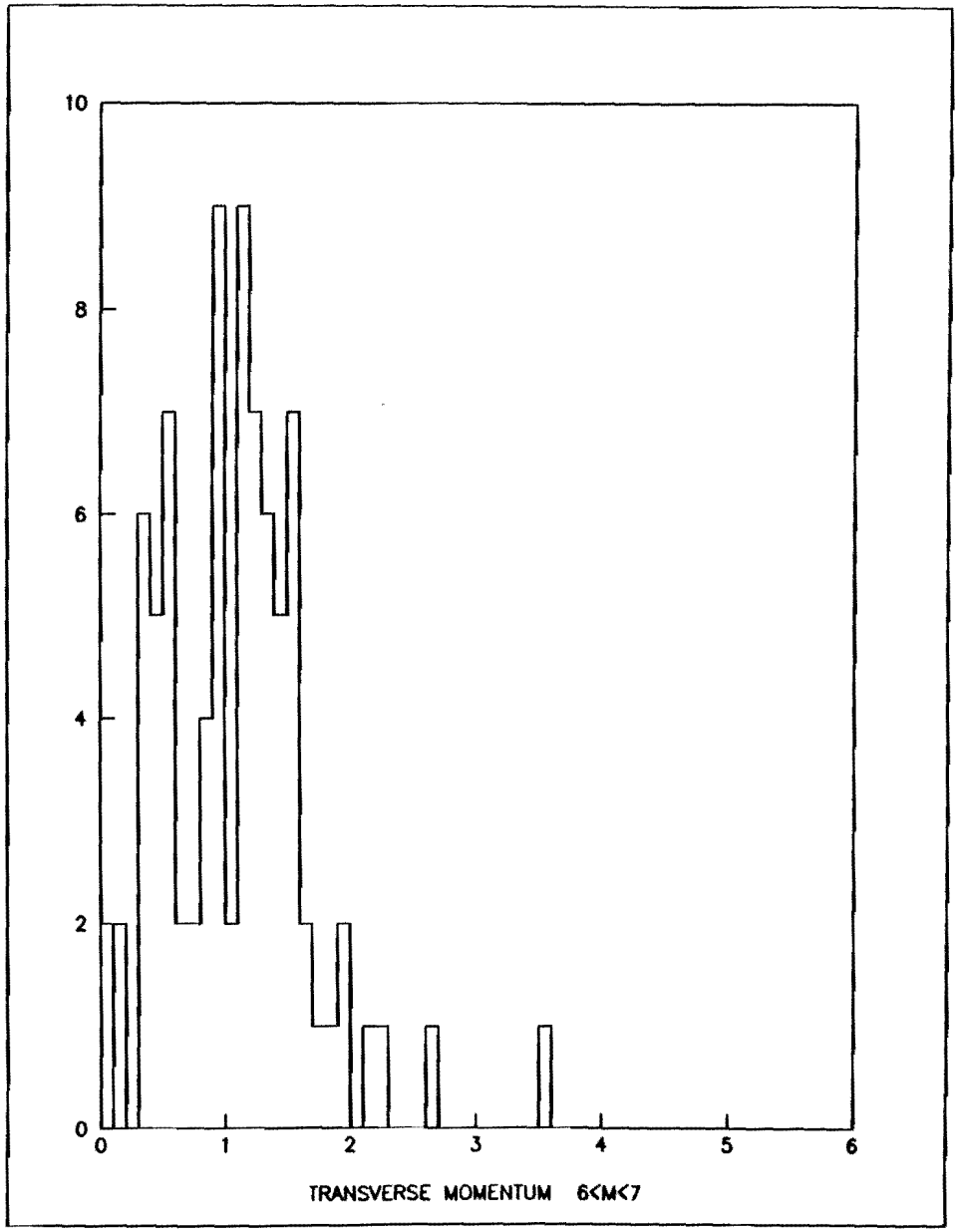

Fig 4b

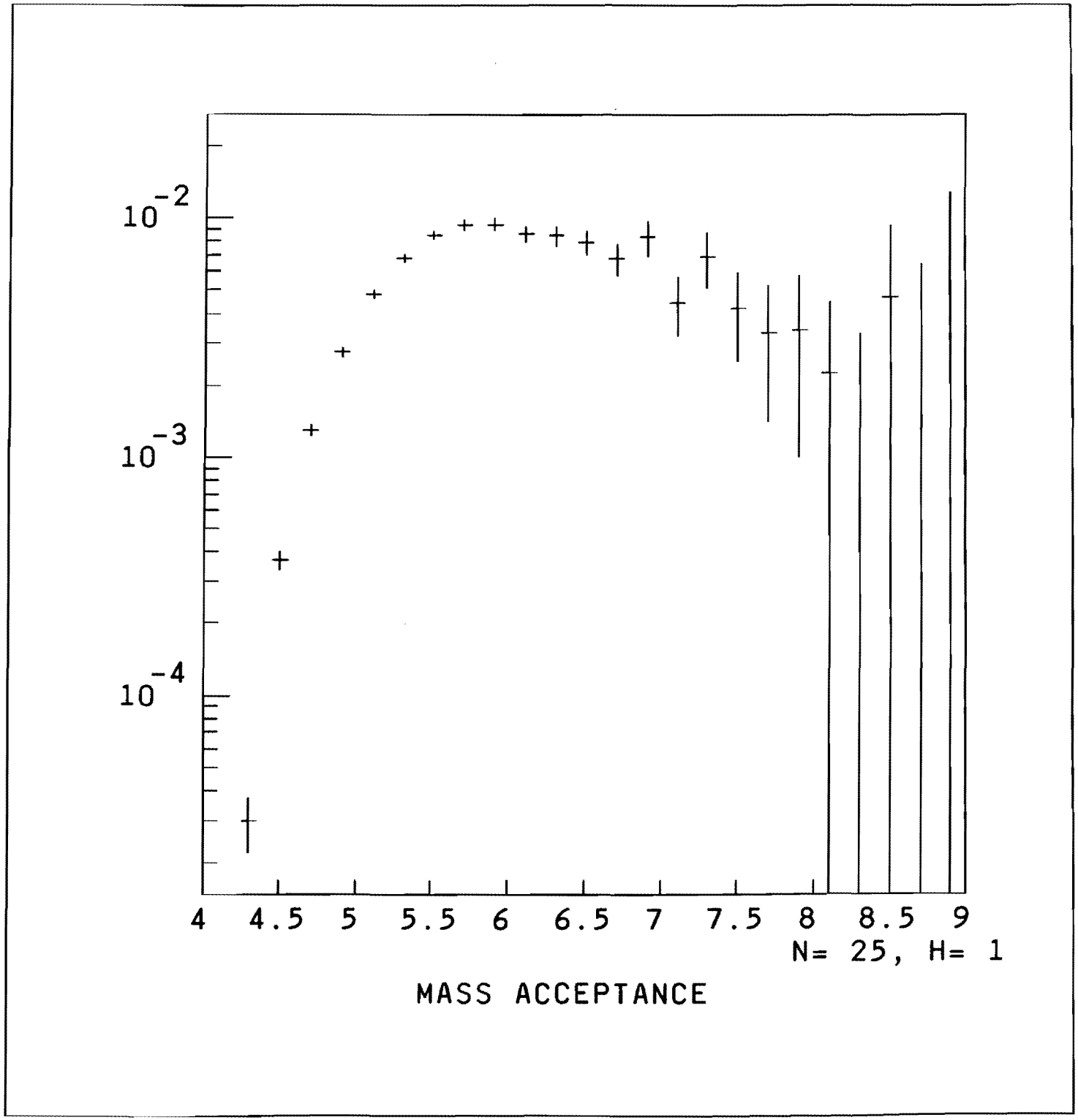

Fig. 5a

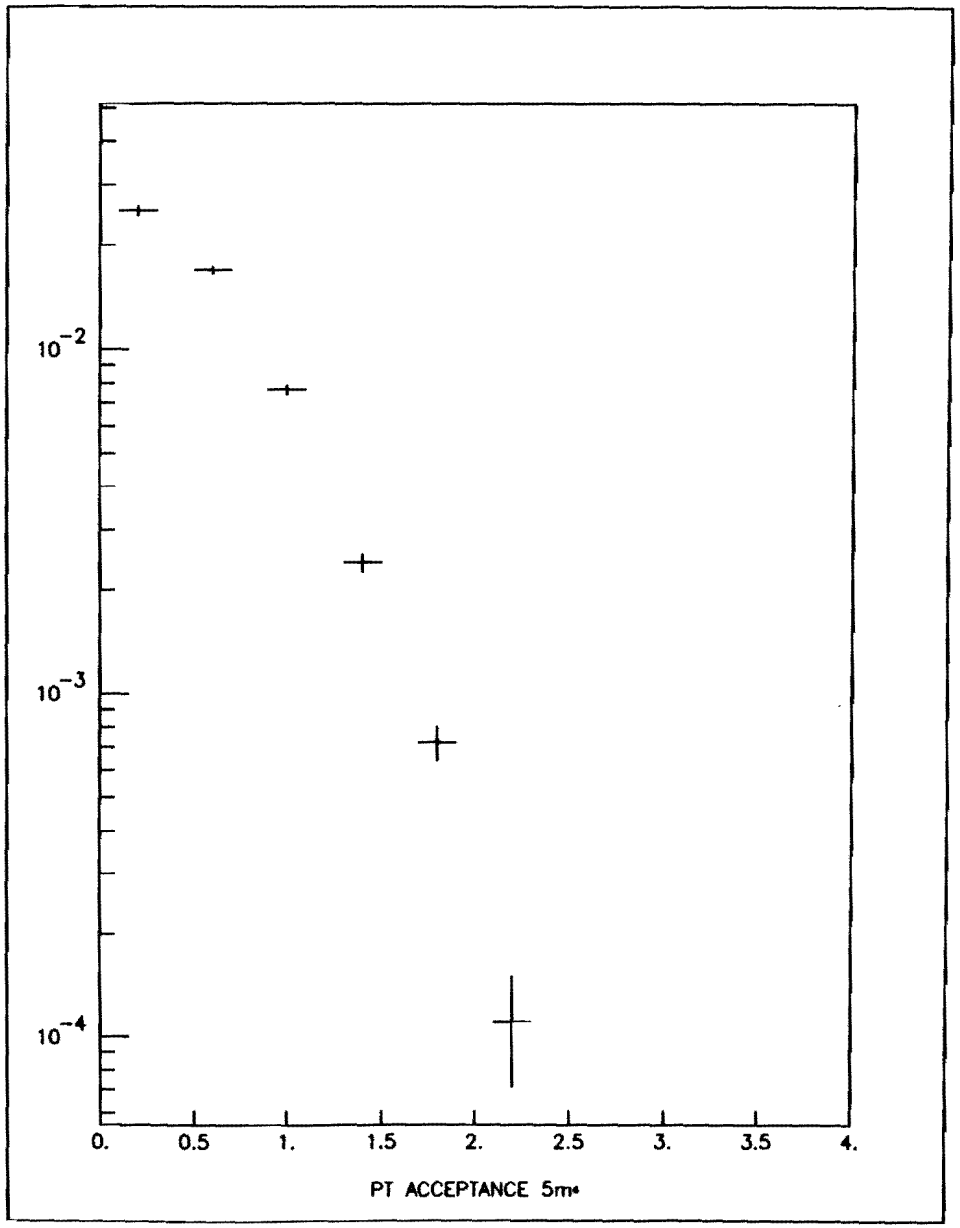

Fig 5b

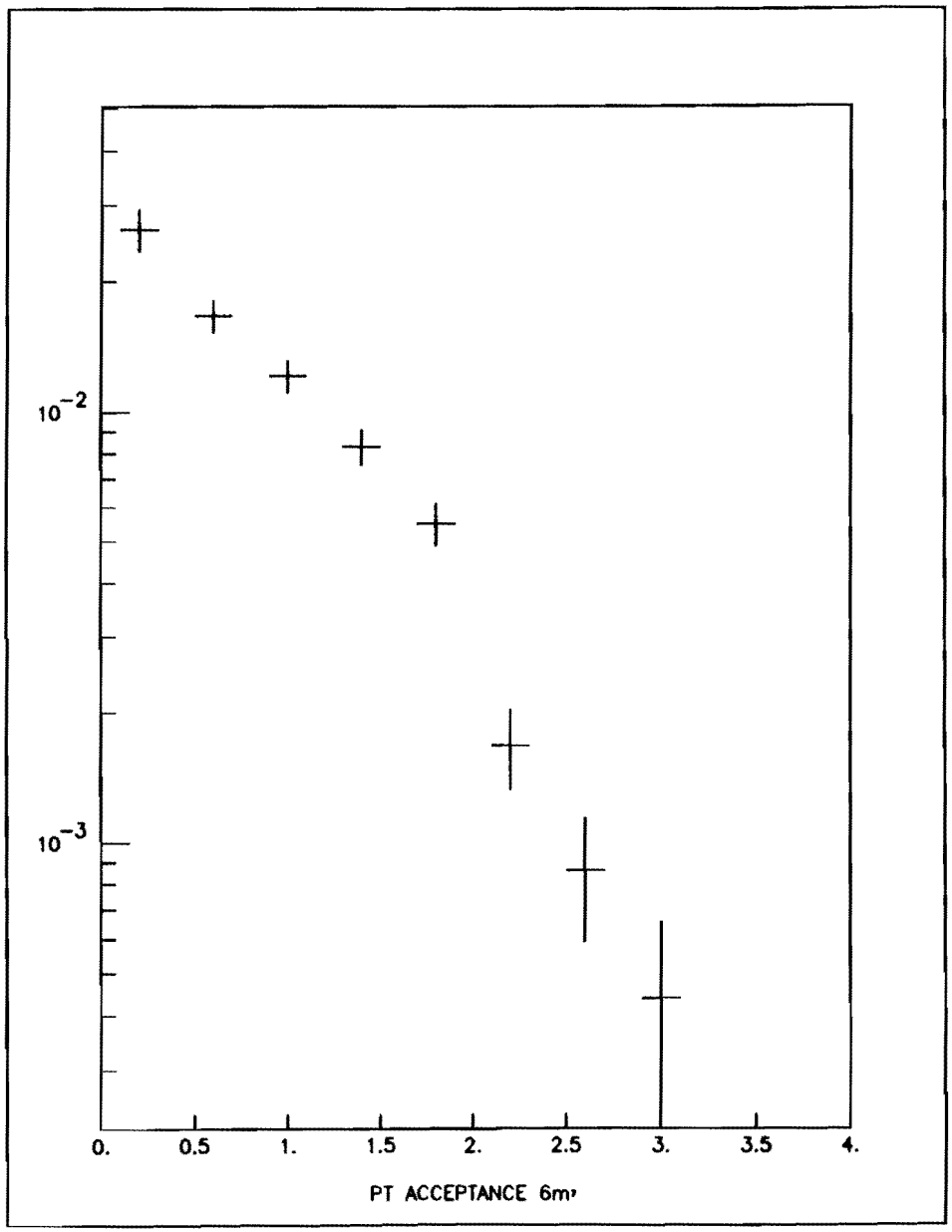

Fig 5c

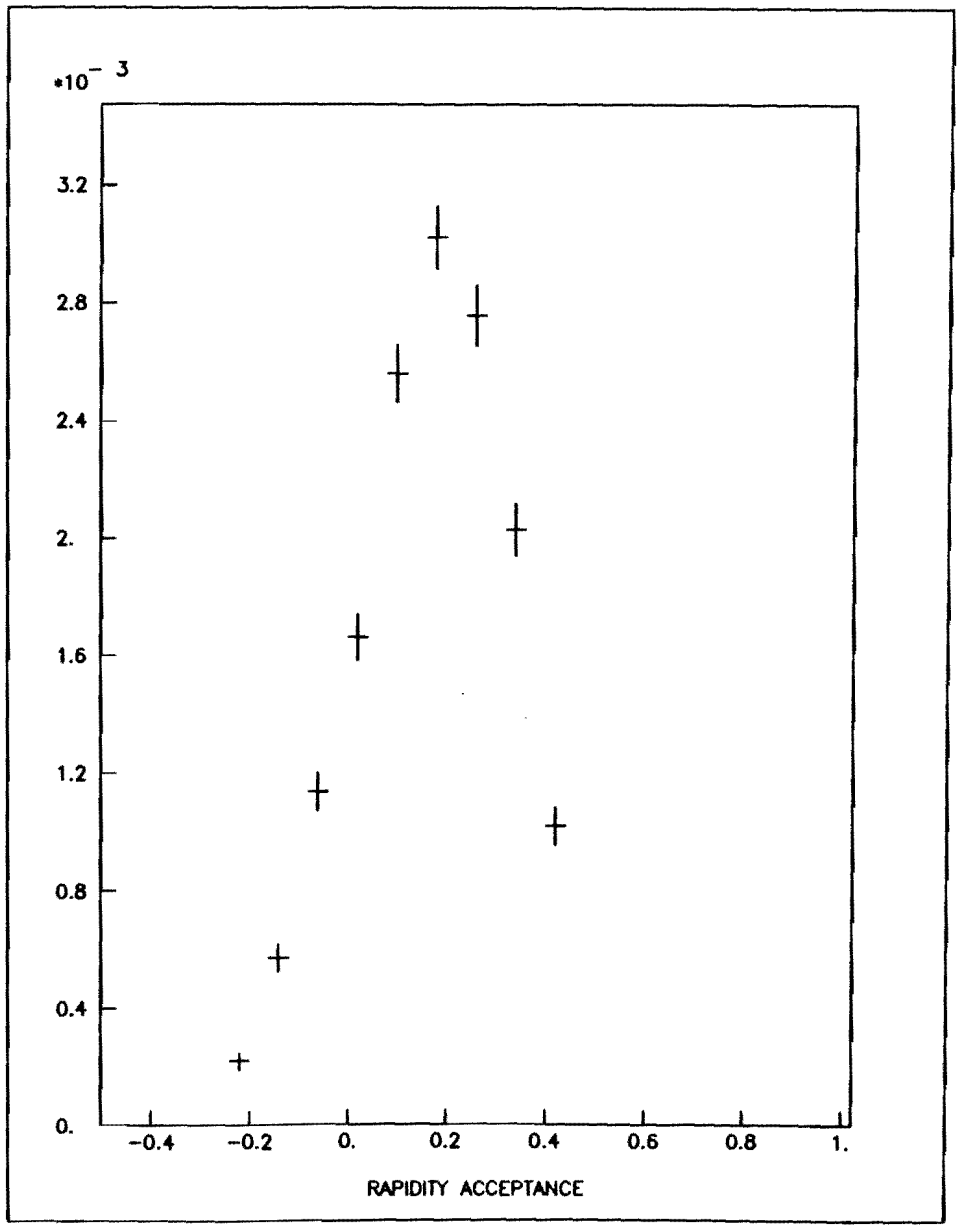
*10^-3
3.2
2.8
2.4
2.
1.6
1.2
0.8
0.4
0.
-0.4
-0.2
0.
0.2
0.4
0.6
0.8
1.
RAPIDITY ACCEPTANCE

Fig. 5d

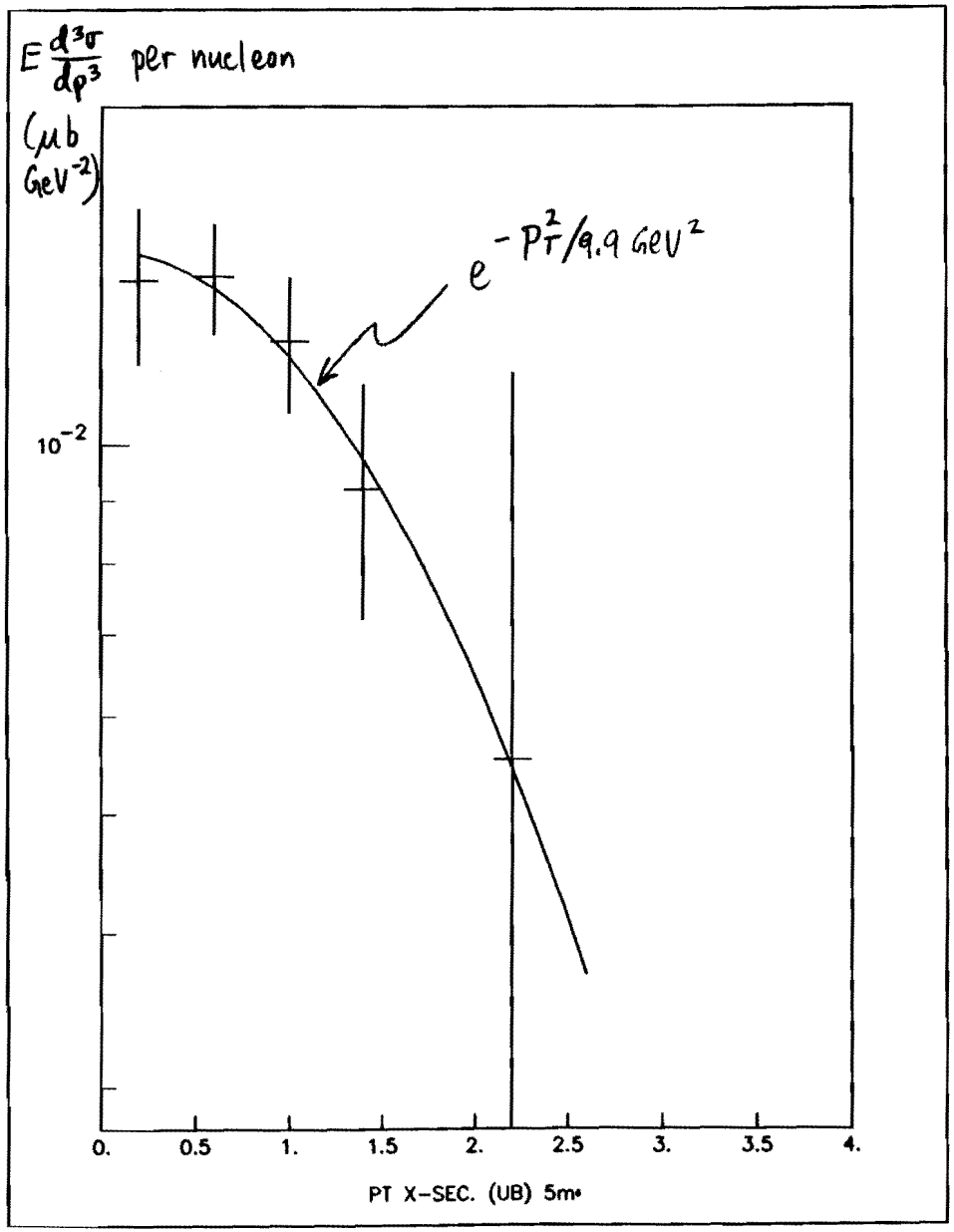
$E\frac{d^3\sigma}{dp^3}$ per nucleon
(μb GeV^{-2})
$e^{-P_T^2/9.9\ GeV^2}$
10^{-2}
0.
0.5
1.
1.5
2.
2.5
3.
3.5
4.
PT X-SEC. (UB) 5m

Fig. 6a

5 x m < 6

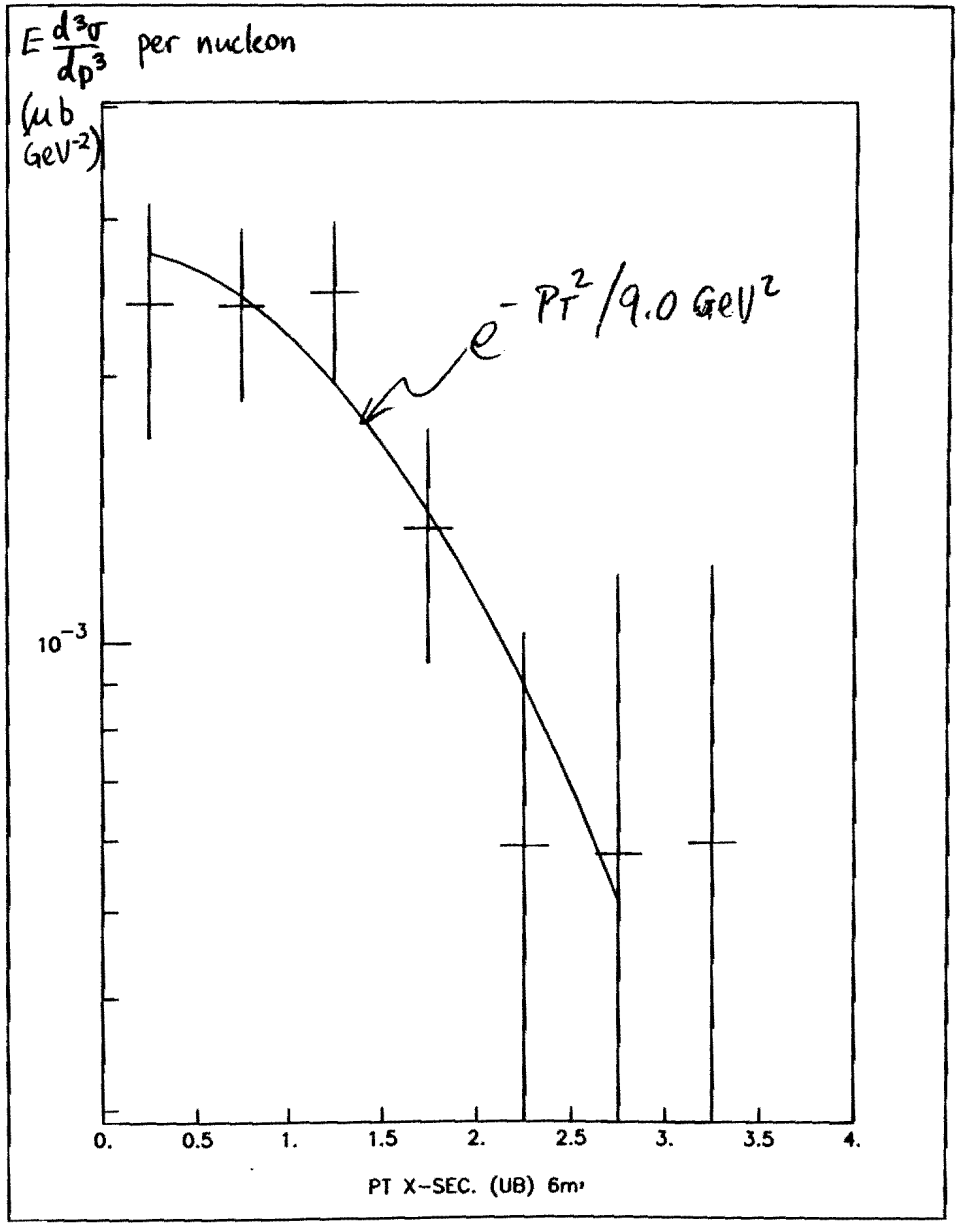
$E\frac{d^3\sigma}{dp^3}$ per nucleon
(μb GeV^{-2})
$e^{-P_T^2/9.0\ GeV^2}$
10^{-3}
0.
0.5
1.
1.5
2.
2.5
3.
3.5
4.
PT X-SEC. (UB) 6m

Fig. 6a

$6 < m < 7$

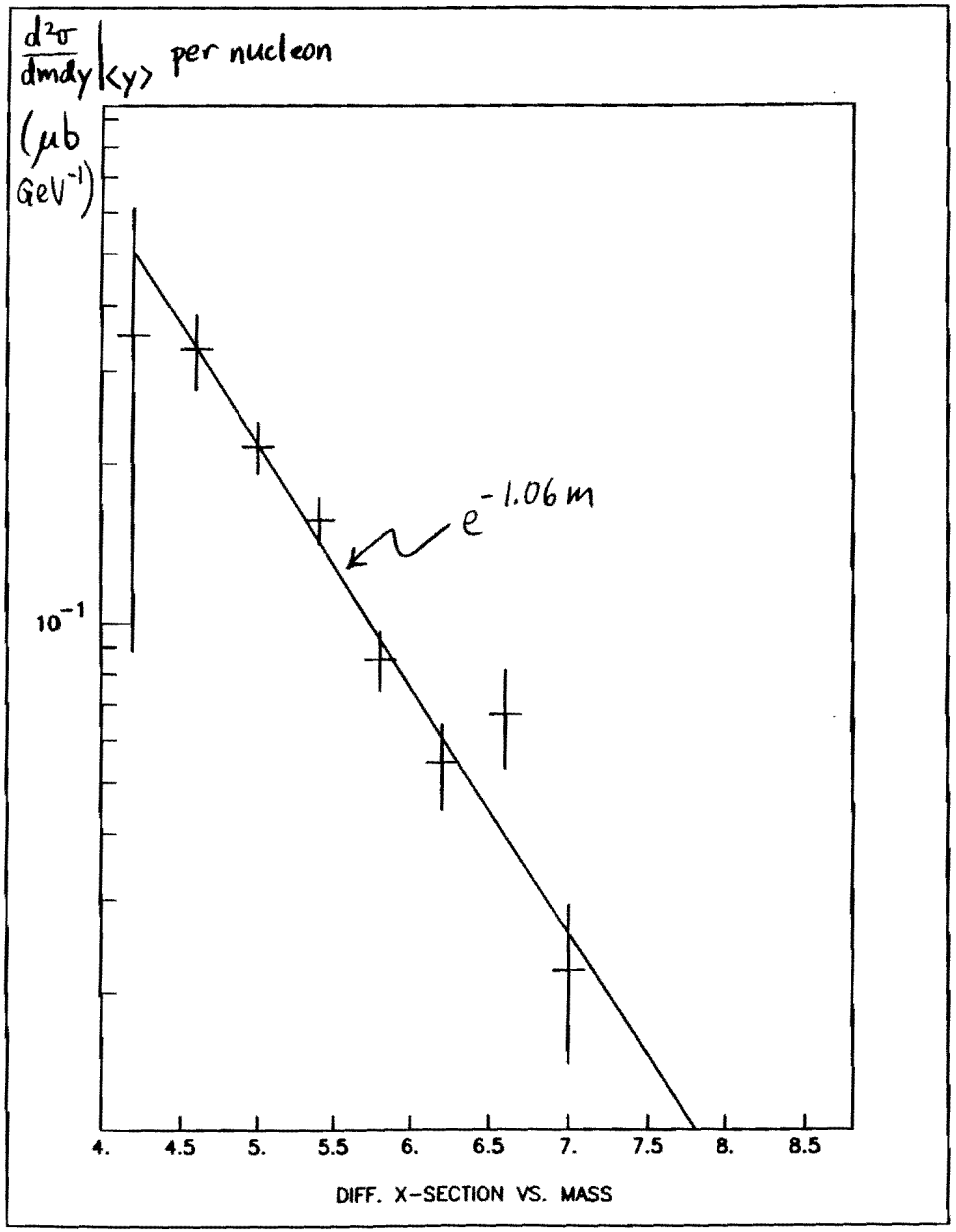
$\frac{d^2\sigma}{dmdy}\Big|_{\langle y\rangle}$ per nucleon
(μb GeV^{-1})
$e^{-1.06\,m}$
10^{-1}
4.
4.5
5.
5.5
6.
6.5
7.
7.5
8.
8.5
DIFF. X-SECTION VS. MASS

Fig 6b

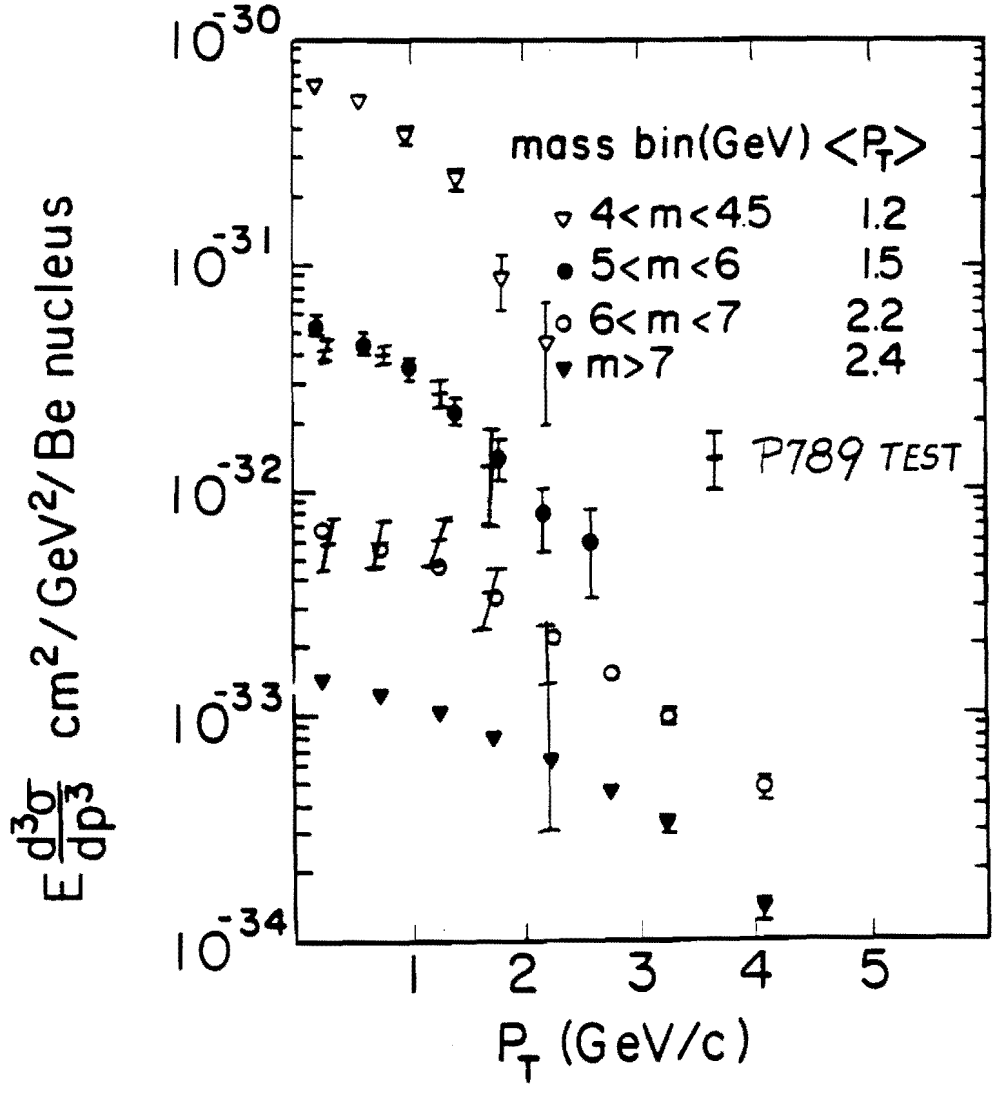

FIG. 3. The invariant pair cross section as a function of the dihadron p_T for various mass ranges.

Figure 7 (from Figure 3, Kephart et al.)

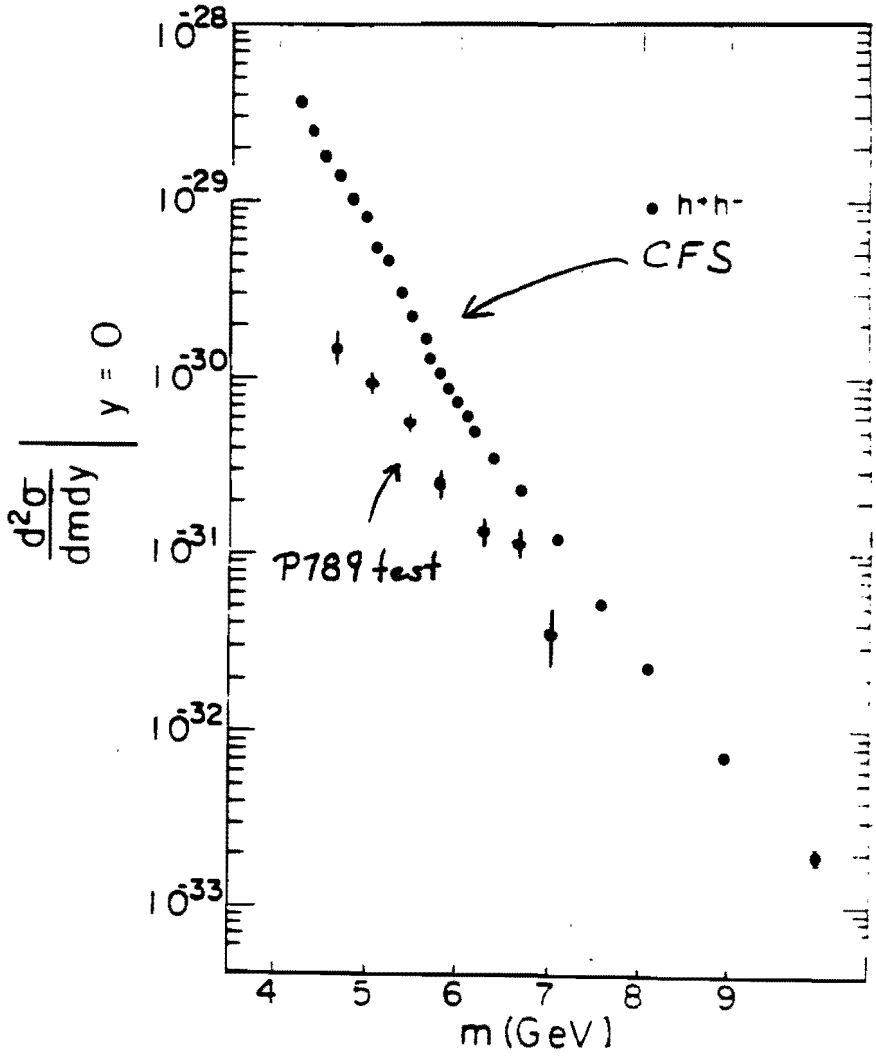
$\frac{d^2\sigma}{dmdy}\Big|_{y=0}$
10^{-28}
10^{-29}
10^{-30}
10^{-31}
10^{-32}
10^{-33}
h^+h^-
CFS
P789 test
4
5
6
7
8
9
m (GeV)

Fig. 8

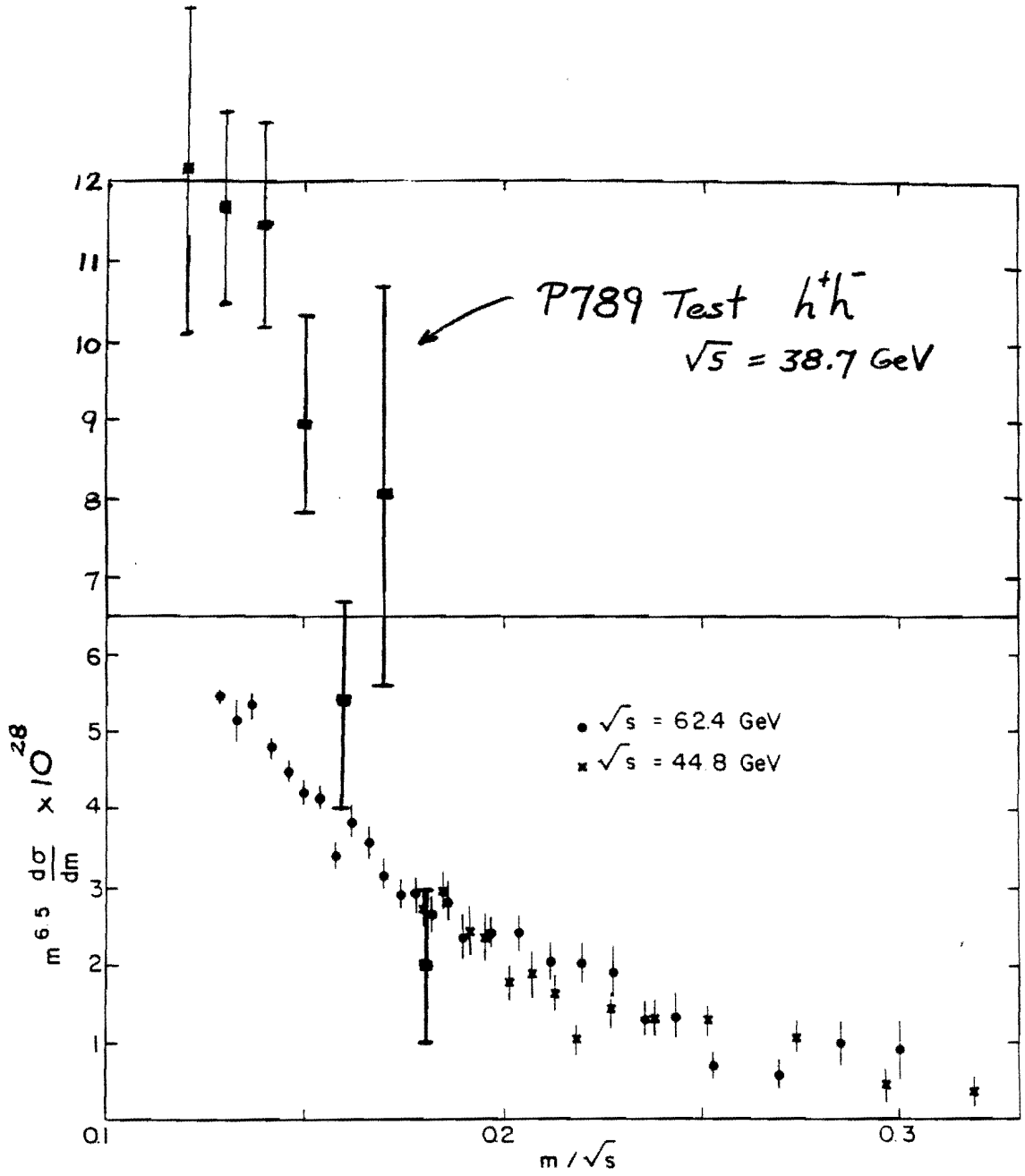

Fig. 6. $m^{6.5}\,d\sigma/dm$ as a function of $m/\sqrt{s}$ for $\sqrt{s} = 44.8$ and $\sqrt{s} = 62.4$ GeV.

Fig. 9

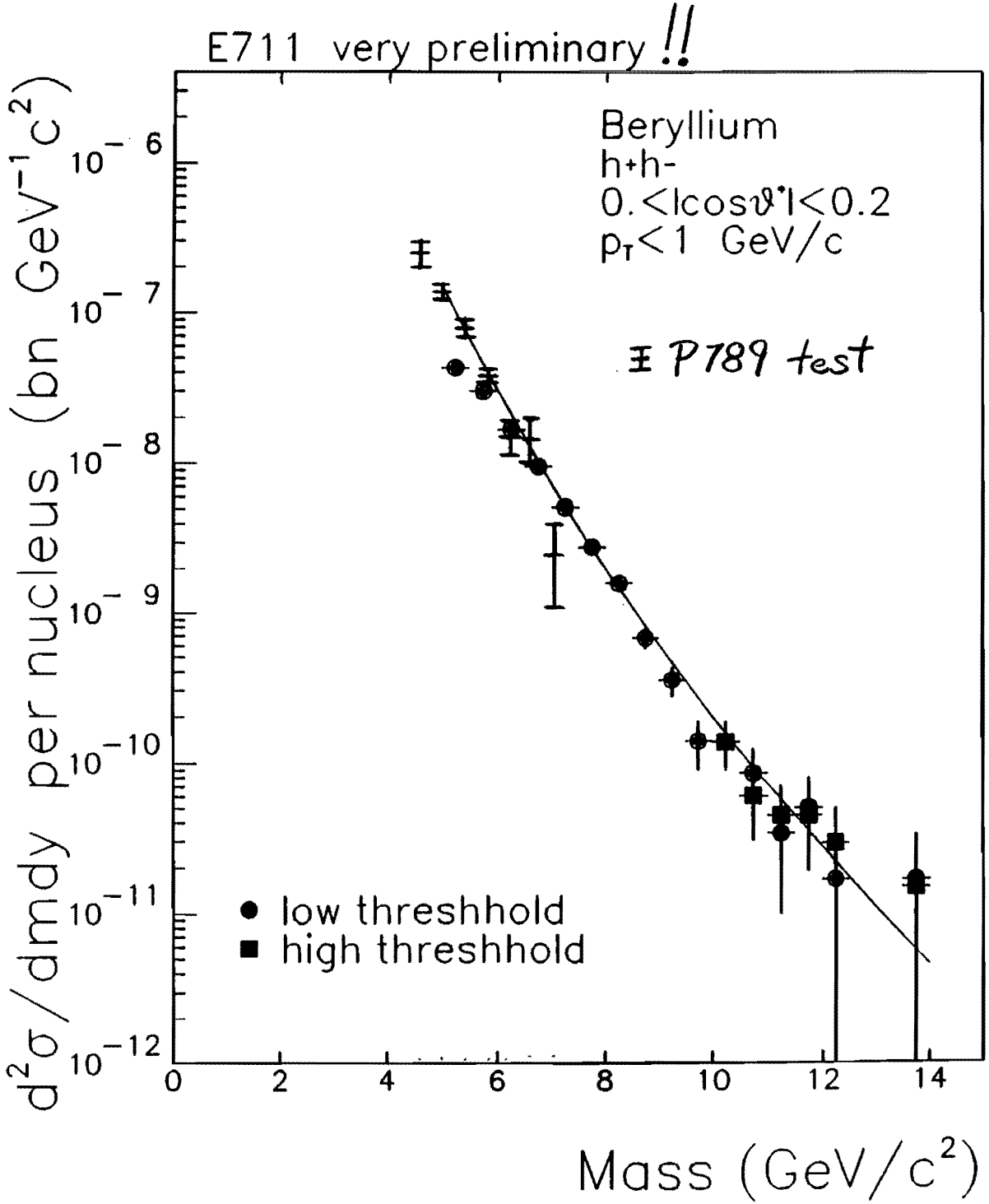
E711 very preliminary !!
Beryllium
h+h-
0.<|cosϑ*|<0.2
pT<1 GeV/c
∓ P789 test
low threshhold
high threshhold
d²σ/dmdy per nucleus (bn GeV⁻¹c²)
Mass (GeV/c²)
10⁻⁶
10⁻⁷
10⁻⁸
10⁻⁹
10⁻¹⁰
10⁻¹¹
10⁻¹²
0
2
4
6
8
10
12
14

Fig. 10

E-789

Supplement to E789 Letter of Intent
December 5, 1989

John Peoples, Director
Fermilab

We wish to clarify the issues raised in our Letter of Intent of October 25, 1989 expressing our desire to run E789 as soon as possible. E789 proposes to study low-multiplicity decays of beauty particles at high luminosity using a silicon-strip vertex spectrometer and triggering on decay vertices downstream of a short (≈few mm) dense target. While the vertex spectrometer is new, all other techniques to be used in E789 have been used successfully in E605/772. In the early months of E789 our main goal is to debug new or modified equipment and understand how to trigger on and reconstruct decay vertices. As described below, the best way to do this is with charm data. This entails little expense; in particular, construction of the new Fermilab silicon readout electronics may be deferred with little adverse impact. We are now engaged in intensive efforts to ready our apparatus for data-taking. We anticipate that all equipment needed for charm running of E789 will be available and working by March 1, 1990.

Charm Running

In commissioning an exploratory experiment of this kind it is extremely valuable to use known large signals for tuneup and calibration. The recently-modified spectrometer elements and the vertex trigger processor can be debugged using the dilepton decays of charmonium and the dihadron decays of the neutral D meson. In the process we can do valuable physics as well. Since the charm cross sections are three orders of magnitude larger than those for beauty, we can work at much reduced interaction rate, with reduced rates in the silicon detectors and simplified vertex reconstruction. Since the current in the main analyzing magnet will be reduced to maximize the acceptance at lower mass, the rates in the downstream detectors will be comparable to those at the beauty setting. We have been planning lower-mass running for several months. We attach as an Appendix a memo written in July detailing acceptances and sensitivities, and we summarize them here.

We estimate an interaction rate of 0.1 interaction per RF-bucket. Our acceptance at the D is 5×10^{-3}, yielding $\sim 10^5$ $D \to K\pi$ events on tape per month. Since the D^0 lifetime is one-third that of the B, a 200-μm platinum wire target will be used to maintain good separation between primary and secondary vertices. At 5×10^{10} protons per pulse incident, we can set the world's best limit on $D \to e^+e^-$, $D \to \mu^+\mu^-$, and $D \to e\mu$ while commissioning our apparatus. One-event sensitivity is 2.5×10^{-7} per 10^5 $D \to K\pi$ reconstructed.

Silicon Detector Electronics

The new Fermilab silicon-strip readout electronics will be unavailable until at least the middle of next year, in part for budgetary reasons and in part due to delays incurred in the

complex and challenging process of designing four advanced semi-custom integrated circuits for the "Postamp/Comparator" (discriminator) module. The charm running described above does not require the full E789 vertex spectrometer (16 planes, 13,312 instrumented strips). The 5°-stereo views provide redundancy for reconstructing B decays in the presence of some 60 accidental background tracks per event. The background rate in the silicon will be 100 times lower for the charm running. 4,096 strips in the 8 bend-view planes will be adequate to identify charm decays (Monte Carlo simulations verify this). We can instrument 4,096 channels using our existing MWPC electronics to latch the signals from the new Fermilab preamps (which are already being fabricated using FY89 money). The MWPC electronics have become available as we are replacing the old E605 MWPC's with new small-cell drift chambers. Tests show that the old electronics have 1 to 2 RF-bucket time resolution and 2 to 3 RF-bucket deadtime, quite adequate for reduced-intensity running.

After we have successfully commissioned the apparatus by studying D decays, we will have various options for instrumenting the remainder of the silicon channels if (as simulation indicates) they are needed to see beauty. If the Fermilab system is then available we will install it. If budget constraints prevent construction of the full 13,312 channels, we may still be able to afford some 5,000 to 9,000 channels to supplement those already instrumented, moving the old electronics to the large-angle, low-rate silicon channels. Alternatively, we have the option of building additional electronics similar to our MWPC design, which is cheaper and simpler than the Fermilab design. (The full cost would not have to be borne by Fermilab but could be shared with some of our collaborating institutions.) As more channels of high-speed electronics become available we will be able to increase the interaction rate; a valuable exploratory study of beauty can be carried out if the luminosity can be raised above 1 interaction per RF-bucket. In the above alternatives, we assume installation of the additional detectors and electronics during the summer shutdown. If budget constraints prevent all of these alternatives, we can continue taking charm data to improve rare decay limits another order of magnitude.

Budget Impact

The cost of the proposed charm running is minimal. Since the main analysis magnet will be operated at 20% of full current, it uses little power (this is also true at the beauty setting). Power consumption is dominated by the secondary analysis magnet and the (largely superconducting) beamline. The total power dissipation is $\approx$ 1 MW. Operating funds would be needed to cover chamber and Cherenkov gases, magnetic tapes, and so forth; these funds are currently allocated in the FNAL Physics Department and collaborating institution budgets.

We believe that the physics value of running E789 far outweighs the small cost of operating the experiment. The goal of ascertaining the potential of this unique and promising approach to the study of heavy quark decays is of immediate importance to Fermilab.

Daniel M. Kaplan and Jen-Chieh Peng
Spokesmen for E789

Appendix

ACCEPTANCE OF E789 FOR B AND D DECAYS

E789 Memo, July 11, 1989
J. C. Peng and C. S. Mishra

The purpose of this memo is to summarize the results of acceptance studies with the new SM12 field maps, and to discuss the feasibility to measure D decays at the tune-up phase of E789.

During the February collaboration meeting, Chuck Brown suggested that the first module of the SM12 pole insert be pulled out so that SM12 can run at a higher current for a given Pt kick. The reconfiguration of SM12 was carried out in May and the new field maps were measured by D. Jensen and J. Peng. The new SM12 field is greatly reduced upstream of the beam dump, but is essentially the same as the old field downstream of the beam dump. In the E789 proposal we assumed 1800 amp for SM12. With the new SM12 configuration, the magnet current can be set at 2400 amp to get the same Pt kick.

We have calculated the acceptance using the new SM12 field maps for the following decays considered in the E789 proposal.

1) $B \to h^+h^-$

2) $B \to \ell^+\ell^-$

3) $\eta_b \to p\bar{p}$

4) $B \to J/\psi X, \psi' X$

5) $B^- \to J/\psi K^-$ and $B^- \to D^\circ\pi^-$

6) $B\bar{B} \to \mu\mu X$

The results of some of these calculations are shown in Figs. 1-3. For the exclusive three-body B decay modes $B^- \to J/\psi K^-$ and $B^- \to D^\circ\pi^-$, we assume that two of the decay products are accepted by the spectrometer and the third particle hits the silicon microstrip detectors. If the straw tubes, being contemplated by B. Luk and G. Gidal, are installed, the acceptance for these three body decays will be significantly increased.

In the April collaboration meeting, J. Peng mentioned the possibility of detecting the rare decay mode of $D \rightarrow \ell^+\ell^-$. This was not taken seriously, since SM12 has to run at very low current to have any acceptance for this decay. However, the new SM12 configuration allows us to run at a reasonable SM12 current to accept the D decays. Mike Witherell sent us an electronics mail in June suggesting that we look into the possibility of measuring D decays in E789. This prompted us to calculate the acceptance for the following D decays:

7) $D \rightarrow h^+h^-$

8) $D \rightarrow \ell^+\ell^-$

9) $D^* \rightarrow \pi D \rightarrow \pi K\pi$

10) $D^+ \rightarrow K^-\pi^+\pi^+$

11) $D \rightarrow K\pi$ tagged by $\bar{D} \rightarrow \mu X$

12) $D\bar{D} \rightarrow \mu\mu X$

The results of some of these calculations are shown in Figs. 4-5. In the $D^* \rightarrow \pi D \rightarrow \pi K\pi$ decay, we assume the soft π from the $D^* \rightarrow \pi D$ decay hits the silicon detectors while the $D \rightarrow K\pi$ decay products are accepted by the spectrometer.

From the acceptance curves, it seems reasonable to have two separate SM12 field settings for the E789 runs. The D decays can be first measured at 1000 amp and the B decays can then be measured at 2000 amp. It is not clear what the maximum interaction rate one can tolerate at 1000 amp. It seems reasonable to assume that we can survive $2\text{x}10^8$ interactions/spill, a factor of 50 lower than the proposed rate at 2000 amp. In Table I, we list the expected yields for B decays at 2000 amp (assuming one fixed-target run) and for D decays at 1000 amp (assuming two-month beam time). The large production cross sections ($\sim 20\mu b$) and large branching ratios account for the huge yields for the D decays. We plan to use a 250-μm-diameter tungsten wire as the target for D-decay measurements.

The average momentum for D-mesons is about three times smaller than that of B-mesons. This scales roughly with the mass of these mesons and reflects the fact that the

spectrometer acceptance centers around X_F=0. The lifetime of D° is ~0.43 ps, 2.5 times shorter than that of B°. The average distance D travels before decaying is only 3.7 mm. This necessitates the use of a point target, approximated by the tungsten wire. C. Mishra calculated the rejection factor for target dihadrons to be better than 10^5 with an impact parameter cut of 150 μm. About 12% of the $D \to K\pi$ decay events survive such cut. This factor has been taken into account in Table I.

The threshold of the RICH detector is presently chosen at $\gamma \simeq 40$. This gives Cherenkov light for both the K and π in B decays, but not for the lower energy kaons from the D decays. This might still be adequate for studying D decays, since tracks without an RICH signal can be identified as kaons. One can not distinguish kaons from protons, but fortunately, D decays do not produce protons.

The D-decays will provide an excellent means to tune up the E789 spectrometer. The silicon microstrip detectors will run very quietly with an average rate of ~0.5 hit/R.F. bucket. In fact, we do not require single-bucket resolution for the SSD electronics during this measurement. The vertex processor and the RICH detector can also be debugged.

In the following, we discuss some physics which can be addressed in the measurements of D-decays.

1) Production Asymmetry Between D° and $\bar{D}^\circ$ Mesons

The production asymmetry is defined as

$$A = (\sigma(D^\circ) - \sigma(\bar{D}^\circ))/(\sigma(D^\circ) + \sigma(\bar{D}^\circ)).$$

In proton-nucleus collisions, the elementary processes responsible for charm productions are $gg \to c\bar{c}$ and $q\bar{q} \to c\bar{c}$. No asymmetry between c and $\bar{c}$ production is expected at this stage. However, one expects some asymmetry in the hadronization process and in the final-state interaction. In proton-nucleus collision, the presence of valence quarks suggests that the probability for a $\bar{c}$ to pick up a u quark to form $\bar{D}^\circ$ is greater than for a c to pick up a $\bar{u}$ quark to form a D°. Similarly, one expects the charm-baryons (cqq) to be formed more abundantly than the charm-antibaryons ($\bar{c}\bar{q}\bar{q}$).

The final-state interaction can also cause asymmetry. D° can disappear through the final state interaction such as $D^\circ + n \rightarrow \pi^- + \Lambda_c^+$. On the other hand, $\bar{D}^\circ$ can not convert into charm-baryon in final-state interactions.

Both the hadronization process and the final-state interaction favor the production of $\bar{D}^\circ$ over D°. To our knowledge, there is no experimental data on the $D, \bar{D}$ asymmetry yet. In E789, this asymmetry can be well measured by comparing the $D^\circ \rightarrow K^-\pi^+$ yield with the $\bar{D}^\circ \rightarrow K^+\pi^-$ yield.

Similar consideration also applies to the asymmetry in the $B, \bar{B}$ system. The knowledge on $D, \bar{D}$ asymmetry will be useful for a rough estimate on the $B, \bar{B}$ asymmetry. As discussed later, one promising method to measure the $B_s - \bar{B}_s$ mixing is to make use of the production asymmetry.

2) $D - \bar{D}$ Mixing

There are two methods to search for evidence of $D-\bar{D}$ (or $B-\bar{B}$) mixing. The first method does not require tagging. As discussed in the E789 proposal, the time-dependence of a neutral meson decaying into the $K\pi$ channel is given as

$$\text{Rate } (B^{neutral} \rightarrow K^-\pi^+) \; \alpha \; exp(-\Gamma t)[1 - A \; cos \; \Delta \; mt]$$

where A is the production asymmetry between B° and $\bar{B}^\circ$. Similar expression holds for $D^{neutral} \rightarrow K^-\pi^+$ decay. Note that the $K^-\pi^+$ decay product can come from both $\bar{B}^\circ \rightarrow K^-\pi^+$ and $B^\circ \rightarrow \bar{B}^\circ \rightarrow K^-\pi^+$. The mixing in $B_d - \bar{B}_d$ is known to be $\Delta m/\Gamma = 0.73$, while the $B_s - \bar{B}_s$ mixing is not known, but expected to be $\Delta m/\Gamma \simeq 5$. Assuming an asymmetry of 0.2, the time dependences of the $B \rightarrow K^-\pi^+$ decay is suitable for detecting $B_s - \bar{B}_s$ mixing (provided that σ.BR is sufficiently large and the asymmetry is not small), but not appropriate for detecting $B_d - \bar{B}_d$ (or $D - \bar{D}$) mixing. Note that the present upper limit for $D - \bar{D}$ mixing is $\Delta m/\Gamma < 0.08$.

A more conventional method to search for mixing is to use tagging. One can study the reaction $D \rightarrow K\pi$ tagged by $\bar{D} \rightarrow \mu X$ (Reaction (11)), or the $D\bar{D} \rightarrow \mu\mu X$ decays (Reaction 12). The estimated sensitivity for

$$r = \Gamma(D \to \bar{D} \to \bar{f})/\Gamma(D \to f)$$

is $\sim 10^{-3}$. The current upper limit for r is 3.7 x 10^{-3}, determined from a quite different technique.

3) Rare Decay Modes of D

The current upper limit for the branching ratio of the lepton number violating $D \to e\mu$ decay is 1.2 x 10^{-4}. The upper limits of the $D \to e^+e^-, D \to \mu^+, \mu^-$ flavor-changing-neutral-current decays are set at BR = 1.3 x 10^{-4} and 1.1 x 10^{-5}, respectively. As shown in Table I, we expect to have a sensitivity at the level of BR = 10^{-7} for these decays.

TABLE I. Number of Events Reconstructed for Various Decay

Decay Mode	σ	Accp(%)	B.R.	Vertex Eff	No. of Events
$B \to \pi^+\pi^-$	6nb	1.5	10^{-5}	0.3	30
$\eta_b \to p\bar{p}$	200pb	0.45	5×10^{-4}	1.0	50
$B \to J/\psi X$	12nb	0.1	0.011 x 0.14	0.3	600
$B \to \psi' X$	12nb	0.55	0.0046 x 0.018	0.3	178
$B^- \to K^- J/\psi$	6nb	0.1	.0008 x 0.14	0.3	20
$B \to D\pi$	6nb	0.1	0.006 x 0.038	0.3	45
$BB \to \mu^+\mu^- X$	6nb	0.075	0.1 x 0.1	0.3	1400
$D \to K\pi$	22μb	0.25	3.8×10^{-2}	0.12	1.7×10^5
$D \to KK$	22μb	0.1	0.45×10^{-2}	0.12	8.2×10^3
$D \to \pi\pi$	22μb	0.3	0.13×10^{-2}	0.12	7.1×10^3
$D \to e^+e^-$	22μb	0.4	10^{-7}	0.12	1
$D^* \to \pi D \to \pi K\pi$	22μb	0.025 (900 amp)	$0.5 \times 3 \times 10^{-2}$	0.12	8.6×10^3
$D^+ \to K^-\pi^+\pi^+$	26μb	0.0002 (800 amp)	7.8×10^{-2}	0.3	8.3×10^2
$DD \to \mu^+\mu^- X$	22μb	0.015	0.14 x 0.14	0.12	5.3×10^3
$D \to K\pi, \bar{D} \to \mu X$	22μb	0.005	0.038 x 0.14	0.12	4.8×10^2

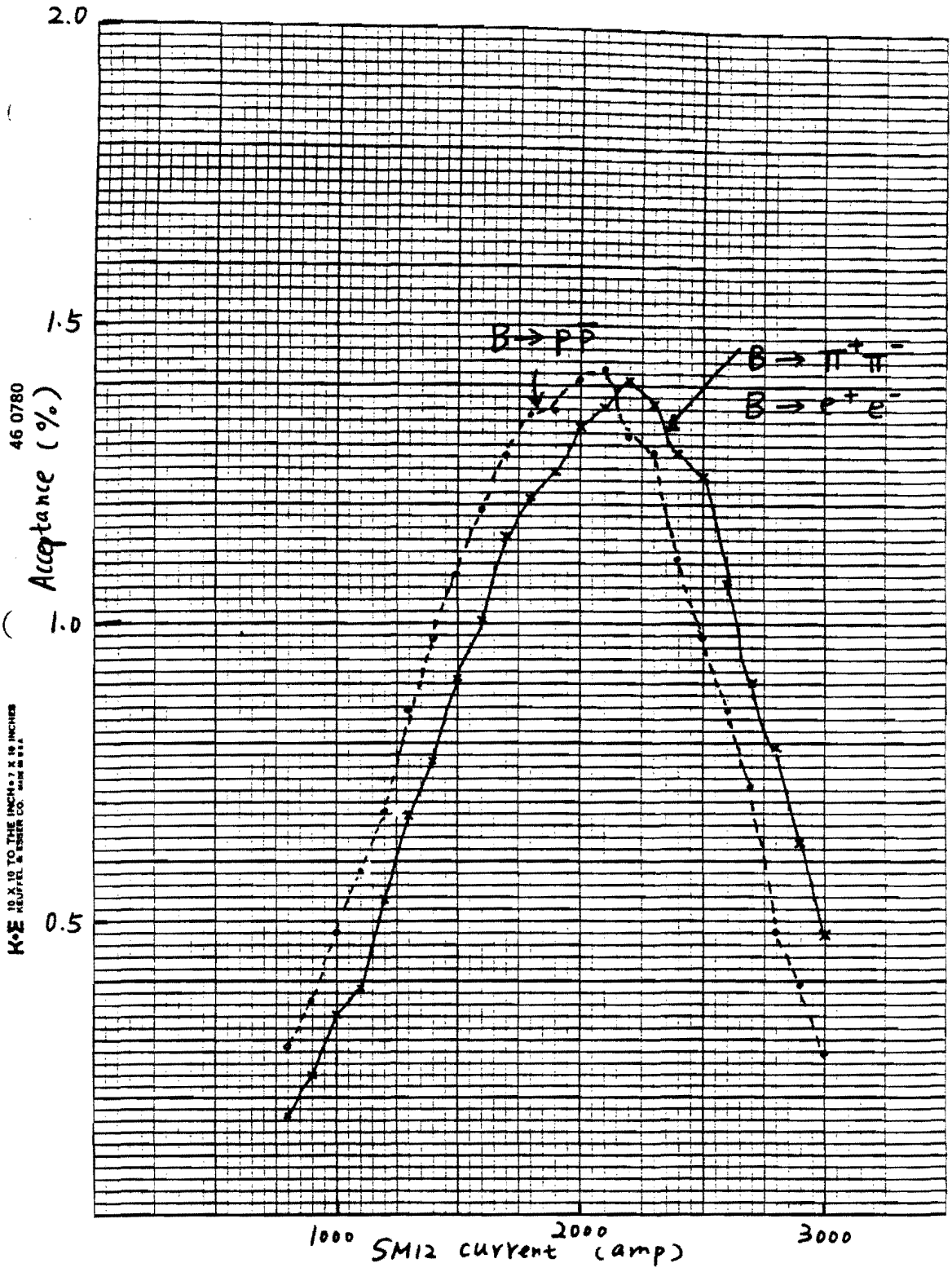
2.0
1.5
1.0
0.5
Acceptance (%)
46 0780
K·E 10 X 10 TO THE INCH • 7 X 10 INCHES
KEUFFEL & ESSER CO.
B→pp̄
B → π⁺π⁻
B → e⁺e⁻
1000
2000
3000
SM12 current (amp)

Fig. 1

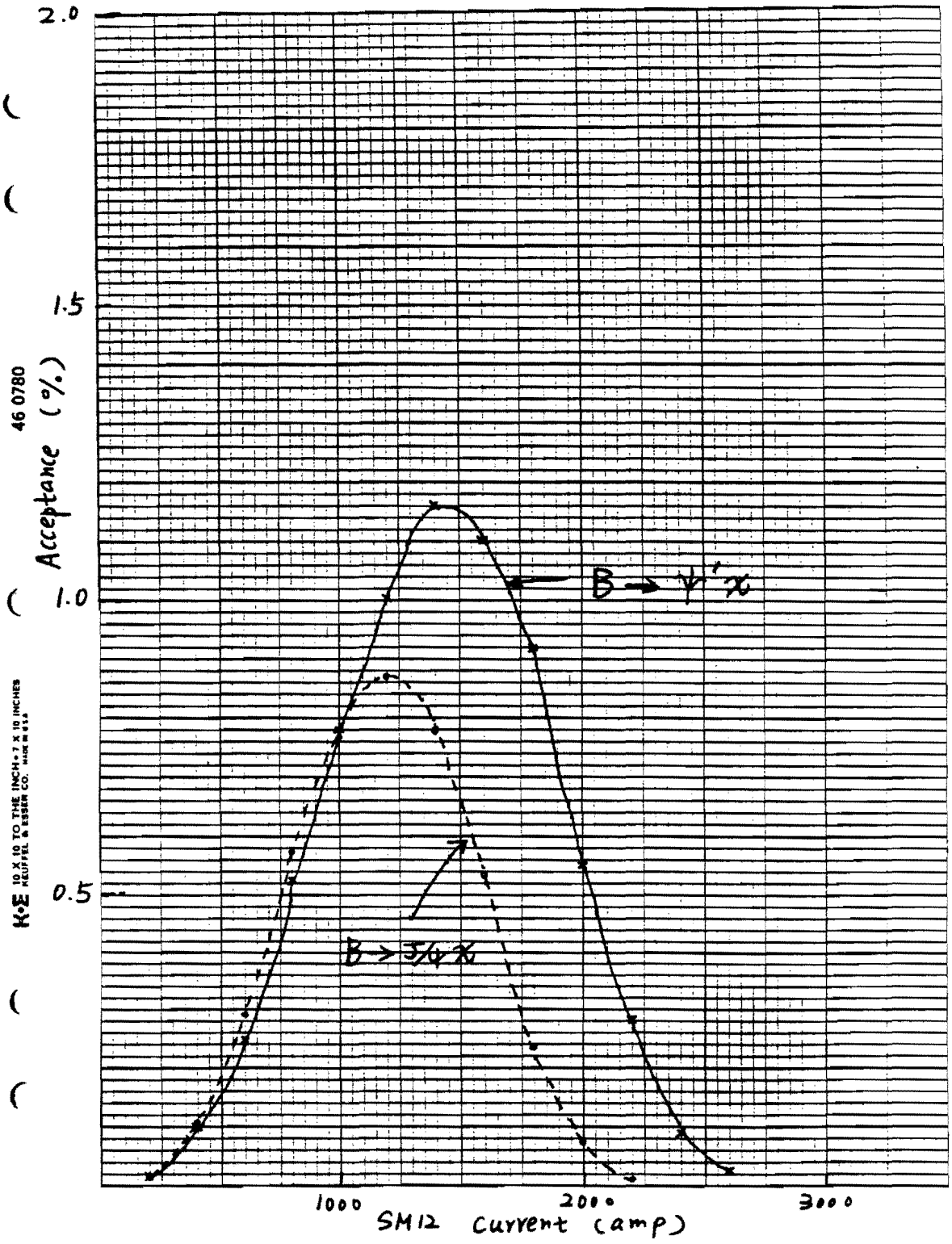
2.0
1.5
1.0
0.5
Acceptance (%)
B → ψ'x
B → J/ψx
1000
2000
3000
SM12 current (amp)
46 0780
K&E 10 X 10 TO THE INCH • 7 X 10 INCHES
KEUFFEL & ESSER CO. MADE IN U.S.A.

Fig. 2

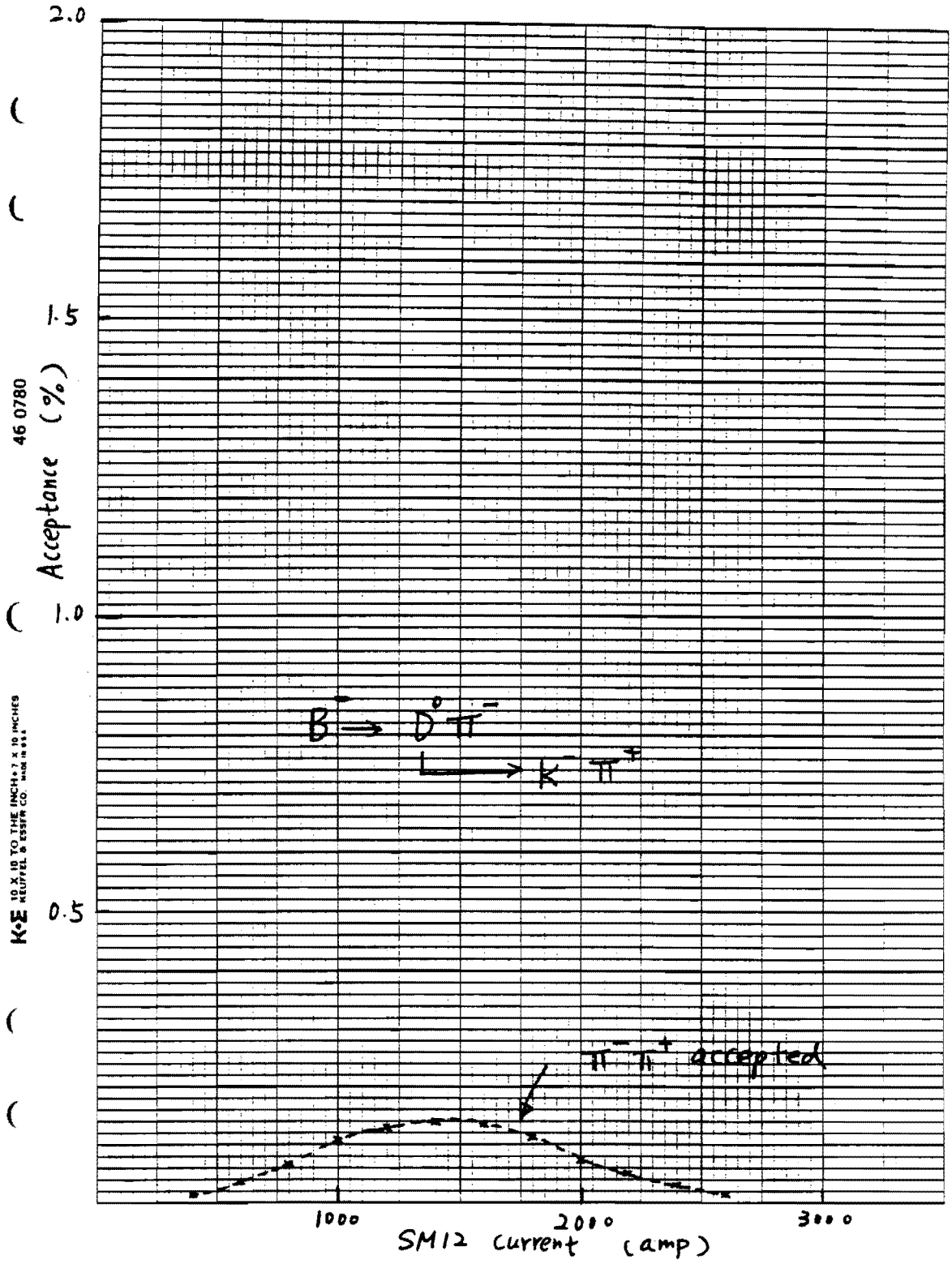
2.0
1.5
1.0
0.5
Acceptance (%)
46 0780
K&E 10 X 10 TO THE INCH • 7 X 10 INCHES
KEUFFEL & ESSER CO.
$\bar{B} \Rightarrow D^0 \pi^-$
$\hookrightarrow K^- \pi^+$
$\pi^- \pi^+$ accepted
1000
2000
3000
SM12 current (amp)

Fig. 3

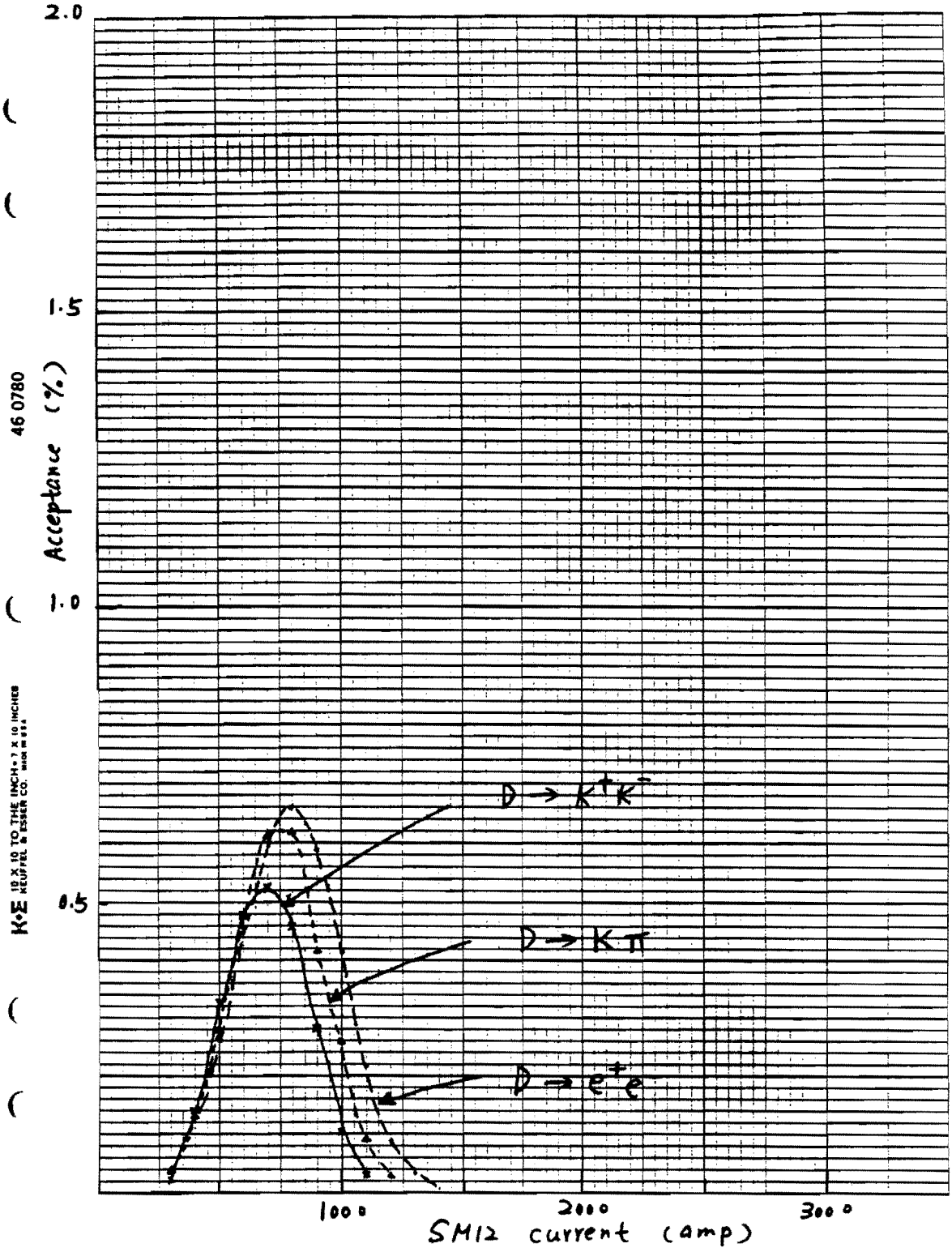
2.0
1.5
1.0
0.5
Acceptance (%)
46 0780
K&E 10 X 10 TO THE INCH • 7 X 10 INCHES
KEUFFEL & ESSER CO.
D → K⁺K⁻
D → Kπ
D → e⁺e⁻
1000
2000
3000
SM12 current (amp)

Fig. 4

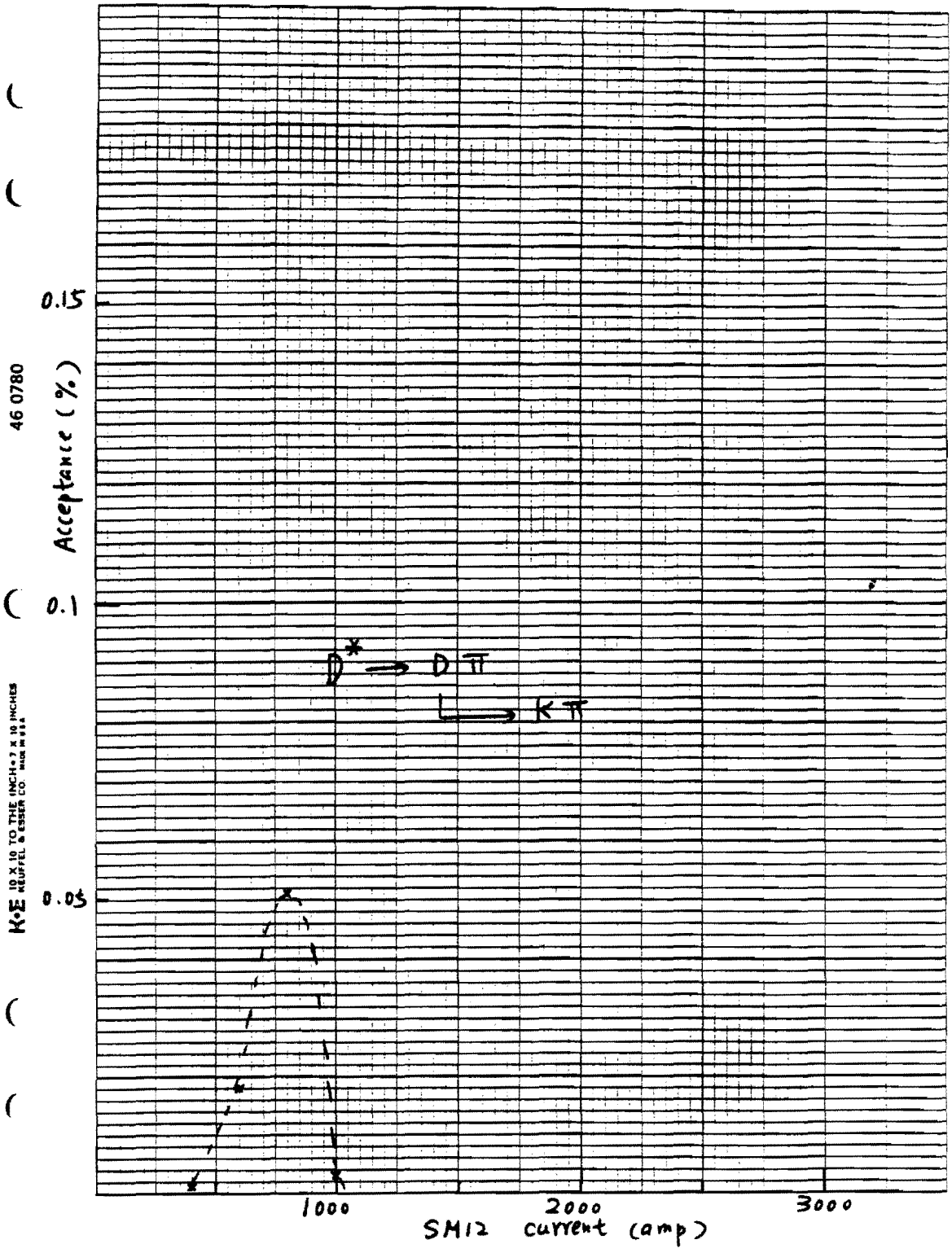
0.15
0.1
0.05
Acceptance (%)
$D^* \rightarrow D\pi$
$\hookrightarrow K\pi$
1000
2000
3000
SM12 current (amp)
46 0780
K·E 10 X 10 TO THE INCH • 7 X 10 INCHES
KEUFFEL & ESSER CO.

Fig. 5

E789 Letter of Intent, October 25, 1989

John Peoples, Director
Fermilab

This letter is intended to clarify our view of the options available to us in turning on E789. The most important new system required for E789 is the silicon vertex spectrometer and associated readout electronics. Since it appears unlikely that the readout electronics will be developed for use during the early months of the upcoming fixed-target run, we have considered two options. (All other required systems will be available for use by February 1990.)

Since E789 will probe new running conditions for the Meson East spectrometer, it is essential to tune up all apparatus at the earliest possible time in order to begin the doubtless complicated tasks of understanding background rates, tuning triggers, etc. The new small-cell high-rate drift chambers at Station 1 and the renovated ring-imaging Cherenkov counter will both require extensive tune-up. Learning to trigger at masses as low as the D and B mesons will also require understanding our calorimeter, trigger matrices, and drift-chamber track processor in a new regime. A necessary preliminary step to all of these studies is a thorough checkout of the scintillation hodoscopes, which were rebuilt over the summer to improve their granularity.

The J/ψ and ψ' resonances will yield very important tune-up and calibration data. At the same time, we have the opportunity to do some nice physics by extending the range of Feynman-x over which the nuclear dependence of their production cross-sections has been measured. Our high-statistics E772 data have generated considerable interest in obtaining additional data at negative Feynman-x, since the observed (and unexplained) A-dependence is strongly x_F-dependent. We estimate that a measurement at the few-% level in the range $-0.15 < x_F < 0.0$ can be carried out in less than one month's running.

If it appears that the Research Division silicon readout electronics will not be ready at the end of this one or two month tuneup period, we have the option of reinstalling our existing 5000 channels of MWPC electronics (with the new Res. Div. preamps which will be available) to instrument a partial vertex spectrometer with $\approx$ 2-rf-bucket time resolution. This would allow us to accomplish two further objectives: 1) tuning up the vertex detector and vertex trigger processor at low intensity, and 2) observing 10^5 D decays to $K\pi$. We would also be sensitive to possible dileptonic D decay modes at the 10^{-7} level. This is another one to two month measurement. Given our intriguing E772 results on A-dependence of hidden charm, we may also choose to study the A-dependence of open charm production.

We are thus requesting that Fermilab allow us to take beam in M-East before our silicon readout system is complete. We believe that only minimal resources are required for the two options described above (we will proceed to estimate these costs carefully). The requested beam time would greatly enhance the ability of E789 to probe rare B decays as soon as the full silicon electronics becomes available.

Daniel M. Kaplan and Jen-Chieh Peng
Spokesmen for E789